AFRL-VS-TR-2000-1520

Development of Methods to Generate High Resolution Climatological Databases to Support DOD Modeling and Simulation Programs

John W. Zack
Glenn E. Van Knowe
Pamela E. Price

Mary D. Bousquet
Kenneth T. Waight III
Charles E. Graves

MESO, Inc
185 Jordan Rd
Troy, NY 12180

March 2000

Scientific Report No. 1

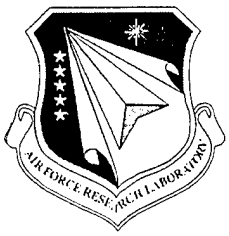

AIR FORCE RESEARCH LABORATORY
Space Vehicles Directorate
29 Randolph Rd
AIR FORCE MATERIEL COMMAND
Hanscom AFB, MA 01731-3010

This Technical Report has been reviewed and is approved for publication.

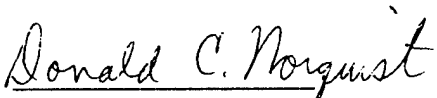

Donald C. Norquist
Contract Manager

Robert R. Beland, Chief
Tactical Environmental Support Branch

This report has been reviewed by the ESC Public Affairs Office (PA) and is releasable to the National Technical Information Service.

Qualified requestors may obtain additional copies from the Defense Technical Information Center (DTIC). All others should apply to the National Technical Information Service (NTIS).

If your address has changed, if you wish to be removed from the mailing list, of if the address is no longer employed by your organization, please notify AFRL/VSIM, 29 Randolph Rd., Hanscom AFB, MA 01731-3010. This will assist us in maintaining a current mailing list.

Do not return copies of this report unless contractual obligations or notices on a specific document require that it be returned.

REPORT DOCUMENTATION PAGE

Form Approved
OMB No. 0704-0188

1. AGENCY USE ONLY (Leave blank)	2. REPORT DATE	3. REPORT TYPE AND DATES COVERED
	20 Jan 2000	Scientific Report No. 2

4. TITLE AND SUBTITLE
Development of Methods to Generate High Resolution Climatological Databases to Support DOD Modeling and Simulation Programs.

5. FUNDING NUMBERS
F196828-97-C-0025

6. AUTHOR(S)
John W. Zack, Mary D. Bousquet, Glenn E. Van Knowe, Kenneth T Waight III, Pamela E. Price, Charles E. Graves

PE
PR CLMS TA EA WU BA

7. PERFORMING ORGANIZATION NAME(S) AND ADDRESS(ES)
MESO, Inc.
185 Jordan Road
Troy, NY 12180

8. PERFORMING ORGANIZATION REPORT NUMBER
10054-02

9. SPONSORING/MONITORING AGENCY NAME(S) AND ADDRESS(ES)
Air Force Research Laboratory
29 Randolph Road
Hanscom AFB, MA 01731-3010
Contract Manager: Donald Norquist/VSBL WTU

10. SPONSORING/MONITORING AGENCY REPORT NUMBER
AFRL-VS-TR-2000-1520

11. SUPPLEMENTARY NOTES
None

12a. DISTRIBUTION/AVAILABILITY STATEMENT
Approved for public release; distribution unlimited

12b. DISTRIBUTION CODE

13. ABSTRACT (Maximum 200 words)

This project focuses on developing methods to simulate climate statistics at high resolution in data sparse and data rich locations. The method, given the name CLIMOD, is based on the use of a numerical-dynamical atmospheric model to generate a sample of simulated data from which climatological statistics are computed. The major objectives of the project are to: (1) demonstrate the robustness and general applicability of the method; (2) refine the CLIMOD technique to optimally blend available observations and numerically simulated climate data; (3) extend the method to complex derived climate variables; and (4) construct an integrated software package that can be applied to anyplace in the world. The work during the second year included: (1) the evaluation of the quality of both 10-year data sets subjectively and objectively using all available observational data; (2) extensive data denial experiments to determine the impact of observed data on the simulations; and (3) the development of enhanced postprocessing methods to compute complex derived variables.

14. SUBJECT TERMS
Climate modeling, Numerical modeling, Numerical weather prediction

15. NUMBER OF PAGES

16. PRICE CODE

17. SECURITY CLASSIFICATION OF REPORT	18. SECURITY CLASSIFICATION OF THIS PAGE	19. SECURITY CLASSIFICATION OF ABSTRACT	20. LIMITATION OF ABSTRACT
Unclassified	Unclassified	Unclassified	UL SAR

Contents

List of Tables

List of Attachments

Foreword

The Defense Modeling and Simulations Organization (DMSO), through the Air Force Combat Climatology System Modeling and Simulation Division (AFCCC/MS) is supporting the Air Force Research Laboratory contract F19628-97-C-0025. This contract is a three-year project to develop a method for estimating climate statistics at high spatial resolution in both data sparse and data rich regions. The method, given the name CLIMOD, is based on the use of a numerical-dynamical atmospheric model to generate a large sample of simulated atmospheric data from which climatological statistics are computed. The objectives of this project are to: (1) demonstrate the robustness and general applicability of the method by generating and evaluating climatological databases for all seasons in two climatologically distinct regions of the world that are of interest to DOD operations; (2) refine the CLIMOD technique to optimally blend available observations and numerically simulated data to produce the highest quality climate statistics; (3) extend the technique to provide estimates of derived variables and additional statistical parameters that are frequently required by DOD applications; and (4) construct an integrated CLIMOD software package that can be efficiently used to generate high quality simulated climate statistics for any location in the world.

Thirteen tasks were formulated to meet the four objectives. The work during the first year of the project included: Task 1, setup of the computational infrastructure; Task 2, development of a method to optimally blend the available observations and model-generated data into a regional statistical climatology; Task 3, development of a method to objectively assess the quality of the simulated climate statistics in data rich and data sparse regions; and Task 4, the generation and delivery of three-dimensional simulated climate statistics for all months of the year over a 10-year period for two different regions of the world: Korea and the Mideast.

The second year of the project focused on: Task 5, the execution of data denial experiments to assess the impact of each data type on the quality of the climate statistics generated by the CLIMOD approach; Task 6, the development and implementation of methods to compute the statistics of derived variables from the basic meteorological variables produced by the model; Task 7, the use of the derived-variable computational procedures to generate climatological datasets for the derived variables for each of the two regions for which a climatology of basic variables was created in the first year; and Task 8, the development of methods to compute specialized statistics, such as the probability of extreme events, from the basic CLIMOD output. Meeting the Y2K compliance requirements was addressed through the expansion of the effort under the contract's Task 10.

The work during the third year will consist of: Task 9, the documentation and delivery of the derived variable climatological data to AFCCC; Task 10, the construction of an integrated CLIMOD software package that could be used to generate climatological databases or as a tool to further refine the CLIMOD technique; Task 11, delivery of the software package to AFCCC; Task 12 the generation of three-dimensional simulated climate statistics for all months of the year over a 10-year period for a tropical region; Task 13, develop a nonhydrostatic option to CLIMOD; and a modified Task 6, that added a task to develop a wind gust algorithm based upon

1. Introduction

There are multitudes of DOD simulation applications that require statistical values of various environmental parameters that describe the local 3-D climate in great detail. These applications include battle- to global-scale simulations, real-world contingency ("what if") situations, and weapons system testing and development. The most obvious and direct way to obtain local climate statistics is to calculate them from long-term point observations. However, the use of long-term observational datasets imposes at least two limitations: (1) long-term point observational datasets are not currently available for many areas of the world; and (2) the representativeness and quality of observations change in time as observing sites are relocated, the land use around a site is changed, or new instrumentation is used. An alternative is to generate statistics from a set of simulations using a limited-area high-resolution mesoscale model that is based upon the physical processes of the atmosphere.

The objective of this project is to estimate the actual climate statistics for a particular period of time over a specified region. This objective can be addressed by executing the model for a long period of time in a data assimilation mode and allowing the model to fuse the available data into a 3-D climatological dataset. In this mode the model periodically ingests the available observed data through a selected data assimilation technique. The model then dynamically fuses the available observations from the region of interest with its knowledge of the surface characteristics of the earth and the basic principles of physics to generate estimates of local climate statistics at all points on a three dimensional grid that covers the region. This technique has been given the name CLImate statistics by a dynamical MODel™ (CLIMOD).

The initial proof of-concept, funded by the Air Force Research Laboratory, through the Air Force Office of Scientific Research (AFOSR), (AFOSR contract F4960-95-1-0523) has established a proof-of-concept for the CLIMOD method. That project performed a set of experiments, which determined that the climate statistics produced by the CLIMOD technique are of very good quality if properly computed. However, the research also showed that the data assimilation strategies, planetary boundary layer (PBL) schemes, microphysics and the cumulus parameterization schemes employed in the model greatly influence the quality of the statistics. The title given to the current project is Advanced Climate Modeling and Environmental Simulation (ACMES). The research in this project has demonstrated significant success in implementing new data assimilation strategies, PBL schemes and in selecting the appropriate microphysics and cumulus parameterizations for producing good quality climate statistics. The first year of this contract and Scientific Report No. 1 (Zack et al. 1998) focused on these aspects of the research. The second year of the contract and this interim report focuses on computational issues, data availability issues, and enhancing the CLIMOD postprocessing. MESO has developed variations of the CLIMOD technique for specific purposes; please note that all references to "CLIMOD" in this report refer to the CLIMOD variation developed for the ACMES project.

2. Computational Issues

Several computational issues had to be faced concerning both the platform and the operating system required to achieve a production capability.

2.1 Computational Platform

Extensive research of the latest workstation technology was conducted to define the optimum workstation and operating system currently available within the cost constraints of the project budget. Based on cost considerations, the decision was to use DEC Alpha "clones". The specific systems used were three 500 MHz Alpha, and two 600 MHz Alpha processor systems. As is typical when using new systems, several hardware and software issues related to system compatibility had to be resolved in order to use the clones effectively. Most issues were resolved completely, but there is still an apparent compatibility issue related to the Linux operating system issue that remains to be resolved.

Midway through the contract AFCCC selected Sun workstations, operating under the Solaris operating system, to be the projected platform for their CLIMOD system software. However, AFCCC has since changed to Dell dual-processing PCs operating under Solaris. The changes in hardware and operating systems presented challenges to the developers to make a flexible and portable system to meet the Air Force's needs.

2.2 Operating System

In order to maximize the productivity of the resources available for the project, MESO obtained and installed the Redhat Linux operating system. Redhat Linux is considerably lower in cost for the same expected performance level than a system utilizing operating systems from a "brand" name vendor such as Digital UNIX. A Microway Linux Fortran compiler for compiling the Mesoscale Atmospheric Simulation System (MASS) (MESO 1995) was also purchased and tested. This compiler is considerably less expensive than the Digital Fortran compiler. Several problems had to be overcome associated with the Linux operating system. Even though MASS was successfully compiled and executed using the Microway compiler under Linux, the performance of MASS never came close to the performance it can achieve when compiled using the DEC Compiler. MESO worked with Microway in an attempt to find the solutions to optimize the performance of MASS (under the Microway compiler) with limited success. The final best solution found was to compile under the Digital operating system using a DEC Fortran compiler and then porting the compiled MASS program to the Linux systems.

However, an unusual problem surfaced with the DEC-Linux combination that was never completely solved. The Linux operating system apparently lost track of certain key files it created in the run process, resulting in the generation of "file not found" errors which caused the run sequence to abort. It needs to be emphasized that the DEC compiler and Linux operating

system combination are not designed to be compatible so it is a misnomer to call this a "Linux" problem as it may be tempting to do. It also needs to be emphasized that the increased speed of the DEC compiled executable over the Microway compiled executable still made the DEC compiled option the better of the two options. This problem may be solved as the Linux Fortran compilers mature that can compete with the DEC compilers performance. As part of the continued investigation into this problem MESO obtained a beta version of a Linux Fortran compiler from Compaq for testing purposes. The entire code of CLIMOD 1.0 was compiled. The Compaq compiled code successfully ran one month of simulations without the "file not found" errors occurring.

AFCCC is planning to use Solaris 7.0 on Pentium III Xeon processors for their actual CLIMOD production systems. AFCCC and MESO believe that the compatibility problem will not be present on these systems since there was no evidence of the problem in production runs made on Alpha systems running Digital Unix or Sun Ultra systems running Solaris. Extensive testing on the AFCCC Pentium III Xeon processors has not revealed any compatibility problems to date.

3. Evaluation of Baseline Runs

3.1 General Comments

The simulations and data evaluation techniques used in this project are described in detail in sections 2 and 3 respectively of the Scientific Report No. 1 (Zack et al. 1998). The quality of the 10-year datasets (01 Jan. 1973 to 31 Dec. 1982) were both objectively and subjectively evaluated in the Korea and Middle East regions. Except for the surface evaluation stations, all of the available observational data were used in the simulations. For evaluation purposes, the stations used in the assessment of the technique were withheld from the CLIMOD simulations. Both the hourly historical data, as well as point and gridded climate products, were evaluated. The complete results of the analysis of all the simulations and data-denial experiments are presented in graph form in Gagan and Graves (1999a - c), Graves and Gagan (1999), and Graves and Poage (1998). All the volumes have been presented to AFCCC in Asheville North Carolina. The evaluation showed that, in general, the technique works well to produce realistic simulations of both historical and climate conditions. However, the evaluation also demonstrated that the magnitude of the model bias and thus the quality of the output data varies according to the season, location and variable.

The estimates of simulated surface observations for the specific station locations are calculated through an inverse distance weighted (IDW) interpolation from the four surrounding gridpoints to account for the exact latitude, longitude and elevation of the station. The observations created by the model are referred to as "simulated observations" or "simobs" hereafter in the paper.

Seasonal differences appear to be influenced by the following primary factors. (1) There is an increase in the convective precipitation in the warmer months thus causing an increase in the activation of the convective parameterization scheme in the warmer months. (2) The accuracy of the vegetation database in representing the seasonal changes in vegetation may not be adequate. (3) The accuracy of the soil type may not be adequate. In general, the vegetation and soil databases have less impact on the model biases in the colder months, therefore colder months tend to have more consistent biases, in both space and time, than is observed during the warmer months.

There appear to be two primary factors regarding location which influence the model biases. (1) The proximity to the coast is the first factor (i.e., number of grid points surrounding a station that are actually over water). Because of the influence of the over-water points, stations near the coast tended to have smoother simulated diurnal changes, higher simulated wind speeds and higher simulated dewpoints than observed data. The simulated mean temperatures were also higher in the colder months and lower in the warm months. The differences of model elevation from the actual elevation of a point also greatly influenced the biases of the simulated values compared with the observed. In general, if the model elevation was higher than the actual elevation, the temperatures were cooler, dewpoints lower and windspeeds higher. Very often the influence of proximity to the coast and elevation differences tended to offset one another.

Because errors tend to offset one another, one has to be cautious not to over-generalize biases when interpreting point statistics from the model grid.

Model grid spacing is a major factor in the quality of the results. Overall, the 10-km results usually were better than the 40-km results. There are some important considerations when comparing the results from the two grid spacings. A different (more sophisticated) cumulus parameterization and moisture scheme was used in the 10-km simulations. The number of grid points actually over water surrounding the coastal station were typically less in the 10-km simulations. Typically the elevation differences between model and actual were less for the 10-km points than 40-km points, but not always. For some points, the differences in elevation were greater for the 10-km grid spacing and in some cases actually reversed sign from the 40-km grid spacing. Table 1 summarizes location, elevation and over-water points for each model grid for the stations used for evaluation in the baseline simulations. For evaluation purposes, the surface observations from these stations were withheld from the CLIMOD baseline simulations. Attachments 1A and 1B provide a map of each region with comparison stations.

Table 1. Summary of Evaluation Stations.

Sta Num	Station Name	ICAO	Lat	Lon	Elev m	40 Elev	10 Elev	H_2O Pts 40	10
KOREA									
470080	Chongjin	CHO	41.47	129.49	43.0	283.8	35.6	3	3
470220	Pungsan	PUN	40.49	128.09	1206.0	1158.5	1336.1	0	0
470310	Changjin	CHA	40.22	127.15	1081.1	1035.6	1305.7	0	0
470550	Wonsan	WON	39.11	127.26	36.0	322.8	378.4	2	1
470580	Pyongyang	KPY	39.02	125.47	38.1	131.2	38.1	0	0
470600	Nampo	NAM	38.43	125.22	46.9	55.0	37.5	3	3
471100	Seoul	KSS	37.33	126.48	18.9	88.6	47.0	2	1
471180	Hoengsong	KNH	37.26	127.57	100.9	396.7	373.8	0	0
471220	Osan	KSO	37.05	127.02	11.9	102.2	42.0	1	0
471390	Pohang	KTH	35.59	129.25	20.1	121.0	122.3	1	1
471410	Kunsan	KJK	35.54	126.37	9.1	68.0	0.8	2	3
471420	Taegu	KTN	35.54	128.39	35.0	221.7	170.1	0	0
471580	Kwangju	KJJ	35.07	126.49	13.1	133.3	103.0	2	0
MIDDLE EAST									
407470	Sanandaj	ICS	35.29	047.00	1373.0	1922.6	1804.0	0	0
407660	Kermanshah	ICC	34.16	047.07	1321.0	1618.0	1618.6	0	0
406500	Baghdad	RBB	33.14	044.14	34.0	39.8	35.6	0	0
406700	Najaf	NAJ	31.59	044.19	32.0	58.6	39.7	0	0
406650	Kut-Al-Hai	KUT	32.10	046.03	14.9	43.9	58.8	0	0
407690	Arak	IHR	34.06	049.42	17190	1984.2	1914.2	0	0
407540	Tehran	III	35.41	051.21	1191.0	1710.7	1184.4	0	0
406210	Kirkuk	KIR	35.28	044.24	310.0	451.4	383.0	0	0
408310	Abadan	IAA	30.22	048.15	11.0	22.4	30.0	2	2

When interpreting the results of the baseline runs, an important consideration to keep in mind is that it took one and one half years to run the entire 10-year Korea and Middle East simulations. In the course of the one and one-half years multiple changes were made to some of the CLIMOD routines and scripts to improve results. This means that the biases and quality of the results may vary somewhat between months due to these many changes. However, no changes were made within the ten year processing of a given month, changes were only made between months. Thus, the statistics from a particular month are derived entirely from a fixed configuration of CLIMOD.

The most notable change was modifying the 10-km cumulus parameterization scheme from the original Fritch-Chapple scheme to the Kain-Fritch scheme for the months of July through December. Also, because of the lack of availability of observed data for certain regions, (which is the reason for developing this technique in the first place), the evaluation is by necessity limited and can not cover all possible cases. As modeling techniques are improved, current biases may be corrected in the future.

There are several components to consider when evaluating the quality of the model output. First is the evaluation of the overall means and extremes for all hours; second is the evaluation of the diurnal cycle, and finally the evaluation of the spatial and temporal variability. Each of these components was examined in the investigation of the quality of results.

In all three of the above categories, temperature and pressure are the variables that appear to be most accurately simulated when compared to observational data. Dewpoint is also simulated quite well, but tends to have larger biases than temperature or pressure. Wind speed tends to be overestimated when compared to the observed wind speed database, but some of the overestimation is due to the fact that wind measurements of less than 3 knots are often reported as calm. The biases in the simulated data do appear to be reasonably consistent across the model domain. For example, if the model bias was for low daytime maximum temperature for a given month, that tended to be the case throughout the domain. The only exception to this consistency was found (1) for points in close proximity to water or (2) when there were significant differences between model elevations and actual elevations. The coastal stations exception to consistency was found when several of the surrounding data points were over water thus making the simulated observation or climatology more unrepresentative of the actual station which, of course, is over land.

On the other hand, the precipitation variables had positive biases in some parts of the domain and negative biases in other parts of the domain. The precipitation variables are the hardest to verify due to the episodic nature of precipitation and the limitations in the precipitation observed database. In some cases, it might be the case that the simulated data is actually more representative of what actually occurred than the observed database. Graphs and figures that are representative of analysis of the output are presented later in this report.

3.2 Historical Data Analysis

The term "historical data" is defined, for the purposes of this paper, as the hourly simulated grids and simulated observations of the variables produced directly from the CLIMOD system. The quality of the simulated historical data can vary from day to day and occasionally a simulated hour or day was not very representative of the actual conditions, but overall, the hourly simulated observations compared favorably with the actual observations. The warmer months tended to have larger differences between the observations and simulated observations. This is described in more detail in the climate analysis sections. Table 2 shows a representative comparison of the hourly observations with the 10-km simulated observation for a given day (20 January 1973) at Osan Air Base, Korea. The quantities compared are sea level pressure, temperature, dewpoint, wind direction, wind speed, and fractional cloud coverage.

Table 2. Comparison of houly observations with simulated observations (simobs)

Comparison of the hourly observations (Obs) with the 10 km *simulated* hourly observations (Sim) for a given day at Osan Air Base, Korea. Elements compared are sea level pressure (SLP), temperature (TMP), dewpoint (DEW), wind direction (DIR), wind speed (SPD) and fractional cloud coverage (CLD).

KSO Osan, S Korea ICAO 471220 DATE: 730120 LAT/LON: 37.08 127.03 MODEL ELEV: 42.0 m NEST: 10 Km												
UTC Hr	SLP Obs	SLP Sim	TMP Obs	TMP Sim	DEW Obs	DEW Sim	DIR Obs	DIR Sim	SPD Obs	SPD Sim	CLD Obs	CLD Sim
00	1025	1023	27	28	25	23	15	14	3	4	0.0	0.0
01	1027	1024	32	33	27	24	21	20	4	6	0.0	0.0
02	1024	1023	40	40	29	24	25	25	4	4	0.0	0.0
03	1025	1024	45	46	29	25	27	25	6	8	0.1	0.0
04	1023	1023	47	48	27	25	28	29	15	13	0.1	0.1
05	1025	1024	49	48	28	26	25	28	10	12	0.1	0.1
06	1025	1024	48	48	27	27	29	28	12	12	0.0	0.0
07	1025	1025	48	47	25	26	26	27	8	9	0.0	0.0
08	1025	1025	47	46	24	25	28	27	5	7	0.0	0.0
09	1026	1025	44	44	24	24	24	23	4	4	0.0	0.0
10	1026	1027	41	42	25	25	00	27	0	2	0.1	0.0
11	1026	1026	40	41	26	26	00	05	0	1	0.2	0.2
12	1027	1025	40	40	26	26	08	02	2	4	0.6	0.6
13	1024	1024	36	35	30	21	27	26	6	5	0.3	0.1
14	1024	1024	35	34	30	24	33	33	3	5	0.1	0.0
15	1024	1023	33	33	29	27	34	34	3	3	0.1	0.0
16	1024	1023	32	33	30	29	02	02	2	5	0.1	0.1
17	1024	1024	32	32	30	30	00	15	0	3	0.2	0.3
18	1025	1026	31	32	29	31	00	18	0	1	0.4	0.5
19	1024	1025	31	31	29	30	07	09	3	3	0.8	0.7
20	1024	1024	30	31	29	29	09	07	4	1	1.0	1.0
21	1025	1024	30	31	29	30	08	09	2	4	1.0	1.0
22	1025	1026	31	33	29	29	11	10	2	3	1.0	1.0
23	1025	1026	32	32	30	31	36	35	3	2	1.0	1.0

Attachment 2A shows the percentage of time the observations fall within a threshold of 4, 2 and 1 degree F or knots for temperature, dewpoint, and wind speed for all hours. The chart was developed from the analysis of data from 300 randomly chosen days throughout the 10-year period for six sites. The six sites chosen for Attachment 2A are listed in Attachment 2B. These six sites were chosen because they are representative of various types of locations (coastal, inland, low elevation, high elevation, small and large actual-model elevation differences) and they have a reasonable observation count.

3.3 Analysis of Means and Extremes

The general, performance of the model can be demonstrated by looking at the annual means (Attachments 3A-3D) of the six representative sites (Atch. 2B) in Korea. Overall, the model does well on the means. However, inspection of the means of pressure, temperature, dewpoint and wind speed by month as represented by the output for Osan AB (Attachments 4A-4D), shows that the simulated means are more representative in the cold months versus the warmer months, indicating the model bias is more of a problem during the warmer months. As indicated in Section 3.1, the likely cause of the larger warm season biases relates to the increase in convective precipitation, accuracy of the vegetation database and the accuracy of the soil type.

The model does well on simulating the extremes. Attachments 5A and 5B depict a representative example of the model performance in capturing the mean daily high and low temperatures for the month. Tables 3 and 4 give some representative examples for simulated extremes versus observed extremes. The precipitation related variables were the most difficult to compare because of the lack of observational data for precipitation. For the observed data that was compared, at times the observed extremes matched well with the simulated, while other times/locations it did not match as well.

Table 3. Extreme value comparisons for temperature and wind speed.

Station	Month	Temperature			Wind Speed		
		Obs	40 km	10 km	Obs	40 km	10 km
470080	Jan	48/-6	44/-8	47/-2	38	32	30
470080	Jul	93/49	90/47	91/50	25	18	22
471180	Jan	65/-21	58/-23	61/-25	38	40	43
471180	Jul	106/60	102/57	108/60	27	30	32
47122	Jan	56/-16	54/-6	55/-8	38	37	34
47122	Jul	97/55	107/59	102/42	47	32	47
47139	Jan	68/3	63/0	64/-2	44	38	40
47139	Jul	100/50	104/47	109/46	40	30	36
40650	Jan	80/19	78/20	79/15	32	28	31
40650	Jul	123/63	120/60	122/58	36	27	30
40754	Jan	67/9	63/6	60/-1	40	32	47
40754	Jul	106/58	102/59	98/50	45	31	43

Table 4. Extreme value comparisons for temperature, wind speed, precipitation and snowfall.

Osan AB 47122									
Jan	**T avg**	**T high F**	**T low F**	**Speed Kts**	**Cloud Frac**	**Pcp avg inches**	**Pcp max inches**	**Sno avg inches**	**Sno max inches**
Obs	26	56	-16	38	.38	1.0	4.2	7	31
40 km	26	54	-6	37	.43	1.3	3.6	2.4	4.6
10 km	26	55	-8	34	.44	0.9	3.5	6.0	11.0
Jul									
Obs	77	97	55	47	.63	4.8	24.0	0	0
40 km	82	107	59	32	.63	2.9	9.2	0	0
10 km	72	102	42	47	.85	15.0	24.2	0	0

3.4 Analysis of Ability to Capture Diurnal Variability

For the most part the model captures the diurnal cycle for each variable. The method of data assimilation has a significant impact on how well the diurnal cycle is captured. It was found that the more abruptly the data was assimilated into the model the larger the discontinuities around the time of data assimilation which disrupted a smooth diurnal cycle. Two forms of data assimilation were used in performing these specific simulations; (1) discontinuous data assimilation that utilizes optimum interpolation and (2) a new data assimilation technique called incremental analysis update (IAU). IAU was found to produce the best diurnal signal. Due to computational considerations, only the 40-km nest was run using IAU. The 10-km nest used the discontinuous form of data assimilation. If capturing the diurnal cycle is important for a given simulation, then it is recommended that IAU be used for all nests.

3.4.1 Pressure

The overall means were captured extremely well. However, the proof-of-concept study conducted on the eastern Great Lakes region showed two problems with the modeled pressures. One problem was an approximately 4 mb bias in the model pressures (both for 10-km and 40-km models). This consistent bias was due to imbalances introduced by the lateral boundary conditions. Consequently, a mass imbalance was established with more mass leaving the model domain than entering it. This caused the modeled pressure to have a low bias. The lateral boundary condition algorithms were adjusted to ensure the lateral boundary conditions are in mass balance, which helped to eliminate this bias.

The second problem highlighted in the proof-of-concept project was an absence of the diurnal pressure cycle. The reason for this was the fact that the diurnal solar thermal tides have never been built into mesoscale models. A diurnal pressure correction was added as a postprocessing step to the pressure field. The results to this point indicate that there is considerable improvement in the simulated pressure. The Osan Air Base pressure analysis results for the January 1973 simulation are presented in Attachment 6A as a representative example.

3.4.2 Temperature

The temperature comparison was consistent with the results from the proof-of-concept research as it again proved to be the best-modeled element. One difference noted was that the 10-km results were improved over the proof-of-concept results. The reason for this was a change in the data assimilation strategy that included using rawinsonde data for the 10 km (discontinuous data assimilation) as well as the 40-km (IAU) domains. In the proof-of-concept study discontinuous data assimilation was used for the 40-km nest with no data assimilation for the 10-km nest. Also, the Planetary Boundary Layer (PBL) scheme was change from the Blackadar to Turbulent Kinetic Energy (TKE) scheme (see Zack et al. 1998) for the 10 km domain. The combination of changes to the PBL scheme and data assimilation resulted in very representative temperature statistics for both the 10-km and 40-km domains. The Osan Air Base temperature analysis results for the January 1973 simulation are presented in Attachment 6B as an example.

3.4.3 Dewpoint

The modeled dewpoints are also very representative of the observed dewpoints. At 40-km grid spacing, a warm dewpoint temperature bias similar to that found in the proof-of-concept was observed. However, the 10-km dewpoint results were much improved as indicated in Attachment 6C. The improvement in the 10-km results is attributed to the change in data assimilation strategy and using the TKE PBL scheme.

3.4.4 Wind Speed

The analysis of the wind speed at Osan in Attachment 6D reveals the observed wind speeds were slightly greater during daylight hours than the simulated wind speeds. The 10 km simulation was somewhat better than the 40 km domain at capturing the daytime maximum that occurs in the mid afternoon. The nighttime simulated wind speeds were higher than observed. This is likely due to the inability of the model to capture shallow inversions at night resulting in higher modeled wind speeds.

3.4.5 Precipitation

The frequency of precipitation compared reasonably well with the observed at both the 40-km and the 10-km grid spacing. The Osan Air Base temperature analysis results for the January 1973 simulation are presented in Attachment 6E as an example. The frequency of precipitation is defined here as the fraction of the days in the month for which rain occurred at the indicated hour of the day. No clear diurnal pattern was observed in either the observed or the simulated data, and it was not clear that the 10 km modeled data was more representative than the 40 km grid spacing data. However, it is clear the 40-km grid spacing simulations produced a smoother (less noisy) curve than either the 10 km or observed data.

3.4.6 Cloud Coverage

Establishing methods to model clouds, tops and ceilings, were undertaken. The first step was evaluating the model-derived total cloud coverage with the total cloud coverage that is observed. The simulated total cloud coverage is an integrated value for the entire column assuming maximum overlapping of levels. The cloud coverage at each level is obtained by calculating the cloud fraction based upon a simple cloud fraction-relative humidity relationship (see Section 5.1). The evaluation of cloud coverage is particularly difficult because cloud coverage is not always reported in the observation. However, a limited comparison of the modeled versus observed cloud coverage for Osan AB, January 1973, (Attachment 6E) revealed encouraging results.

3.5 Analysis of Ability to Capture the Climate Distribution

When all of the evaluation stations for all months were evaluated for the ability to capture the climate distribution, the model showed a similar capability to capture the mean of the distribution for pressure, temperature, and wind. However, there was considerable difference in the ability of the model to capture the variability of the distribution. The definition of "variability" used in this report refers to the general departure or spread of individual values of a variable from the central tendency of the distribution. The variability of a given variable is primarily determined by calculating the variance. Variance is defined as the mean square deviation from mean, that is, the mean of the squares of the differences between individual values of the variable and the mean. The percentage of the variability captured by the model was defined as the model variance divided by the average observed variance, or

Percentage Variability = (average variance model / average variance observed) x 100.

The model at times had more, and at times less, variability than the observed. To account for this fact, the agreement of the variability captured by the model was defined as:

> the difference between the average observed variance and the absolute difference between the variance of the observed and model distributions divided by the average observed variance for each variable for each of the evaluation stations for all months. That is

Percentage Agreement in Variability =
[(average variance observed - |average variance observed - average variance model|)
/ average variance observed] x 100.

Surprisingly, the model often had greater variability than observations with an average variance actually being higher for the simulated observations than the observed. The absolute agreement between variance values of the observations and simobs were between 70 to 80 %. However, the model only showed an overall agreement with the dewpoint distribution of between 50-60 percent. Usually, the 10-km model showed better capability to capture the variability in distribution. The exception was the wind speed, with the difference primarily due

to warm season problems in capturing the wind variability at 10-km grid spacing. Table 5 and Attachment 7 depict the overall average variability agreement by nest.

Table 5. Impact of Resolution on Model's Ability to Capture Variability

Percentage Agreement in Variability = [(average variance observed - |average variance observed - average variance model|) / average variance observed] x 100.

	Average % Agreement in Capture of Variability	
Variable	**40 km**	**10 km**
Sea Level Pressure	75	78
Temperature	70	75
Dewpoint	52	60
Wind	77	75

3.6 Analysis of Ability to Capture Climate Distribution Variability by Season

The 10-year averages for selected stations, that represent the various climate regions of the Korean and Mideast region, listed in Table 1 from the 10- and 40-km grids in each theater are depicted in Attachments 8-11. In general the winter months were better captured than the summer months, with temperature and pressure having smaller overall biases than dewpoint and wind. For the most part, the magnitude of the biases tends to correlate well to the difference between the model elevation and the actual elevation for any given point. The greater the difference in model and actual elevation for the same point, the greater the bias. The other significant factor is the number of surrounding grid points over water, with the greater the number of grid points over water the larger the bias. On occasion the elevation difference and number of grid points over water would tend to compensate, thus decreasing the bias for a specific variable. However, this situation tended to be variable specific. Using the effects of the bias on temperature as an example, a higher model elevation bias (which is colder) with surrounding grid points over water (which is warmer), tended to cancel each other. But at the same station, these two factors would tend to increase the model bias for wind speed (higher for both factors).

Examining the ability to capture the climate distribution by season, considerable variation was noted based upon the variable and grid spacing. During the colder months, when the respective bias was removed from each variable, the modeled pressure and temperature agreement in observed variance was over 90 percent for both the 10- and 40-km data. That dropped to an agreement between 78-84% during the warm season. The cold season modeled wind agreed to 75 % of the observed variance at 40 km and improved to 90 % at 10 km. The summer months variance agreement ranges for wind were from 50-70 % at 40 km and only 40-50% at 10 km. The modeled dewpoint variability showed the largest differences between the modeled and observed values in July, with the modeled variance being much larger than the observed. The cause of the over estimation of variability by the model seemed to be related to an over mixing of the drier air above the boundary layer which unrealistically lowered the afternoon dewpoint.

In summary, the results tend to indicate that the 10-km model was somewhat better in capturing variability. There was in general more agreement between the observed and modeled variance at the 10-km grid spacing than the 40-km grid spacing. For the variables examined (pressure, temperate, dewpoint and wind speed), although there were exceptions, the magnitude of difference between the observed and simulated observations tended to be larger during the warmer months. Attachments 12-19 give observed and model plots of the distribution for the individual variables for Osan AB, Korea (47122) and Tehran, Iran (40754). In Attachments 12-19 "Var" is the variance, "PRMSD" is the error calculated for the entire distribution and "TPRMSD" is the error calculated for the tails of the distribution (depicted by vertical red lines). Table 6 summarizes the results of the model's ability to capture the magnitude of the variability as represented by the variance.

Table 6. Capture of Variability by Model Nest

Percentage Variability = (average variance model / average variance observed) x 100.
Osan AB, Korea (47222) Tehran, Iran. (40754)

	Average % Capture of Variance by Model Nest			
Variable	**40 km**		**10 km**	
	Jan	**Jul**	**Jan**	**Jul**
Sea Level Pressure Osan	110	112	114	124
Sea Level Pressure Tehran	125	84	149	109
Temperature Osan	103	151	91	196
Temperature Tehran	102	151	112	155
Dewpoint Osan	104	250	90	556
Dewpoint Tehran	154	315	169	195
Wind Osan	109	108	105	208
Wind Tehran	50	50	25	51

3.7 Comparison of Results by Region

On the whole, the model did a reasonable job in simulating the climatologies for both the Korean and Middle East region. However, the Korean model-observed comparisons tended to show somewhat smaller and more consistent bias than the Middle East results. There are three likely factors contributing to this. (1) The observational sites in the Middle East are not as representative of the surrounding areas because observation points are typically put in locations of significant human influence and modification of the local desert climate. (2) The availability of high-quality observations for comparison is quite limited. (3) The available surface characteristics databases such as soil type, land use and terrain are not as representative of the Middle East surface as they are of Korea. In part this is due to the surface characteristic complexity of the Middle East which should improve by running at higher resolution. However, there is a clear need for improved surface databases in this region.

The results from Baghdad, Iraq (station number 406500) are shown to demonstrate the possible problem and solution resulting from poor soil moisture representation. An evaluation of the results from the Mideast simulations revealed a significant discrepancy in the temperature and dewpoint as indicated in Attachments 20A and 20B. The results shown in Attachment 20A and 20B were obtained before the soil moisture content was adjusted. Attachment 20A shows a strong overnight warm bias in the modeled temperature. The dewpoint curve at Baghdad depicted in Attachment 20B showed an even greater problem with a warm model bias. The possible causes for this were examined. It was determined that the most likely case was an unrealistically high initial soil moisture content. Since the soil in that region is very dry, the model's initial soil moisture content was changed to a near zero value. This greatly improved the results.

The Baghdad results depicting surface temperatures and dewpoints using the modified soil moisture content are shown in Attachments 21A and 21B. The temperature results using the modified soil moisture content decreased the overnight simulated low temperature values. The 10-km temperature results were improved more than the 40-km results. As depicted in Attachment 21B, the modeled dewpoint curve showed a remarkable improvement when the soil moisture was adjusted.

However, even with this improvement, the CLIMOD-produced dewpoint statistics over a desert area of the Middle East showed a warm and dry bias when compared to the observed data. The bias is smaller in the 10-km grid than in the 40-km, but still noticeable. An analysis of the problem (Thompson 1999) revealed the following insights. Two stations were chosen for the comparison, one in an urban desert environment (King Khalid Airport in Riyadh, Saudi Arabia), the other in a rural desert environment (Al Kharj, located 35 miles to the southeast of Riyadh) (Table 7). Two more sets of dewpoint and temperature difference curves were produced, one in Nevada, the other in Egypt. Similar circumstances were used in setting up these two studies: an urban desert and a rural desert location were both chosen, within a certain distance of each other, at roughly the same altitude. The comparison from Egypt may prove unreliable, due to proximity of the Nile River. The difference in the Nevada test shows a similar trend to Saudi. The rural desert location shows a significantly smaller average dewpoint, about 3.1F. This provides consistent information with what was observed in Saudi. The observed data at each station was examined and compared with the other.

Table 7. Locations used to compare temperature and dewpoint observations. For each desert region, an urban and rural location were selected.

Region	Ob Site	Blkstn	Latitude	Longitude	Type
Saudi	*King Khalid (Riyadh)*	404370	24.53	46.46	Urban
	Al Kharj	697040	24.08	47.18	Rural: ~35 mi. ESE of Riyadh
Egypt	*Cairo*	623660	30.08	31.24	Urban
	Ismailia	624400	30.65	32.17	Rural: ~60 mi. E of Cairo
Nevada	*Nellis AFB*	723865	36.15	-115.02	Urban
	Mercury	723870	36.37	-116.01	Rural: ~60 mi. WNW of Nellis

For each observation with data at both stations, the difference between the temperature and dewpoint was calculated. The distribution of each difference was fairly normal, with a small amount of skewness in each. The average difference in dewpoint between the city and rural setting was about 7.4F, with the city being the higher of the two. Tables 8 and 9 depict the difference between rural temperature and dewpoints respectively.

Table 8. Temperature comparison.

Values are the difference between urban and rural temperature observations. Positive values indicate higher temperatures ($Temperature_{Urban}$ - $Temperature_{Rural}$).

Loc	Mean	Max	Median	Min
Saudi	-0.94	33.8	-0.9	-33.8
Egypt	0.45	27	0.4	-34.2
Nevada	4.5	29.0	5.0	-40.1

Table 9. Dewpoint comparison.

Values are the difference between urban and rural dewpoint observations. Positive numbers indicate higher dewpoints. ($Dewpoint_{Urban}$ - $Dewpoint_{Rural}$).

Loc	Mean	Max	Median	Min
Saudi	7.4	50.2	6.1	-41.2
Egypt	-0.53	24.1	-0.2	-32.9
Nevada	3.1	46.1	3.1	-29.0

These comparisons suggest that urban locals within a desert domain may be uncharacteristically moist compared to their rural surroundings. This could explain a portion of the dry bias resulting from a comparison of simulated dewpoints from surrounding model grid points with dewpoints from an urban station in the desert.

There are two instrumentation issues with this study. The first was fairly easy to test. Digital sensing equipment has a known deficiency dealing with very small dewpoints (20F and less). Therefore, the data was filtered and all observations with dewpoint below 40 degrees were removed and the statistical analysis was performed on the modified data set. The change in average difference was negligible; in the Saudi case for example, the new result was a difference of about 7.3F. The second issue with instrumentation concerns the differences of quality and calibration of the instruments used to measure dewpoint. There is no way to account for this in this comparison or the CLIMOD model.

Examining the observations provides at least part of the explanation for the dry bias of the CLIMOD model results when compared to the observations. Several examples have shown that an observation taken in an urban desert environment can show higher dewpoints than observations taken in a nearby rural desert location. The urban desert locations are not as representative of the whole as the rural observations, and the CLIMOD model seems to be more representative of the region than the site observational climatologies.

3.8 Analysis of Quality by Variable

AFCCC personnel performed a series of assessments of the quality of CLIMOD-generated grid climatologies for each modeled variable (Doggett et al. 1999; Doggett 2000; Thompson 2000). They compared the model-derived climatologies with the climatologies at existing observing locations for each variable. A portion of the results of these studies is presented in this section to provide a more complete presentation of the evaluation of the CLIMOD products for the Korea and Mideast theaters. The ten-year model derived climatologies (Jan 1973-Dec 1982) were compared with the climatologies at existing observing locations for each variable as available in the 30 year NCDC's Global Historical Climatology Network (GHCN) (Vose et al. 1992) (Attachment 22A). The GHCN was used as the observed standard for these variables. The modeled values for each station location were determined by the inverse distance weighted interpolation method described in section 3.1.

3.8.1 Temperature Results

Typically, when performing a regional climate analysis for AFCCC customers, AFCCC will take the mean temperatures at existing observing sites and construct a contoured analysis for visual interpretation (Attachment 22B). However, this kind of analysis has several severe limitations.

First, while observation sites may be fairly dense in some locations, there are large regions over mountainous terrain and especially the oceans where no surface observation sites exist. Second, is that a simple interpolation scheme like IDW is not representative between sites

where strong mesoscale effects are present (e.g., land/ocean boundaries and mountainous terrain). Another limitation is that climatologies from the GHCN database only include temperature, precipitation, and pressure. While climatologies may be obtained from other sources of surface data, these sources are even more sparsely populated in the Korean region than those in the GHCN.

The use of the CLIMOD method to "fill in the gaps" of the above-mentioned deficiencies is showing some promise. Attachment 23A shows the model-derived mean temperature over the entire model domain (40-km grid spacing). This attachment demonstrates that the model is producing a physically consistent climatology that reflects mesoscale climate influences. Most notable are the colder mean temperatures over the mountainous terrain on a mesoscale level.

Significant differences between the observed and modeled results are shown in Attachment 23B. Overall, the model tends to have a warm bias of 1.6 °C. This bias, however, is largely a result of the analysis over the oceans. Interpolating over water between land-based observation sites fails to account for the moderating effect the oceans have on air temperature. The model does, however, account for this effect and correctly models warmer temperatures over water. Strictly over the land areas, Attachment 23B shows that a majority of the area is within ±1 °C. Another region of significant warm bias is the mountainous terrain in extreme northern China/Russia. Here the model failed to capture the extremely cold mean temperatures seen in this area. There are two possible reasons for this. (1) The vertical grid spacing of the model near the ground, while higher than in the free atmosphere above the PBL, is still not sufficient to capture shallow inversions which often occur in this region in the winter and contribute significantly to a very low mean temperature. (2) The coarse grid spacing of the NCAR -NCEP Reanalysis data used for lateral boundary conditions fails to properly represent these cold shallow inversions. The combination of these two factors results in climatologies that look like the Reanalysis data near the model boundaries.

Many regions where the differences are greatest are located in between the surface observation sites where mesoscale effects such as mountainous terrain or ocean influences are significant. In these areas it is inappropriate to simply interpolate between observations and it is believed the point statistics from the model often makes more physical and climatological sense than the statistics interpolated from the observed values.

The CLIMOD performance also can be measured by analyzing the differences between the modeled climate and the observed climate at the points where surface observations are recorded. The GHCN provides over 500 observation sites in the region with which to compare the modeled mean temperatures. An examination of the modeled and the observed distributions reveals several similarities between them (Attachment 24A). Both modeled and observed show peaks occur near +4, -4, and -18 °C. With the exception of the extreme minimum temperatures, the modeled distribution is remarkably similar to the observed. The model is skewed slightly more toward the warmer temperatures and fails to accurately identify the tail of the distribution at extreme cold temperatures. A scatter plot of modeled versus observed shows a very strong linear correlation with an R^2 of 0.96 (Attachment 24B). Only a handful of modeled temperatures depart significantly from observed. A cursory examination of several of these outliers indicates

the modeled grid spacing of 40 km was insufficient to resolve mesoscale features such as terrain and ocean at these locations. Further examination of the distribution of errors shows that the model has a mean error of +0.8 °C, a mode of +0.3 °C, and is skewed slightly toward a warm bias (Attachment 25A). Forty four percent of the locations are modeled within ±1°C of observed and 75% are within ±2 °C.

These are remarkable results when considering the extremely limited amount of direct observational data that was ingested in the model. Another significant consideration that needs to be made when viewing these results is that this project is only a first attempt at using this method and there is considerable room for optimizing the methodology and model configuration.

3.8.2 Precipitation Results

The monthly modeled precipitation climatology for the Korean region is shown in Attachment 25B. An analysis reveals the following characteristics:

1. Precipitation drops off to zero at the model boundaries.
2. The model correctly identifies mesoscale features such as up-slope precipitation maximums and rainshadow minimums.
3. The rainfall maximum over the ocean southeast of Japan coincides with the observed mean position of the polar frontal zone.
4. The maximum over the northeast region of Taiwan is a result of up-slope conditions from the Northeasterly trade winds.
5. The very dry conditions in continental Asia are consistent with observed.

A comparison of the monthly modeled and observed precipitation distributions reveals several similarities (Attachment 26). The mean precipitation at all sites is slightly higher from the model than the observed but only by about 10%. The model precipitation amounts are somewhat more spread out but this is largely a reflection of the large difference in the extreme maximums. The differences between the quartiles were all less than 0.10 inches.

In general, the model appears to produce a distribution of precipitation climatology consistent with expected conditions. However, when the modeled precipitation is compared with the observed mean precipitation at the GHCN sites, significant differences are observed. A scatter plot analysis of modeled vs. observed shows precipitation modeling is much less skillful than temperature modeling. However, it needs to be noted that a 40-km model grid spacing, which works well for temperature, is not adequate to capture fine-scale precipitation patterns that will likely dominate the climatology in complex terrain. Higher model resolution combined with the more complete microphysics will likely have a significant positive impact on precipitation.

The traditional linear correlation is compared with the ranked correlation (Attachment 27) where the lowest rank corresponds to the driest station. In this analysis, there is a stronger correlation between the driest observed and the driest modeled sites. The locations with the most precipitation are also the same locations where the model is the wettest. The lower traditional R^2 value of 0.53 compared to a much higher rank R^2 of 0.74 indicating that a few deviant pairs are contributing significantly to a low correlation.

Attachment 28 shows the error between modeled and observed mean precipitation. As noted earlier, the model appears to be too dry along its boundaries, and since this appears to be a boundary value problem, these sites are not included in this analysis. The regions that appear to contribute significantly to the correlation in Attachment 27 are identified as: "A" – Taipei, Taiwan; "B" – Continental Southeast China and; "C" – Four sites in Japan.

Taipei's large discrepancy is a result of excessive low-level convergence due to the moisture-rich tropical northeasterly trade winds moving into up-slope conditions along the windward side of the island mountains. The island's close proximity to the model boundary is heavily influenced by the coarse Reanalysis data used for lateral boundary conditions. The Reanalysis data is not fine enough to properly resolve Taipei and Taiwan as a whole but the CLIMOD 40-km simulations do. Thus, a conflict is created in the model between the Reanalysis data and the solution from the model in the vicinity of the Island. This conflict creates added convergence due to the wind differences between the model and the Reanalysis and this leads to extra precipitation. The results for Taipei would likely be significantly better if it were further into the interior of the 40-km grid. This indicates that it is crucial to select the domain locations of the theater, for which climate statistics are desired, in such a way as to minimize the boundary effects at locations deemed important to the user.

The locations at four sites in Japan present a similar problem. However, all are located within the leeward side of a significant mountain barrier. Although the model does demonstrate the "rainshadow" effects on the leeward side of the mountains, it is apparently not precipitating enough moisture out as systems move across the mountains. In general, it appears that the model is over-precipitating at many locations where there is mountainous terrain and an ample source of moisture (see Korea and Japan in Attachment 28).

A contrary problem is seen in the locations over continental Southeast China, which are modeled much drier than observed. The cause for this appears to be a result of boundary conditions. The model does identify this zone as a region of locally higher precipitation (Attachment 25B). However, the precipitation amounts quickly diminish to zero inland from the oceans (toward the model boundary).

Ideally a normal distribution of errors strongly peaked near zero is expected (Attachment 29A). This distribution peaks at 0.04 inches and has a mean of only 0.12 inches. Its skewness is largely influenced by the extreme case at Taipei, Taiwan whose modeled error is in excess of 12 inches (off chart).

Attachment 29B shows the cumulative frequency distribution of the root mean square errors (RMSE) for each of the Januarys in the 10-year period. The RMSE is calculated for each January as the difference between modeled and observed mean precipitation for 383 GHCN locations. While the mean error seems rather excessive at 0.60 inches, 50% of the errors were less than 0.25 inches and 80% of the errors were less than 1 inch.

3.9 Analysis of Ability to Capture Spatial Variability

The locations of the four stations used in the spatial variability experiments are Seoul 471100 (KSS), Hoengsong 471180 (KNH); Osan 471220 (KSO), Taegu 471420 (T). Osan was used as the base station. These stations were selected for two reasons: (1) They provided several cross-sectional options to evaluate different aspects of the model's ability to capture a spatial variability over a variety of situations, e.g., coastal versus inland mountains and latitudinal influence. Also, (2) these stations had a reasonable observation count. Table 10 summarizes the significant characteristics of the four stations.

Table 10. Summary of Evaluation Stations.

Sta Num	ICAO	Lat	Lon	Elev m	40 Elev	10 Elev	H2O Pts 40	H2O Pts 10
471100	KSS	3733	12648	18.9	88.6	47.0	2	1
471180	KNH	3726	12757	100.9	396.7	373.8	0	0
471220	KSO	3705	12702	11.9	102.2	42.0	1	0
471420	KTN	3554	12839	35.0	221.7	170.1	0	0

Four different variables were looked at to examine how well the respective mean diurnal variable curves captured the difference between locations. The differences for each variable between Osan and Seoul were calculated by using Osan minus Seoul (Attachments 31 - 34). These results were typical of the other comparisons. The ability to capture the spatial difference appeared to be dependent on season, the terrain characteristics and the specific variable. For example, the temperature difference was not well depicted in the cold season early morning hours presumably because Osan is located in a "bowl" like valley where a shallow boundary layer can set up in the early morning hours. This effectively decouples the surface layer around Osan and allows unique characteristics to develop. However, the warm season modeled spatial difference was much more representative presumably because of a greater mixing with a deeper boundary layer. It also became obvious that the observing characteristics of the instrument involved have to be accounted for. As an example, in the case of sea level pressure, it appears that much of the difference observed between stations was due to systematic instrument errors and not actual pressure differences.

3.10 Extreme Value Analysis

An analysis of how the model captured extreme values was performed by AFCCC (Doggett 1999). The results of that assessment study are presented in this section to provide a more complete presentation of the evaluation of the CLIMOD products for the Korea and Mideast theaters. An analysis of how well the simulated climatologies compared with observed climatologies for the Korean, 10-km climate statistics data was accomplished. Attachment 35 lists the minimum, maximum, and range for all pressure, temperature, dewpoint, wind and precipitation for the entire domain from 1973-1982. The initial analysis showed that most of the questionable extreme values occur in the four grid point "sponge layer" of outermost grid points. These extreme values are the result of the model adjusting to the larger domain along the lateral

boundaries. The bulk of the questionable extreme values were removed by ignoring the outer four points when analyzing the data. However, there were spurious extremes at the 10 km grid spacing that seem to be associated with too much convective activity over central Korea. The most noted example of this was a mean monthly precipitation of 36 inches in central South Korea, while the nearest stations report only 10 inches. Figures from the AFCCC extreme value analysis, conducted for temperature, dewpoint, and precipitation in July, are shown in the eight pages of Attachment 36.

For example, the analysis of the mean maximum temperatures show the highest values over continental China and southern Pacific in the upper 80s to low 90s (86 -93°F). The lowest temperatures of upper 50s to low 60s (56-62°F) were found in mountainous locations in northern Japan and northeast China. The Korean peninsula averaged highs in the 70s-80s except in the mountains with highs only in the 60s. The observed values agreed reasonably well with the modeled values. The 40-km nest had the hottest temperatures across continental China, in the 90s to over 100°F. This modeled result is about 10 degrees too hot. Northern islands of Japan appear nearly 20 degrees too warm. Japan and Korea in general appear 5-10 degrees too warm in the model. Observed mean daily highs are in the 80s (80-86°F) while modeled are 86-93°F. The 10 km nest showed temperatures generally ~6 degrees (one category) cooler than shown in 40 km. Daily highs were much closer to observed than in the 40 km simulations. The most dramatic difference between the 40 and 10 km simulation is over the oceans which are as much as 12 degrees (two categories) cooler than in the 40 km domain.

The extreme maximums were found over continental China with extremes of 100-110°F. A large portion of the rest of the area sees maximums of 90-100°F. The northern islands of Japan were the coolest with extremes only in of 70-80°F. Extremes on the Korean peninsula ranged from 90-100°F. All were in reasonable agreement with the model values.

3.11 Baseline Simulation Summary

Ten years of simulation data for both the 40 and 10 km nest were produced and evaluated for the Korean and Middle East theaters. A complete set of climatological statistics was created for each theater and nest. The climate products and databases were delivered to AFCCC who are now using them for customer support.

4. Data Denial Experiments

4.1 Description of Experiments

Five years of simulation experiments were performed (1973, 74, 75, 77 and 79) for January, April, August, and October over the region of the Korean Peninsula. It became evident after evaluating the results of the initial data denial experiments that the quality of the high-resolution climatologies for a given month was impacted by both the availability of observed data and whether the simulation was started without a spin-up time (cold start) or was a continuation of a longer simulation (warm start). Therefore, a series of cold and warm start experiments were performed, during which data was systematically withheld for both cold and warm starts. The complete list of the specific experiments performed is given in Table 11.

Table 11. List of Data-Denial Experiments.

Experiment	Description
A. Control Warm	All available surface and upper observed data used with warm start
B. Total Denial Warm	All surface and upper observed data withheld with a warm start
C. Control Cold	All available surface and upper observed data used with a cold start
D. Total Denial Cold	All surface and upper observed data withheld with a cold start
E. Upper Air Only Warm	All available upper observed data used with a warm start
F. Upper Air Only Cold	All available upper observed data used with a cold start
G. 50 % Denial Uniform Warm	50 % surface and upper air observed data withheld in a uniform manner
H. Sfc Only Warm Start	All available surface observed data used with a warm start
I. 50 % Denial Hole Warm	50 % surface and upper air observed data withheld non-uniform manner

The warm start runs used at least 30 days of climatological spin-up time before the output data was used to compile statistics, where as a cold start used no spin-up time. Of course even in the case of a cold start, the model would build up simulated antecedent conditions throughout the month. However, for this set of experiments, the smallest climatological unit was considered to be one month so the accumulation of antecedent conditions within the month were not explicitly evaluated. When data was assimilated, IAU was used as described in Van Knowe et al. 1999.

4.2 Results of Experiments

The results indicate that the type of start (warm or cold) and the amount of observed data did impact the model biases approximately equally. Table 12 lists the mean experimental temperature results for three representative stations, Osan AB (47122), Hoengsong AB (47118) and Taegu AB (471420) in the Republic of Korea for January and July. These results are typical

of the results for each variable studied. The results in Table 12 show that the biases usually were reduced by both the warm start and including observed data.

Table 12. List of selected experimental results for temperature.

Data Availability Experiments by Month							Data Availability Experiments by Month						
Temperature							Temperature						
Experiment Type	Avg T °F		Avg Max T °F		Avg Min T °F		Experiment Type	Avg T °F		Avg Max T °F		Avg Min T °F	
	Jan	Jul	Jan	Jul	Jan	Jul		Jan	Jul	Jan	Jul	Jan	Jul
Obs	25.6	74.2	33.1	79.2	18.9	70.1	E	20.9	78.1	26.9	85.3	15.6	72.8
A	24.9	76.3	31.1	82.3	18.8	71.8	F	20.5	79.1	26.1	87.5	14.1	73.1
B	22.8	77.0	30.1	85.9	17.2	72.5	G	20.2	78.8	25.7	86.0	14.9	72.9
C	21.8	79.8	24.9	86.2	12.4	73.4	H	23.9	76.9	30.8	82.4	17.7	72.0
D	18.2	80.3	23.7	91.2	10.0	73.9	I	22.5	77.4	25.6	84.9	13.1	72.9

The full impact of data denial on temperature, dewpoint, wind, precipitation, and snowfall is presented in Table 13.

Table 13. Osan AB Korea statistics for Jan. 1973, 74,75,77, and 79. Temperature (T) in °F.

Data Src	Tmax Avg	Tmin Avg	Tavg	Tmax	Tmin	DP avg.
OBS	35.1	16.5	26.8	53	-6	16.1
OBS 30Y	35	16	26	56	16	16
10K A	35.1	17.5	27.2	48.9	4.4	15.5
40K A	34.6	19	27.7	48.9	1.8	16.9
10K D	36.7	17.6	28	52.7	2.9	14.2
40K D	35.2	20.2	28.8	49.3	1.8	17.5
Data Src	Wind Dir	Spd	Pcp	Snow	Snow Depth	Cld Cov
OBS	60	3	9999	9999	9999	9999
OBS 30Y	60	3	1	7	999	38
10K A	333	1.6	0.89	4.9	0.1	42
40K A	321	2.4	1.6	1.3	0	44
10K D	306	1.8	1.26	4	0.1	46
40K D	279	2.9	0.94	1.1	0	47

The plots of representative results of the data denial experiments for temperature and dewpoint are presented in Attachments 37-40.

5. Methods to Compute Complex Derived Variables

AFCCC requested nontraditional, complex, derived variables, e.g., icing indices and turbulence indices, that impact aviation and military operations. MESO surveyed the algorithms available for deriving numerous complex variables from the ACMES-CLIMOD output. A significant amount of information was found about some variables such as clouds, icing indices, turbulence indices, and visibility that included some fairly comprehensive verification studies. Some variables, such as wind gusts and thunderstorm occurrence, had a small amount of information about them. Others, such as IR transmissivity, have no published information available.

The following is a summary of the algorithms jointly selected by AFCCC and MESO and implemented to diagnose these variables. A description all of algorithms considered and an explanation for why a particular algorithm was chosen for each derived variable is included in a report entitled "Research of Methods to Generate Complex Derived Variables to Support Military Operations in Support of the Advanced Climate Modeling and Environmental Simulation Project". It is available upon request from the authors of this report.

5.1 Cloud Related Variables

A simple relative humidity (RH)-cloud fraction relationship, depicted in Figure 1, was used in CLIMOD. An independent RH-cloud fraction analysis was performed, resulting in the depicted relationship: cloud fraction = $(4RH - 3)^3$. More sophisticated cloud fraction schemes have been formulated. However, the uncertainty in surface observations of cloud fraction as a standard for verification did not warrant their use in this project.

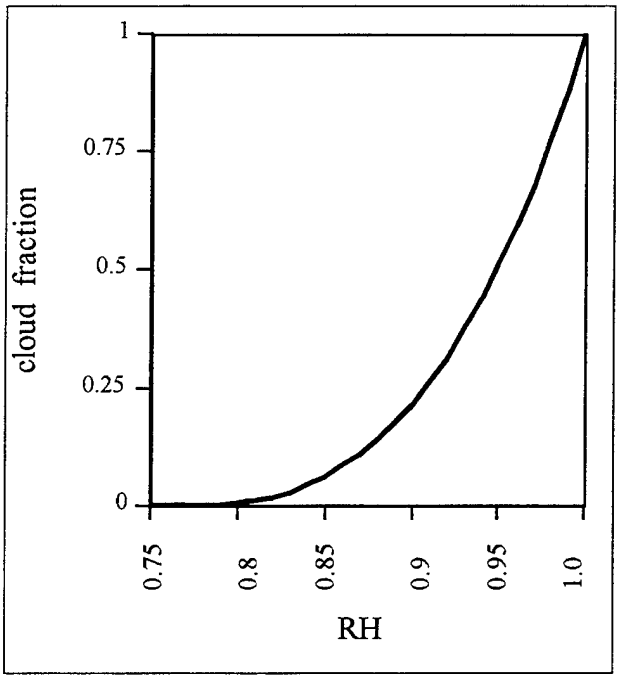

Figure 1. Cloud fraction vs. relative humidity relationship used in CLIMOD.

The 900 mb, 625 mb and 275 mb levels are approximately at the middle of the layers used to represent low, mid and high clouds. The low cloud layer is approximately 1000-800 mb, midcloud layer approximately 800-550 mb, and high cloud layer approximately 550-150 mb. A conversion from model sigma levels to pressure levels leads to a problem in mountainous areas. Pressure levels lying below (in altitude) the surface cannot have clouds diagnosed for them, and in areas of high terrain this often means a non-diagnosis of low clouds. The pressure levels can be correlated with approximate Mean Sea Level (MSL) height levels. The low clouds are approximately 0-6500 ft (with the middle of the layer being at 900 mb or 3000 ft), the mid clouds are approximately 6500 to 16,500 ft (with the middle of the layer being at 625 mb or approximately 13,000 ft) and the high clouds are approximately 16,500 to 45,000 ft (with the middle of the layer being at 275 mb or approximately 32,000 ft).

In the low, mid and high cloud estimations the cloud fractions are calculated for each sigma level (layer) that falls within the Low, Mid or High Layer described above. The cloud fraction for each sigma layer is then summed for the whole layer using a "random overlap" method (Pielke 1984). For example, if there are two cloud layers, each with 0.5 coverage, the random overlap assumes that the 0.5 in the lower layer would be half inside and half outside of the 0.5 coverage above or below it, leading to a total cloud cover of 0.75.

For an example, if a three-sigma layer low-cloud layer were used, then:

```
--------------------------------- sigma 3  (Top of Low Layer)

        Cloud Frac = .30

---------------------------------sigma 2

         Cloud Frac = .60

---------------------------------Sigma 1

        Cloud Frac=  .10

---------------------------------Sfc
```

In this case the total cloud fraction for the layer would approximately equal .15 + .60 + .05 or .80.

An alternative cloud vertical structure calculation available in the current CLIMOD post processing uses the same cloud fraction calculation, but the clouds can be calculated based on all the sigma layers of the model, and interpolated to any height Above Ground Level (AGL) versus just low, mid or high.

5.2 Visibility

5.2.1 Description of the Method

CLIMOD uses an algorithm that is used at the National Oceanic and Atmospheric Administration Forecast Systems Laboratory (NOAA/FSL). The visibility is calculated using the natural log of visibility, V', so that negative visibilities are not possible. The basic formulation of the visibility algorithm is

$$V' = a + bR^3 + d_p + d_{BS} + d_{BD} \tag{5-1}$$

where V' = natural log of visibility a= 3.831594, b = -3.288893, and R is the relative humidity as a fraction. For CLIMOD, R is calculated as the integrated relativity average between the surface and the first model sigma level.

The values of d_p, d_{BS}, and d_{BD} are incremental contributions of visibility restrictions due to precipitation, blowing snow, and blowing dust. The contributions of d_p, d_{BS}, and d_{BD} are calulated separately and are based on a precipitation type algorithm developed by Ramer (1993) and described thoroughly in Cairns et al. (1994).

The calculation of visability Restriction Due to Precipitation (d_p) is set to:

0.01 with no precipitation,
–0.26 – (Sr*I*P) where Sr = 10, I = 1 with snow, P = precipitation rate
–0.26 with all other forms of precipatation

There are limitations to this algorithm, for example, the lowest visibility that can be obtained with fog (and no precipiation) is 1.7 miles. The problem lies in the heavy reliance of RH fraction. Also, fog, snow or rain can realistically develop with a T-Td spread of greater than zero that will decrease the RH to less than 100%. Since the visibilty calculation uses the natural log (ln) of visibility, this has a significant effect of unrealitically increasing the visibility for certain meterological situations.

The visibility restrictions due to snow involve the calculation of the ice or snow fraction I. This technique calculates I by following an idealized precipitation parcel down to the ground. The parcel is followed to the ground beginning at the precipitation generation level, which is calculated using relative humidity criteria. The ice fraction of the parcel, from the precipitation generation level, is modeled according to the environmental wet-bulb temperature at each level. The ice fraction of the precipitation parcel as it reaches the surface and the surface wet-bulb temperature determine the precipitation type, with thresholds for entirely liquid, entirely solid, mixed, and freezing. The actual algorithms for the contributions to visibility from precipitation and blowing snow depend on I and the precipitation rate P (obtained directly from the MASS model as mm/hr).

5.2.2 Assessment of the Method

The visibility was evaluated in two ways. One was evaluation of real-time plots of the visibility grids and comparison with the visibility analysis based upon observations. The other was to compare point visibility observations with the modeled point visibility values. In general the modeled visibility values tended to be lower than observed in the early morning hours and also frequently too low over water surfaces. The reason for this was the high dependence of the visibility algorithm on the relative humidity. Table 14 gives a summary of an observation-model visibility comparison study performed by MESO for a random selection of stations in the U. S.

Table 14. Summary observation-model visibility comparisons

Weather Condition	Number of Cases	Mean Observed Visibility	Mean Model Visibility
No weather reported	43	12.9	10.6
Rain without fog	27	5.3	5.4
Rain with fog	38	1.6	1.3
Drizzle with Fog	19	0.7	1.3
Wet Snow (RH > 98%)	15	2.1	1.5
Snow (RH = 90-98%)	19	2.3	3.2
Dry Snow (RH < 90%)	12	2.7	5.6
Fog but no precip	12	3.2	2.8
Haze only	17	6.2	16.3

Table 15 gives the calculated values for various weather scenarios based upon the visibility algorithm used in CLIMOD.

Table 15. Visibility values produced by visibility algorithm for various weather scenarios

RH Fraction	Weather	Visibility (mi)
0.00	None	46.6 (Max model visibility)
0.50	None	31.0
.75	None	11.6
1.00	None	1.7 (Lowest Fog or haze vis)
.95	Rain	2.1
1.00	Rain	1.3
.95	Lgt Snow	2.0
1.00	Lgt Snow	1.2
.95	Mdt Snow	.4
1.00	Heavy Snow	.1

5.3 Visibility Restriction due to Precipitation

The value of d_p is set to 0.01 with no precipitation, and to –0.26 for all values other than snow. For snow $d_p = -0.26 - (S_r * I * P)$, where

S_r is the "snow reduction factor" which is now set = 10,

I is the ice fraction equal to 1 for all snow, set equal to .8 for if sleet is falling, to .5 if a mixture of rain and snow is falling, and set to 0 for all rain, and

P is the rate of fall of precipitable water in mm/hr.

5.4 Fog Calculation

Fog is assumed to exist when:
(1) the visibility is less than 3.4 miles,
(2) the relative humidity is greater than 90%,
(3) the wind speed is less than 7 ms^{-1}.

5.5 Haze Calculation

Haze is assumed to exist when:
(1) there are no other obstructions to visibility,
(2) the visibility is less than 3.6 miles,
(3) the wind speed is less than 4 ms^{-1}.

5.6 Visibility Restriction due to Blowing Snow and Blowing Dust

NOAA/FSL developed algorithms for contributions to visibility from blowing snow and dust (d_{BS} and d_{BD}) Cairns et al. (1994a). The criteria for blowing snow are:

$$T \le -2,\ P \ge 0,\ I = 1, \text{ and } U*(40-T) > 450. \qquad (5\text{-}2)$$

where T is the surface temperature (°C) and U is the surface wind speed in ms^{-1}. I is assumed to be equal to 1 if snow is falling. If blowing snow exists then $d_{BS} = -0.5$, and otherwise $d_{BS} = 0$.

The criteria for blowing dust are:

$$U*(40+T)/R > 4000. \qquad (5\text{-}3)$$

If blowing dust exists, then $d_{BD} = -2.$, and otherwise $d_{BD} = 0$.

5.7 IR Transmissivity

5.7.1 Description of the Method

The following method is used for calculating the surface transmissivity (transmittance) 8-12 micrometer band. The path is assumed to be horizontal and 4 km in length. The values of the various variables/factors (e.g. B1, B2, etc.) may be modified if additional information dictates. The algorithms are designed so they will work for both the A (40 km) and B (10 km) grid output.

Calculation of IR transmittance for 8-12 Micrometer band:

Exponential Relationship:

$$T = [B1^{Ah}] + [(Rh - R1) \times (R2)] + [P \times P1] \qquad (5\text{-}4)$$

Basic Factor Rh Factor Precip Factor

T= IR Transmittance in 8-12 micrometer band

Basic Factor = Value with rural aerosol and no precipitation or fog

B1 = 0.906252249 (best fit exponential slope of rural aerosol T vs. Absolute Humidity curve)

Ah = Absolute Humidity in grams/meter^3

Rh Factor = Does not turn on until Rh > 80%. Rough approximation of impact of maritime and hygroscopic aerosols as well as fogs.

Rh = Relative Humidity as a decimal fraction

R1 = .80 (threshold to turn on influence of Rh)

R2 = -0.3 (rate of change in impact T vs. RH. = -0.06/0.2)

Precipitation Factor = Accounts for impact of precip based upon rate of liquid equivalent precipitation during past hour.

P = Liquid equivalent precipitation rate in mm/hr (use accumulation during previous hour)

P1 = -0.1 (rate of change of impact of precip T versus Precip rate -1.0/10)

Note: Can't allow values of T less than zero. All T values less than zero need to be set to zero.

5.7.2 Assessment of the Method

AFCCC performed an assessment of the algorithm for the 8-12 micrometer band. The algorithm for the near surface IR transmissivity was compared with LOWTRAN 7 (Kneizys et al. 1988) transmissivity for the same waveband. Overall, the algorithm performed quite well with an "R squared" value of .87". Attachment 41 gives a plot of the LOWTRAN 7 transmissivity values versus the algorithm transmissivity values. The comparison was performed by calculation of the 8-12 micrometer transmissivity using both LOWTRAN 7 transmissivity values (x axis) and CLIMOD algorithm transmissivity values (y axis) for various meteorological conditions. Most of the difference between the two calculations occurs for conditions which result in transmissivity values of less than 0.4. The primary reason for the difference is that the CLIMOD algorithm tends to give somewhat lower values than the LOWTRAN model when precipitation is occurring. Details of the comparison can be obtained from AFCCC/DOC.

5.8 Precipitation Types

Four categories of precipitation are distinguished in CLIMOD postprocessing: Rain (R), Snow (S); Sleet (IP) and Freezing Rain (ZR).

5.8.1 Snow

The occurrence of snow reaching the ground will be determined directly from the current MASS algorithm.

5.8.2 Rain, Sleet, and Freezing Rain

If MASS indicates rain at the surface, there will be a further determination between rain, freezing rain and sleet based upon the following relationships. Thermal profile categories are:

(1) If model indicated rain, freezing level is above 2000 feet = rain.
(2) If there are two freezing levels and the surface is below freezing the following are possible:

(a) If model has rain and upper freezing layer is greater than 500 feet thick and the lower freezing level is greater than 1000 feet = Ice Pellets (Sleet).
(b) If model indicates rain and upper freezing layer is greater than 500 feet thick and the lower freezing level is equal to or less than 1000 feet = Freezing Rain.

(3) If there are three freezing layers and the surface is above freezing the following are possible:

(a) If model indicates rain and if the lowest freezing level is less than 1000 feet, the lowest below freezing layer is greater than 500 feet thick, and the upper freezing layer aloft is greater than 1000 feet = Ice Pellets (Sleet).
(b) If the model indicates rain and the lowest freezing level is more than 1200 feet, and the upper freezing layer aloft is greater than 500 feet = All Rain.
(c) If the lowest freezing level is greater than 500 feet but less that 1000 feet, the lowest below freezing layer is less than 500 feet thick, and the upper freezing layer aloft is greater than 500 feet and less than 1000 feet thick = Whatever the model indicates.

5.9 Precipitation Intensity

Estimates of intensity are possible by using the precipitation that the model generated over the past hour; however, currently no instantaneous model intensities are directly produced by the model.

5.10 Precipitation Amounts

Precipitation accumulation is a product directly obtained from the current CLIMOD output for rainfall, water equivalent, and snowfall. Anything that improves the overall quality of the model, e.g. improvements in grid spacing, cumulus parameterization schemes, moisture physics and data assimilation will tend to improve precipitation results. The current recommendation is to use the model output as it is now available.

5.11 Probability of Thunderstorm Occurrence

The criteria to be used for the occurrence (yes) of a thunderstorm will be the triggering of the convective precipitation scheme at any level, stability, and a minimum cloud thickness and cloud temperature. The method selected allows for thunderstorms to occur without precipitation reaching the ground. Such thunderstorms can occur in the desert locations such as the Southwest U.S. region.

T = yes if convective precipitation is triggered and cloud thickness reaches a specified threshold. The occurrence of thunderstorm criterion currently being used is:

(1) Convective scheme turned on?

(2) Cloud depth 10 k feet thick

(3) Top of cloud reaches -4 deg C

(4) Stability index criterion e.g. Lifted Index (LI), Showalter Stability Index (SSI), Total Totals (TT) can be computed if determined it is needed.

5.12 Wind Gusts

5.12.1 Description of the Method

The wind gust method used is based on the work of Lee and Girodo (1998). The method uses static stability as the basis to predict the maximum surface wind gust. In this method:

Surface Gusts in knots (G) = % of model (b) wind at the top of the unstable layer (Vt).

$$G = bVt \tag{5.5}$$

Currently over land b= 65%; over water b = 75%

The depth of the unstable (mixed) layer is defined simply as the highest level at which the lapse rate (defined as the temperature difference between that level and the 2 m temperature) is at least dry adiabatic.

It was determined that it made a more usable product to have no lower limit to the gust criterion (presence of an unstable layer) to avoid creating 2-D fields with large areas of missing values. So, if the unstable gust criterion is not met, *G* is set to equal the surface wind.

However, it was found necessary to set an upper limit to the wind gust to avoid incompatibility with the surface wind such as winds "2 G 30". So an upper limit was placed on the gusts in knots (Gul) of:

$$Gul = A + Vm + [A\,(Vm/B)] \qquad (5\text{-}6)$$

Where A= 5
Vm = mean model surface wind
B = 0.1

Examples: if mean wind is 5 knots the upper limit is

Gul = 5 + 5 + [5 (5/10)]
= 10 + [5 (.5)]
= 10 + [2.5]
= 12.5 knots

if mean wind is 25 knots then the upper limit of the gusts would be

Gul = 5 + 25 + [5 (25/10)]
= 30 + [5 (2.5]
= 30 + [12.5]
= 42.5 knots.

5.12.2 Assessment of the Method

The maximum wind algorithm has been qualitatively analyzed using results from the MESO MASS daily real-time runs and the results seem reasonable. However, an objective analysis is still needed.

5.13 Icing

5.13.1 Description of the Method

The icing algorithm used is a NCAR/RAP algorithm which is a modification of the Schultz-Politovich and Forbes algorithm. The basic algorithm and code information were obtained from the Air Force Weather Agency (AFWA). It is described in Thompson et al. (1997) and Brown et al. (1997). The AFWA criteria of the algorithm (Table 16) is calibrated for the MM5 model output and is used as the first approximation for the CLIMOD output.

Table 16. AFWA icing algorithm, from Thompson et al. (1997).

Icing category	Temperature Range (C)	Relative humidity threshold
Freezing Rain	$T \leq 0$	RH ≥ 80% (with RH ≥ 80% above T > 0 C)
Stratiform	$-12 \leq T \leq 0$	RH ≥ 85% (with RH ≥ 85% above T < -12 C)
Unstable	$-20 \leq T \leq 0$	RH ≥ 56% (with max RH ≥ 65% within unstable layer)
General	$-16 \leq T \leq 0$	RH ≥ 63%

The severity of icing is based upon the supercooled liquid water content available in the model. The value needed from the model is QCONDSIG, which is defined as the mixing ratio of the condensed water vapor. The documentation does not make it clear exactly what is to be included in QCONSIG, but by direct contact, AFWA indicated that all forms of the liquid equivalent of the water content should be used. This was consistent with MESO's test results, which had the best results when both cloud and liquid precipitation mixing ratios are used in calculating QCONDSIG. So if the prognostic microphysics are used, use (QCONDSIG = QR + QC) where

QR - Precipitation mixing ratio (kg/kg);
QC - Cloud water mixing ratio (kg/kg)

In the case of the diagnostic routine Q (Mixing Ratio) - QS (Saturation Mixing Ratio) must be used which only approximates QC. QR is not directly available in the diagnostic routine. The first step in the severity calculation is to convert the liquid water content to g/m^3 from kg/kg using the code:

```
QCONVERT = (PSIG(K)*QCONDSIG(K))/(0.287*TSIG(K))
```

then to

```
ADD ADJUSTMENT FACTOR TO LIQUID WATER IF T(K) ABOVE TZLLIM
where TZLLIM = -261.16
      IF (TSIG(K) .GE. TZLLIM) THEN
        ADJ = 0.1
      ELSE
        ADJ = 0.0
```

The severity levels are then calculated from:

```
IF ((QCONVERT + ADJ) .LE. 0.1)
        ICINGSIG(I,J,K) = 0 (NONE)
    IF ((QCONVERT + ADJ) .GT. 0.1)
        ICINGSIG(I,J,K) = 1 (LIGHT)
    IF ((QCONVERT + ADJ) .GT. 0.6)
        ICINGSIG(I,J,K) = 2 (MODERATE)
    IF ((QCONVERT + ADJ) .GT. 1.2)
        ICINGSIG(I,J,K) = 3 (SEVERE)
```

5.13.2 Assessment of the Method

A qualitative assessment of the real-time results of the icing algorithm seemed to produce reasonable frequency of occurrence of any icing (either yes or no) using either the diagnostic or prognostic microphysics. However, reasonable severity values were only obtained when the prognostic microphysics scheme was used with only light icing being produced for the diagnostic scheme.

5.14 Turbulence

5.14.1 Description of the Method

The selected turbulence algorithm, the Knapp-Ellrod turbulence index, is based upon the work from the Army Research Lab and is defined by the relationship of deformation times the vertical wind shear. This index is described in Ellrod and Knapp (1992). The basic algorithm and code information was provided by AFWA. Equation TI2 in the Ellrod and Knapp paper is the equation used in the selected algorithm. The turbulence index (TI) uses the deformation and convergence of the wind field at each sigma level, and the vertical wind shear calculated in the layer +/- one sigma level from the original sigma level.

The equation used for calculating the TI is:

$$TI = VWS * (DEF + CVG), \tag{5-7}$$

where $DEF = SQRT [(du/dx - dv/dy)^2 + (dv/dx + du/dy)^2]$,
VWS is the vertical wind shear and CVG the convergence.

Converting the TI output to turbulence severity is done according to the following categories:

0 - SMOOTH/NONE	(0.0 - 3.0)
1 - LIGHT	(3.0 - 9.0)
2 - MODERATE	(9.0 - 14.0)
3 - SEVERE	(14.0 +)

5.14.2 Assessment of the Method

A qualitative assessment of the real-time results of the turbulence algorithm seemed to produce reasonable frequency of occurrence of all turbulence categories using either the diagnostic or prognostic microphysics.

5.15 Atmospheric Stability

Any of the standard stability indices SSI, LI, etc. can be easily calculated from the model output. Currently only the surface LI is calculated.

5.16 Soil Temperature/Frozen Ground

The soil temperature is currently a value available as part of basic model output. Thirty degrees Fahrenheit is used as the threshold for frozen ground.

5.17 Soil Moisture/Percent Saturation

The soil moisture is currently a value available from the model. The form of the soil moisture is provided as both the absolute value and the percentage of saturation. The fractional saturation value for typical soils ranges from about 0.39 to 0.48 with an average of about 0.43.

5.18 Snowfall Accumulation

Snowfall and accumulated snowfall is a value available from the basic model output.

5.19 Snow Depth

Snow depth is a value available from the basic model output. There has been a noticeable bias for low snow depth totals which is currently being evaluated. AFCCC did an extensive snow evaluation for the Balkan region that illustrates the low snow bias (Doggett 2000)

6. Y2K Compliance

6.1 Y2K Compliance Overview

CLIMOD was ensured for Y2K compliance under a contract modification to the project "Development of Methods to Generate High Resolution Climatological Databases to Support DOD Modeling and Simulation Programs", under contract AFRL Contract No. F19628-97-C-0025.

Meeting the Y2K compliance requirements was addressed through the expansion of the effort under the contract's Task 10 "Construction of the Production Version of CLIMOD". The objective of Task 10 is to construct the final version of the CLIMOD system, which was delivered to AFCCC under the contract's Task 11. The objective of the Y2K compliance tasks ensured all software delivered under the contract satisfied the requirements listed in the "AF Year 2000 Compliance Checklist" (HRS Form 21, March 1998). The Y2K compliance requirements were met through a three-step process. The first step was a review of all components of the CLIMOD software to identify all occurrences of dates or date operations. The second step was the analysis of each occurrence to determine if it satisfies the Y2K criteria contained in the "AF Year 2000 Compliance Checklist". Any deficiencies that were identified were corrected in this step. The third step was the testing of the full CLIMOD to verify that CLIMOD satisfies all of the Y2K checklist items.

The three major components of the CLIMOD software that MESO modified for Y2K compliance are: (1) a data preprocessing system that transforms raw atmospheric observational data into a dataset suitable for the initialization of the CLIMOD atmospheric simulation model; (2) the CLIMOD numerical-dynamical simulation model; and (3) the post-processing package which consists of several program modules that ingest output from the simulation model and generate a variety of statistical quantities that describe the atmospheric climatology for a particular point or region. Any dates referenced and operations that were not Y2K compliant were modified to be Y2K compliant. One component of the modeling system outside the control of MESO was the date handling of nationally archived external databases needed for the model. The only data of this type which uses two digits to store the year information is the upper air rawinsonde data archive. Logic has been built into the CLIMOD system to handle the two digit dates, which will work until approximately the year 2050 when 100 years of this data are archived. It is anticipated that since this database is maintained by national meteorological centers, and used by the entire international meteorological community, a solution will be forthcoming long before this becomes a real issue in 2050. However, the modeling system has been constructed to include the logic to NEVER fail even if date confusion arises because of two digit dates in the rawinsonde data field. In this case the data would be skipped, and the user would be notified of the problem. The rawinsonde data are not required to run the model.

6.1 Y2K Compliance Details

Three simulation sequences were successfully executed for the CLIMOD system: (1) a sequence which crosses the 1999 to 2000 boundary; (2) a sequence which begins before midnight of February 29, 2000 and ends after midnight March 1, 2000; and (3) a sequence which begins at an arbitrary date after March 1, 2000 (March 2, 2000 and July 1, 2000).

Each part of the CLIMOD processes was examined for Y2K compliance with all date-dependent operations in the CLIMOD software system identified. Seven distinct areas were identified and addressed. They were:

1. Input date formats

2. Model preprocessor

3. Mesoscale atmospheric simulation model (MASS)

4. Output date formats

5. CLIMOD postprocessor

6. CLIMOD scripts

7. Create ability to be "backward" compatible to handle old date (i.e., 2 digit) formats (both input and output).

There were external (e.g. file names) and internal (e.g. operations involving dates) issues that needed to be considered in each area.

There were three input data types that were found to be date sensitive. All were atmospheric data. They are: (1) reanalysis gridded data; (2) rawinsonde upper air data; and (3) surface data. The surface data format was within MESO control. In conjunction with AFCCC, an internal and external Y2K compliant four-digit year format was created. The reanalysis data use four-digit years (century plus year) so MESO-developed code made all the necessary changes that allows the use of this data for all dates. However, the rawinsonde data, which is from databases from U.S. government archived sources, use two-digit years internally and externally. It must be emphasized that even with the two-digit years the system will not have a problem until 100 years of rawinsonde data have been produced. This will occur approximately in the year 2050. Since this is a U.S. government maintained data archive issue for these two types of data, the plan is to ensure CLIMOD is compatible to whatever changes take place in the nationally archived databases.

The reanalysis data are in GRIB format. GRIB is a standard data format used by many organizations including AFCCC and the DOD's Master Environmental Library. In the gribbed

format, each variable is assigned a number or position within the database. Some variables have mandatory position numbers within a gribbed database, and others have a user-defined position. For example, standard meteorological variables such as surface temperature and dewpoint would have mandatory positions within the database, but variables such as snow depth are defined by the user. The GRIB data that were obtained from NCAR have a two-digit year, and a century indicator. MESO created a "degribbing" code that extracts the reanalysis data in the gribbed format and converts it to a model readable format. The degribbing code also converts the NCAR data to a four-digit year. The degribbing code provided to AFCCC, called readgrib, has been modified so it can now write the files with four-digit years, e.g., 1995030100H.mrfY.Z and 2000030100H.mrfY.Z.

The rawinsonde data is obtained from NCAR, which uses the ON29 raob data format that only has a two-digit year. The assumption has to be made that the 00 indicates 2000, not 1900. The preprocessing code makes this assumption so there is no failure during or after year 2000. So it is Y2K compliant. The problem will come about when 100 years of rawinsonde data is reached around the year 2050. Since this is an international standard database maintained at national meteorological centers and NOAA it is assumed that modifications or replacement to the database will be made long before there is a problem. Currently, the rawinsonde files have names such as Rnmc74070900.Z. The rawinsonde files could be renamed with four-digit year file names by making the assumption that years 00-50 are 2000-2050 and years 51-99 are 1951-1999. But that really doesn't improve the fundamental Y2K compliance issue. The same would be true of the first line in the rawinsonde data using the following example:

"0000740701ADPUPA WASHINGTON"

where the "74" could be changed to "1974" making the previously mentioned assumptions.

7. Summary

All indications are that the CLIMOD method will provide high quality climate statistics for most regions of the world. The remaining tasks in this project, to be undertaken during FY2000, are: (Task 12) complete the execution and evaluation of CLIMOD in a tropical region, (TASK 13) add and test an option for using a nonhydrostatic formulation of the MASS model within CLIMOD, and (TASK 6a) develop and test a wind gust derived-variable algorithm based on a turbulent kinetic energy formulation.

ATTACHMENTS

Attachment 1

Comparison Stations in Blue

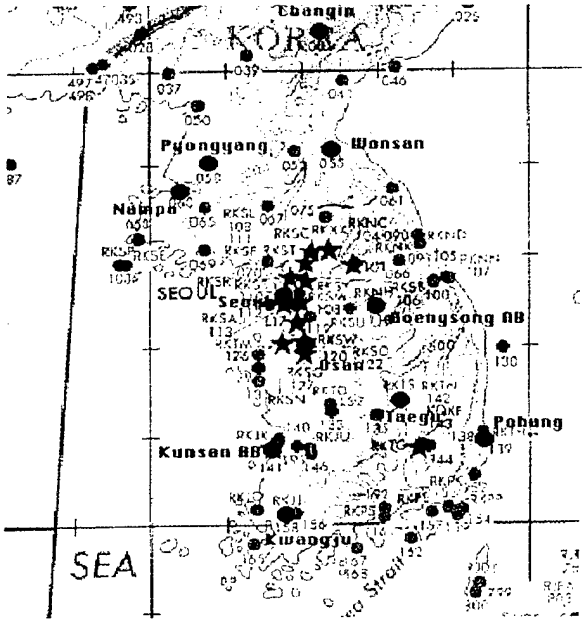

Attachment 1A Korean comparison stations used for evaluation.

Comparison Stations in Blue

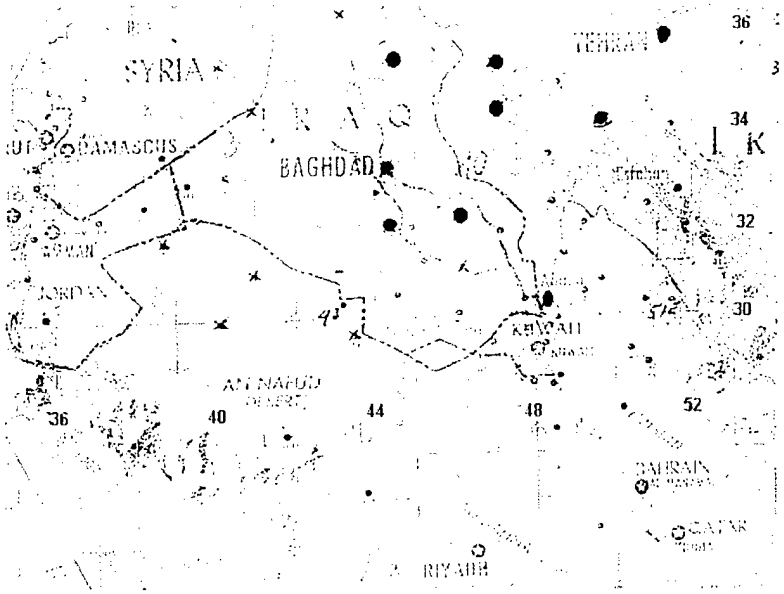

Attachment 1B Mideast comparison stations used for evaluation.

Attachment 2

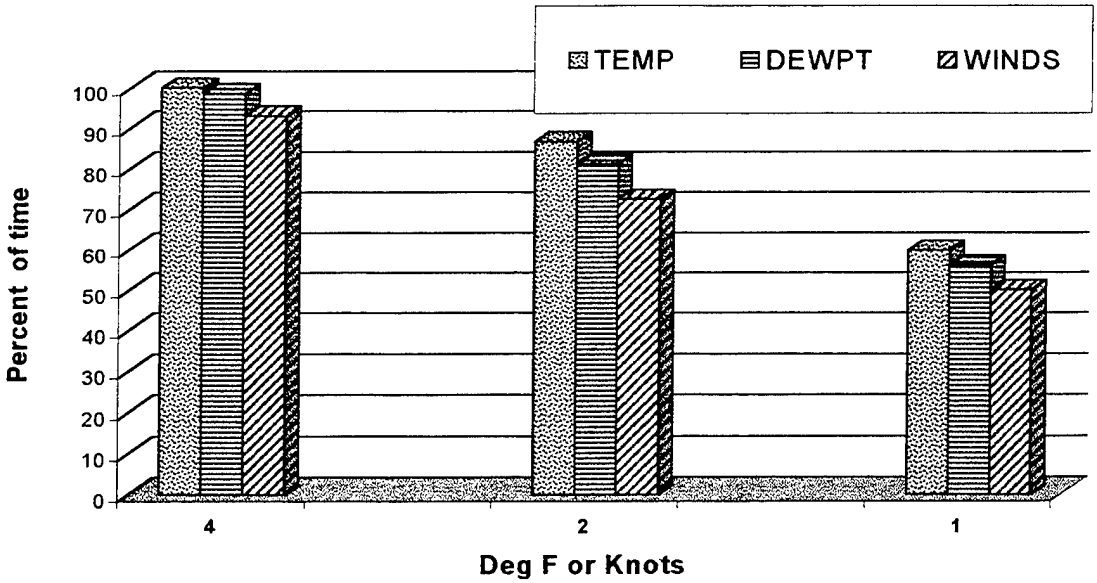

Attachment 2A. Percentage of time the observations for 6 sites fell within a threshold of 4, 2 or 1 F deg or knots from analysis of data from 300 randomly chosen days from 10-year(1973-82) period.

Attachment 2B. Details of the six representative sites used in Attachments 2A, and 3A-3D. Sites chosen because they are representative of various types of locations (coastal, inland, low elevation, high elevation, small and large actual-model elevation differences) and have a reasonable observation count.

Sta Num	ICAO	Station Name	Lat	Lon	Elev m	40 Elev	10 Elev
470080	CHO	Chongjin, N. KO	41.47	129.49	43.0	283.8	35.6
471180	KNH	Hoengsong, S. KO	37.26	127.57	100.9	396.7	373.8
471220	KSO	Osan, S. KO	37.05	127.02	11.9	102.2	42.0
471390	KTH	Pohang, S. KO	35.59	129.25	20.1	121.0	122.3
406500	RBB	Baghdad, IQ	33.14	044.14	34.0	39.8	35.6
407540	III	Tehran, IR	35.41	051.21	1191.0	1710.7	1184.4

Attachment 3A and 3B

3A. Annual Mean Sea Level Pressure Comparisons

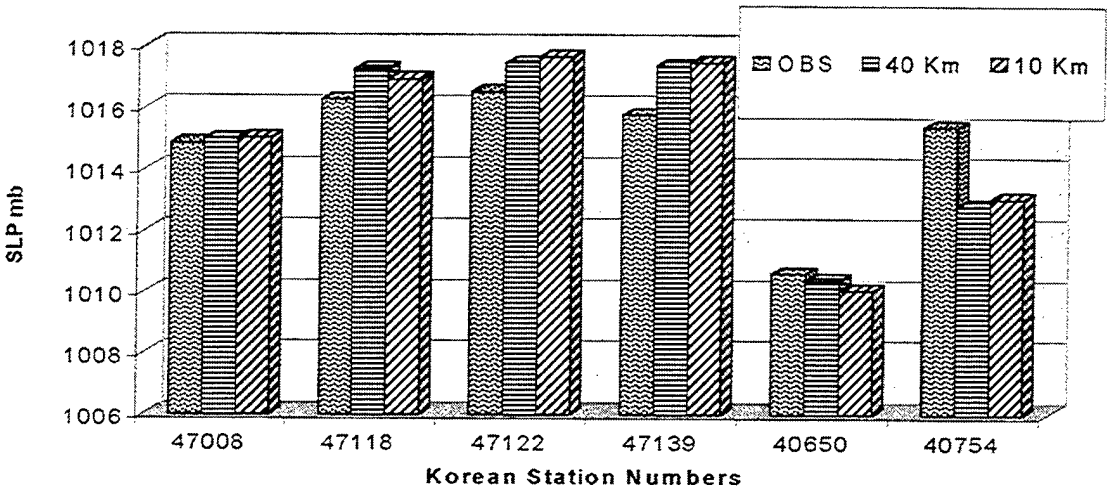

3B. Annual Mean Temperature Comparisons

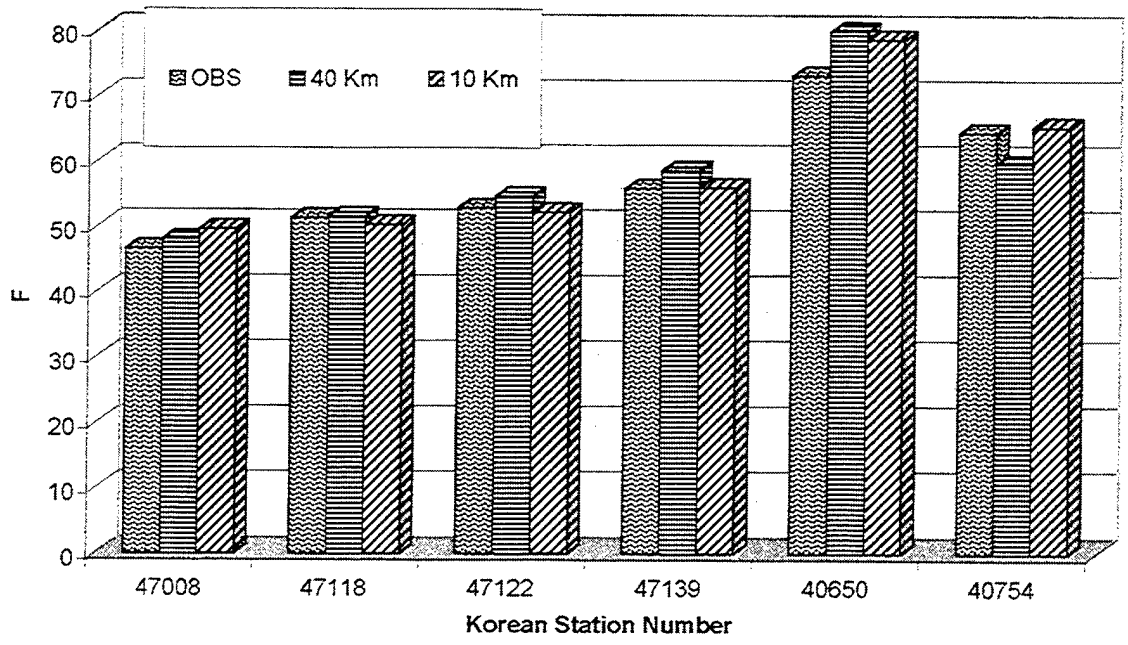

Attachment 3C and 3D

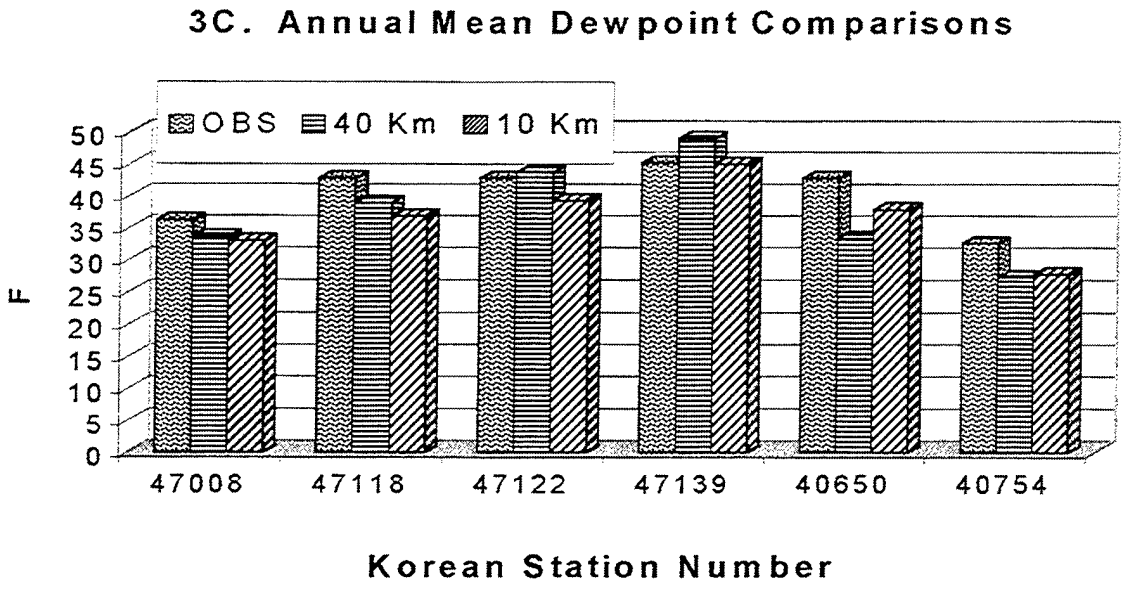

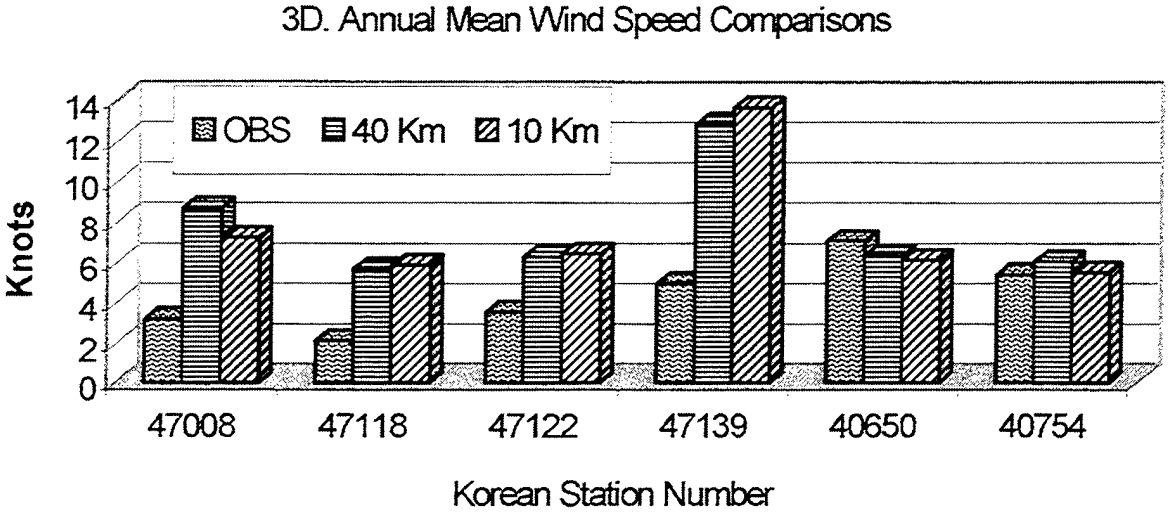

Attachment 4

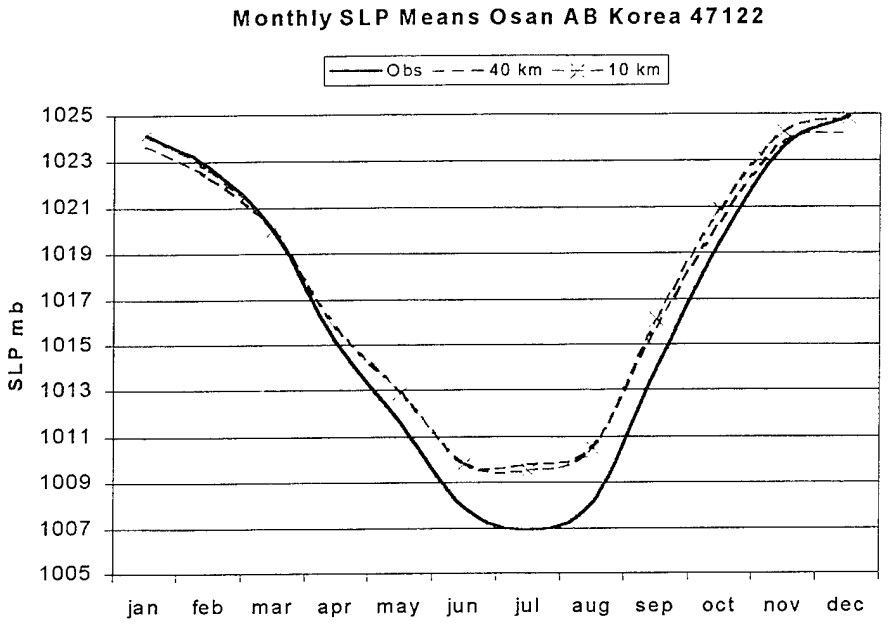

Attachment 4A

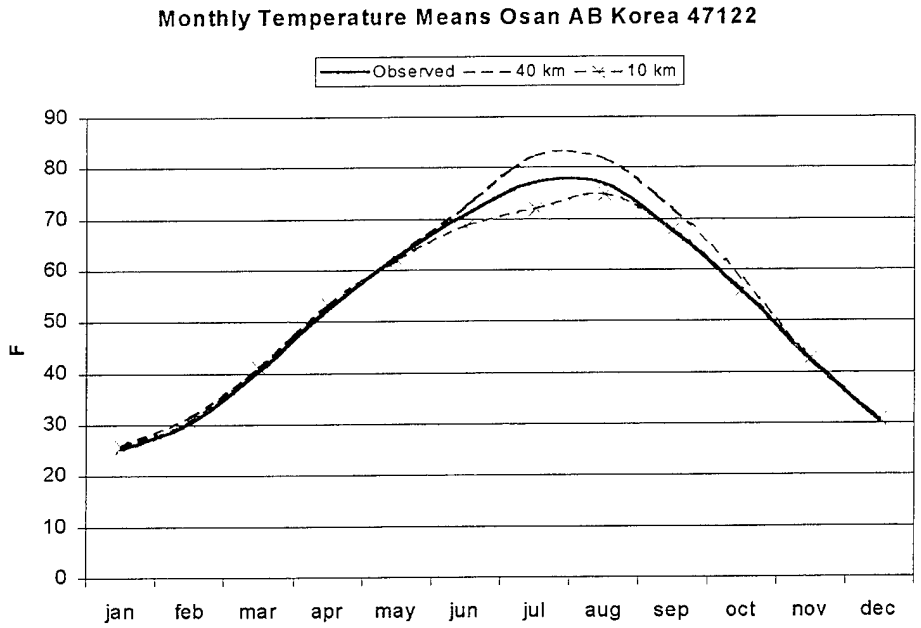

Attachment 4B

Attachment 4

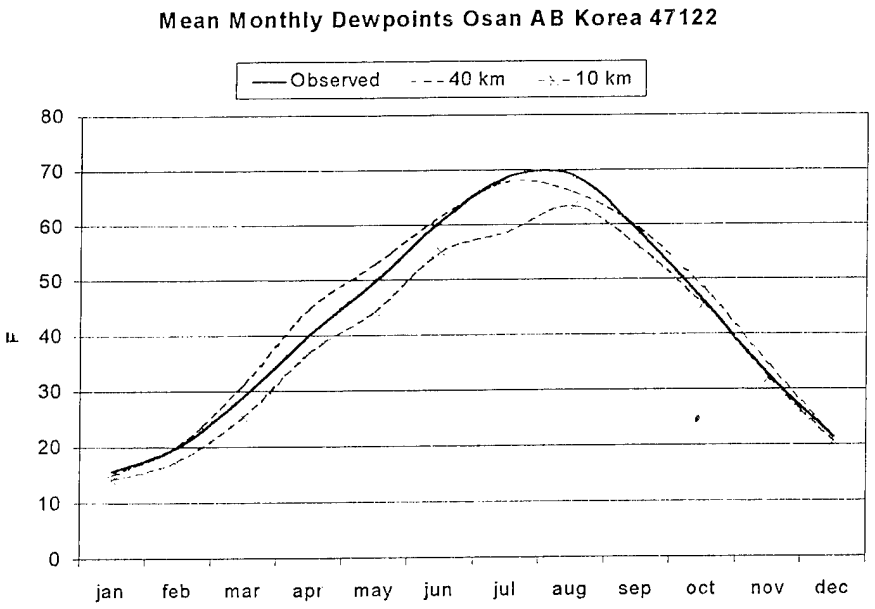

Attachment 4C

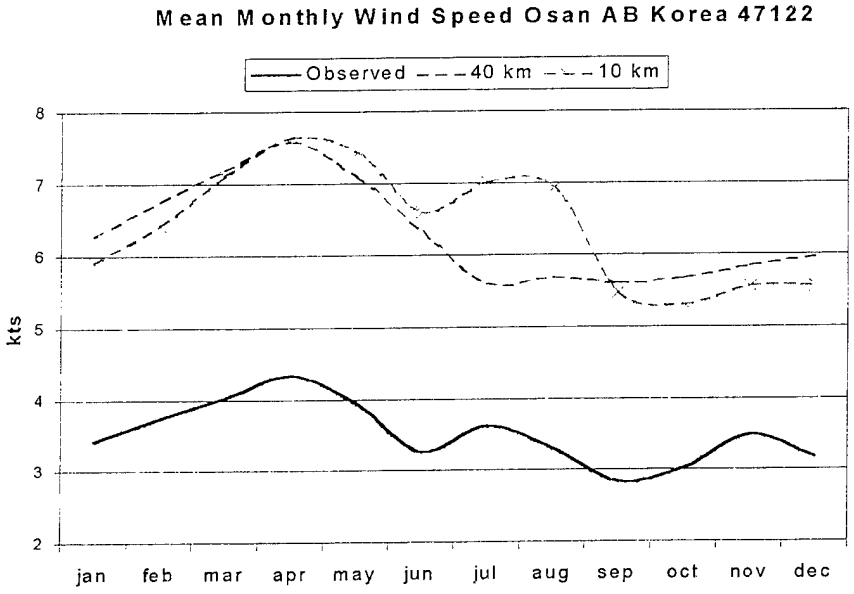

Attachment 4D

Attachment 5

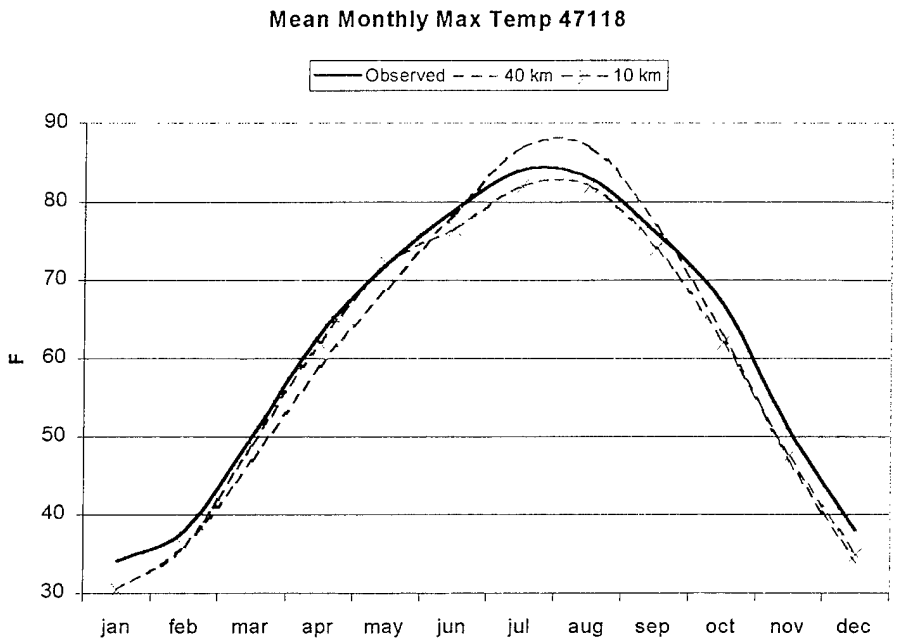

Attachment 5A. Station 47118 is Hoengsong, South Korea.

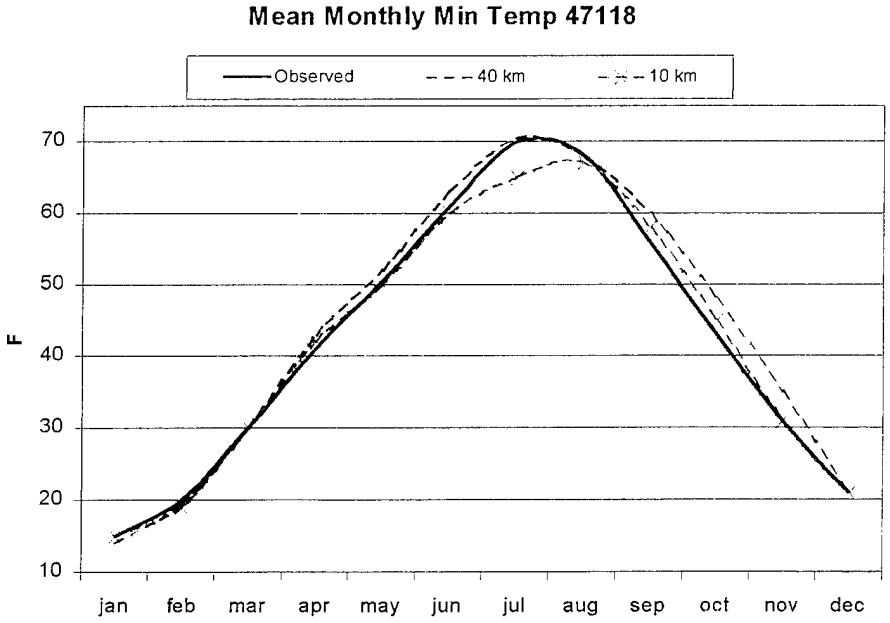

Attachment 5B. Station 47118 is Hoengsong, South Korea

Attachment 6 A and 6B

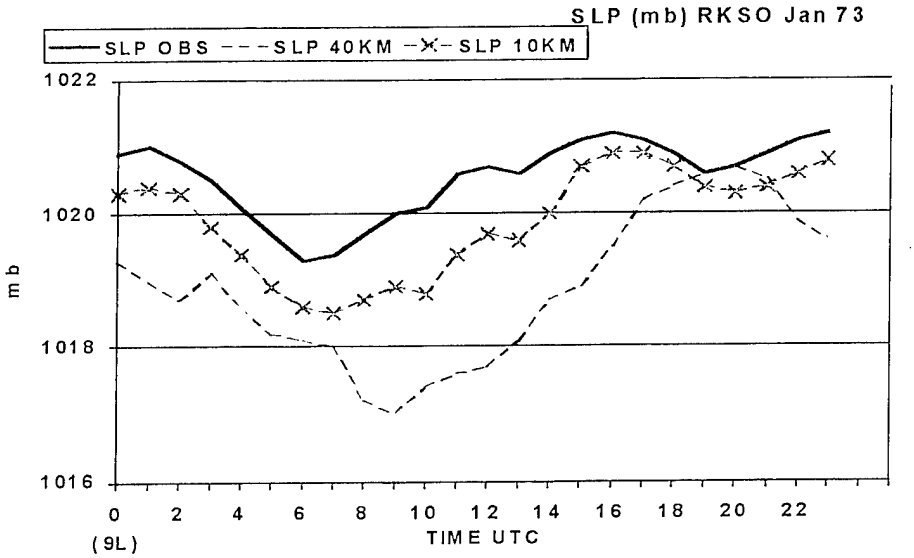

Attachment 6A. Hourly mean sea level pressure (SLP) comparison for the observed (OBS), 10-km and 40-km diurnal pressure curve for the month of January 1973 at Osan Air Base (RKSO).

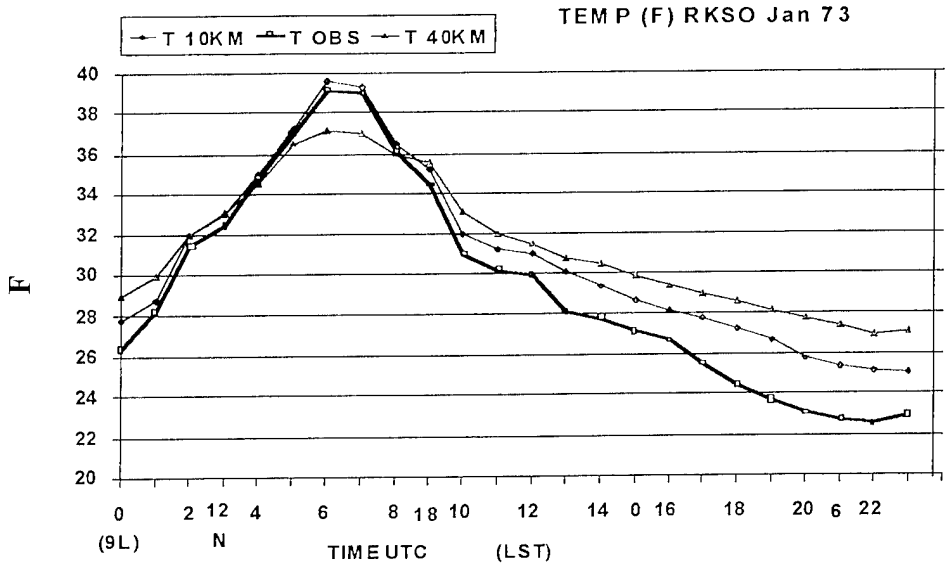

Attachment 6B. Hourly mean surface temperature (T) comparison for the observed (OBS), 10-km and 40-km diurnal curves for the month of January 1973 at Osan Air Base.

Attachment 6C and 6D

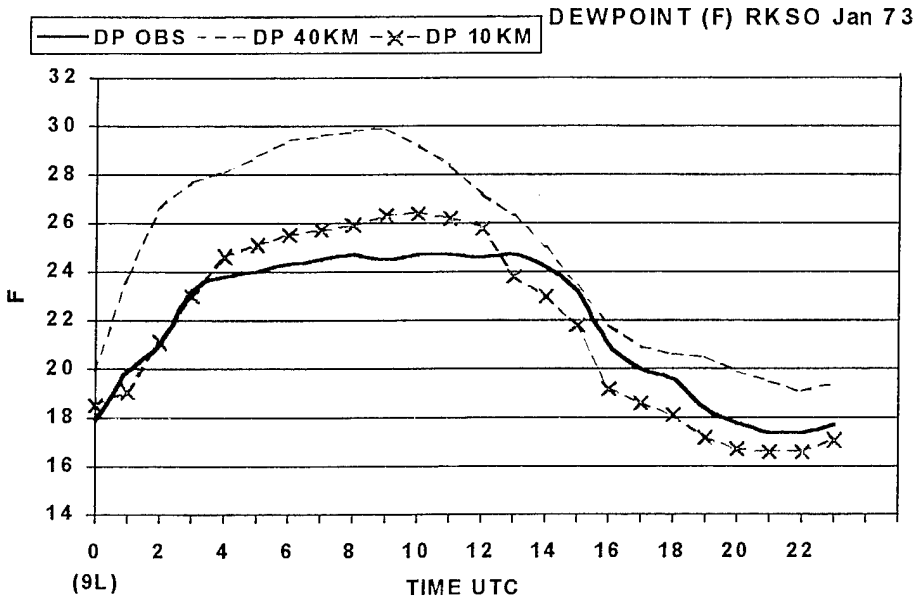

Attachment 6C. Hourly surface dewpoint (DP) temperature comparison for the observed (OBS), 10 km and 40 km diurnal pressure curve for the month of January 1973.

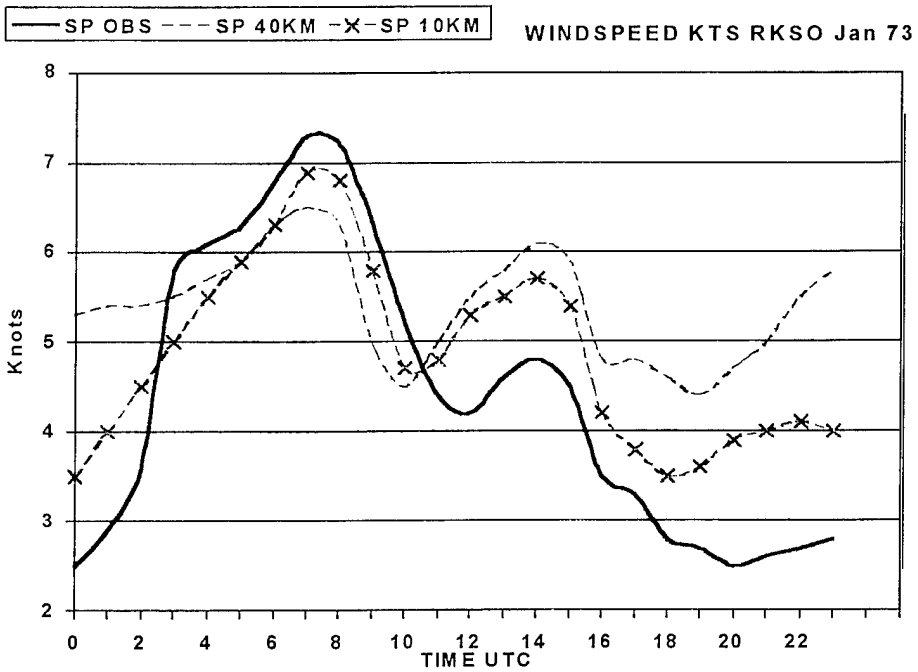

Attachment 6D. Hourly mean surface wind speed (SP in knots) comparison for the observed (OBS), 10 km and 40 km climate statistics for the month of January 1973 at Osan AB (RKSO).

Attachment 6E and 6F

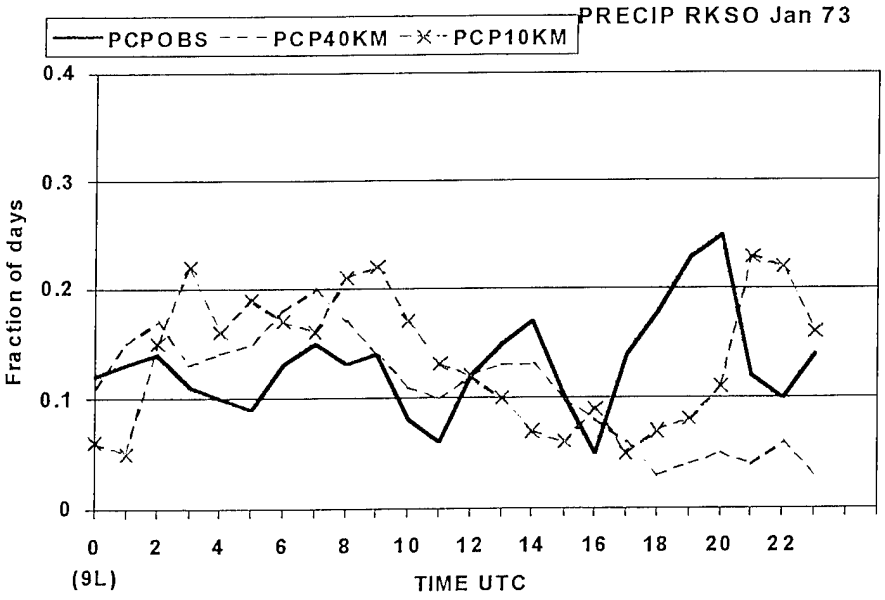

Attachment 6E. Frequency of precipitation (PCP) occurrence comparison for the observed, 10-km and 40-km climate statistics for the month of January 1973 Osan AB (RKSO). (Frequency of precipitation defined here as the fraction of the days in the month for which rain occurred at the indicated hour of the day.)

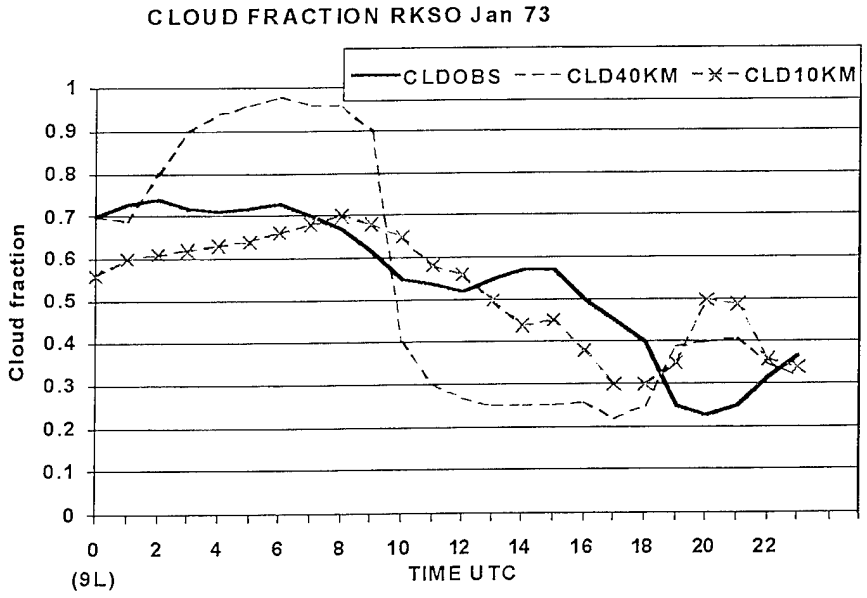

Attachment 6F. Hourly mean total cloud coverage (CLD) comparison for the observed, 10 km and 40 km climate statistics for the month of January 1973 at Osan AB (RKSO).

Attachment 7

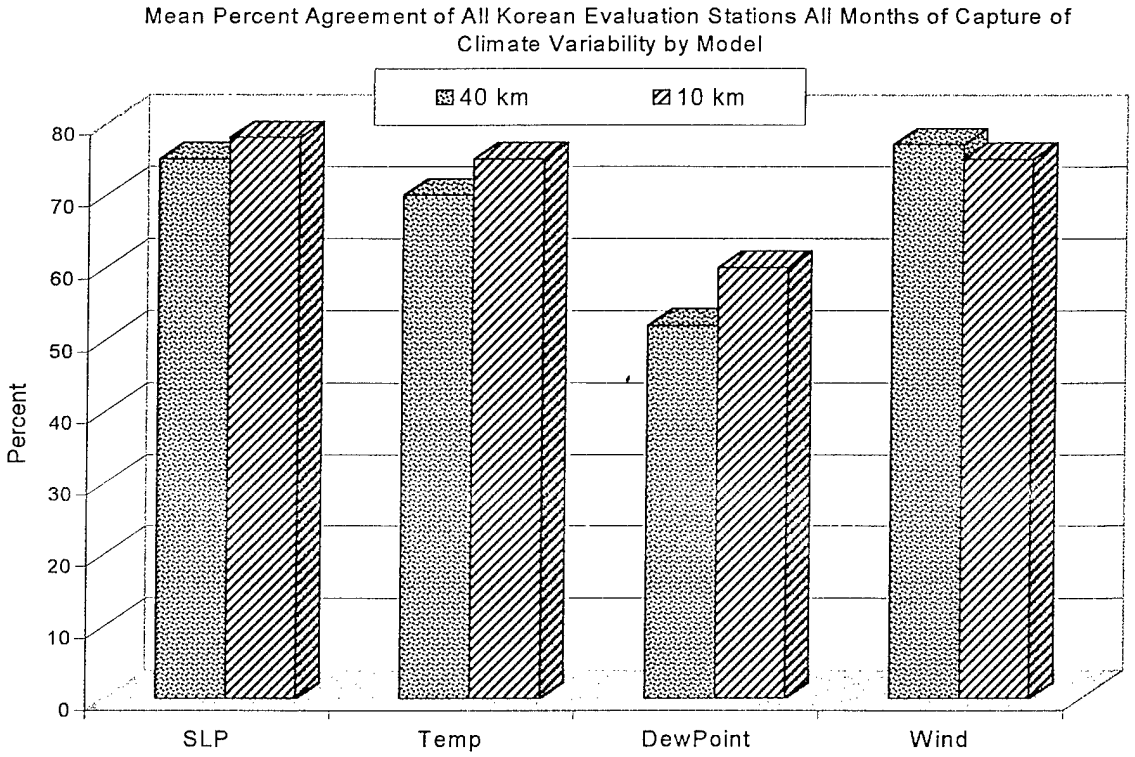

10 Year Averages for Jan

Observations
40 km Model
10 km Model

Selected Korean stations

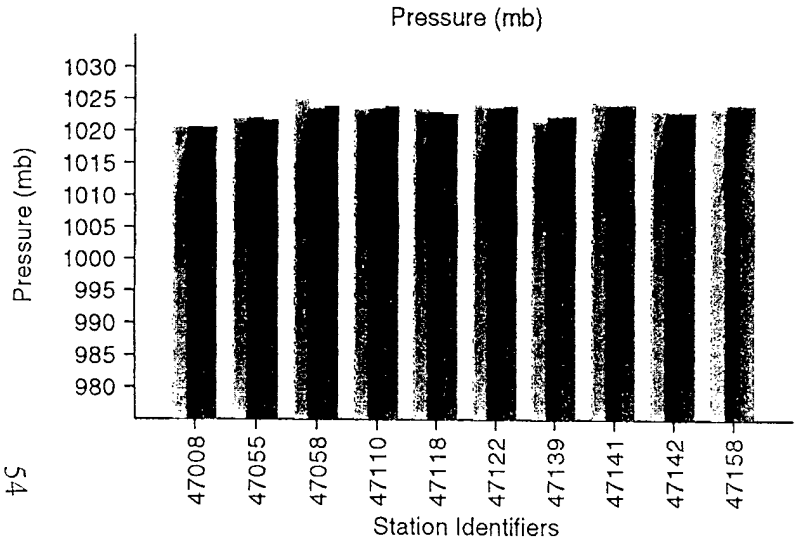

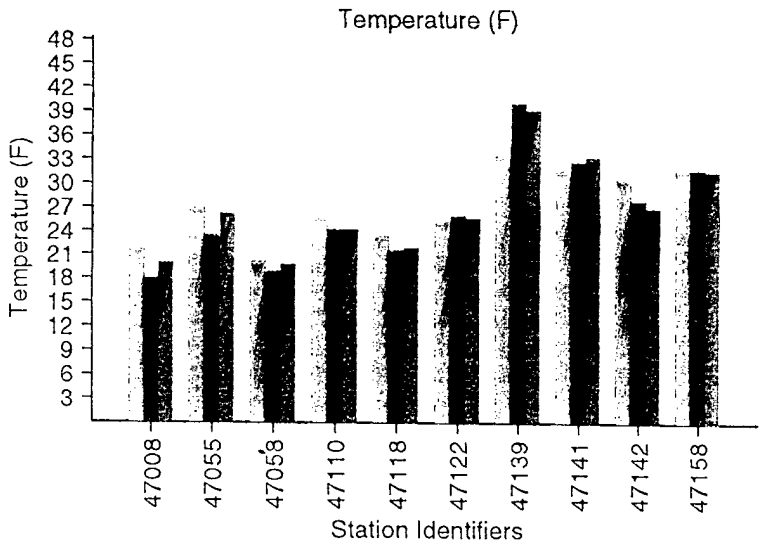

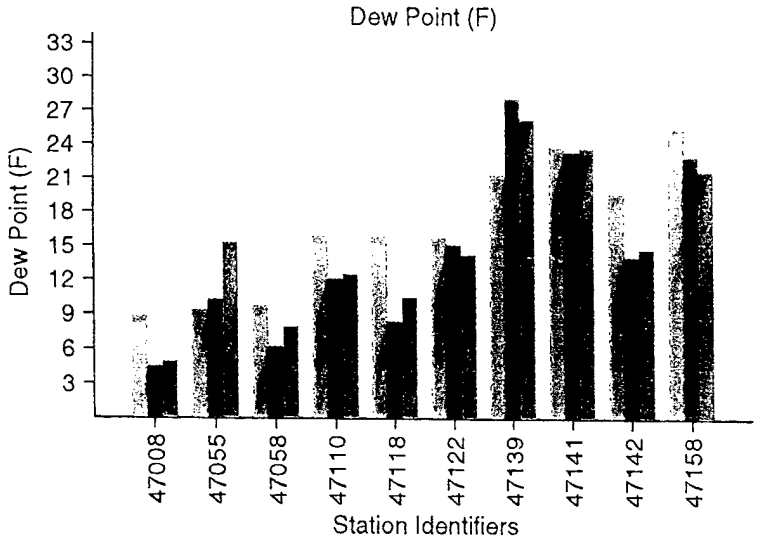

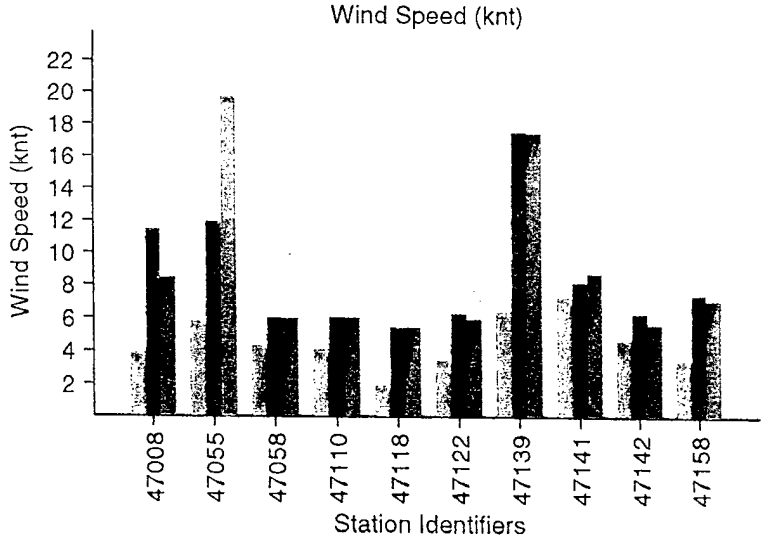

Attachment 8

10 Year Averages for Jul

Selected Korean stations

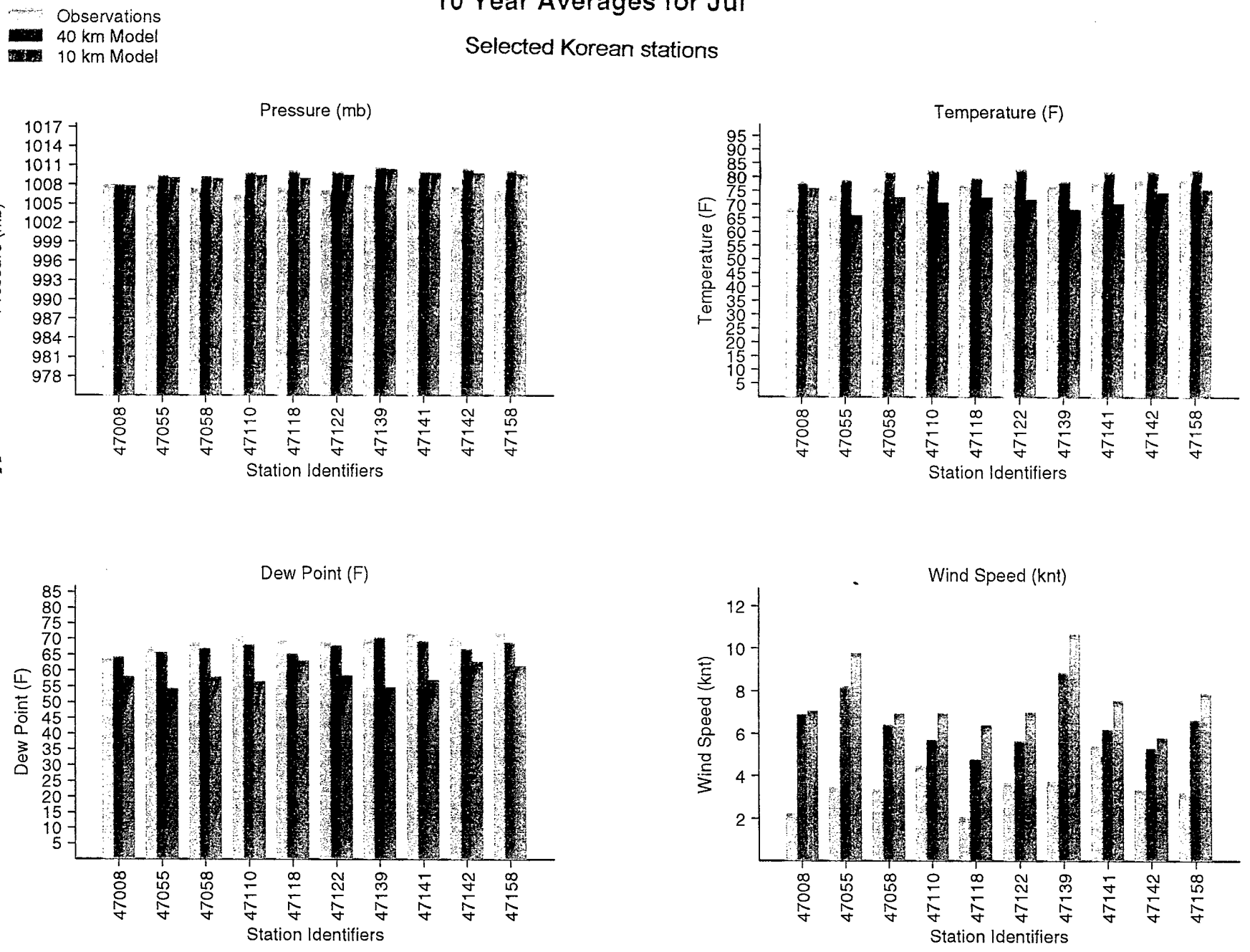

Attachment 9

10 Year Averages for Jan

Observations
40 km Model
10 km Model

Selected Mideast stations

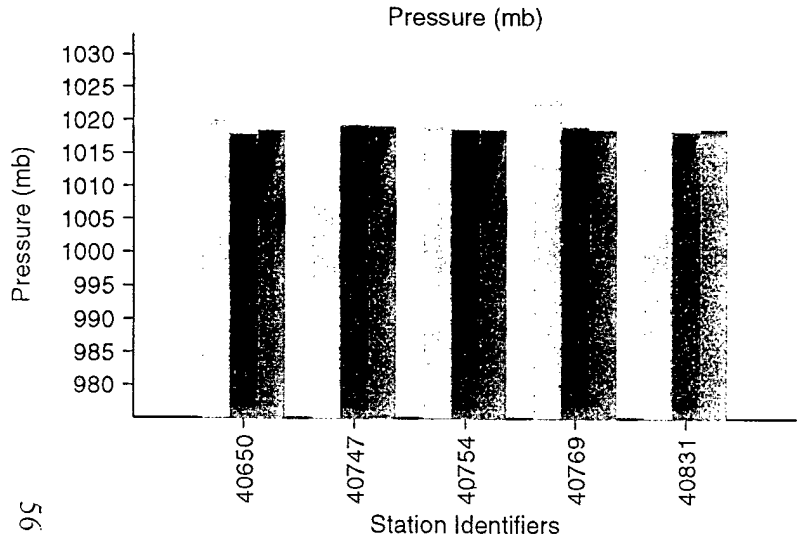

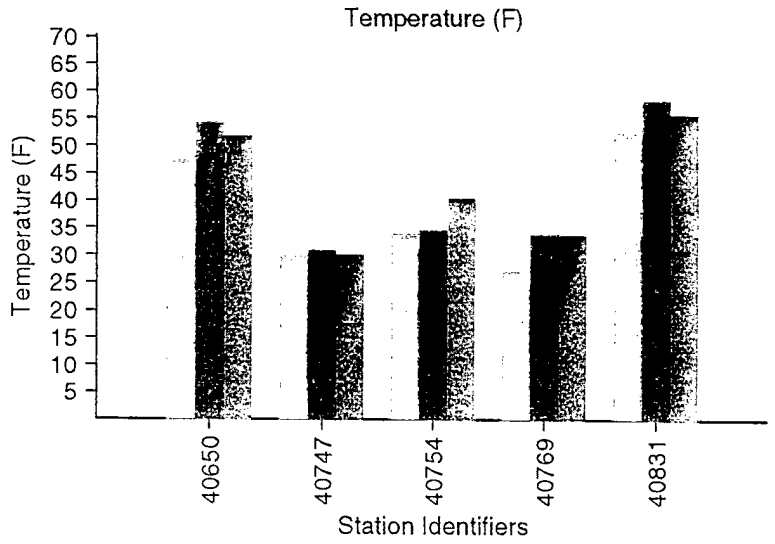

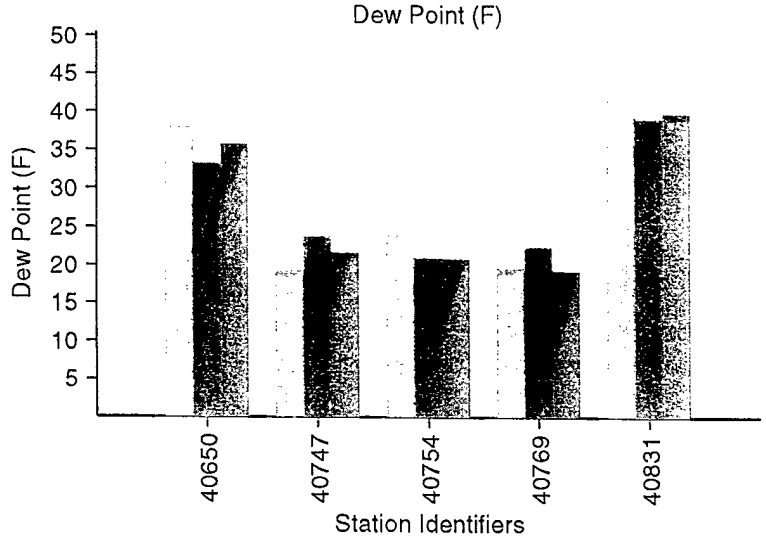

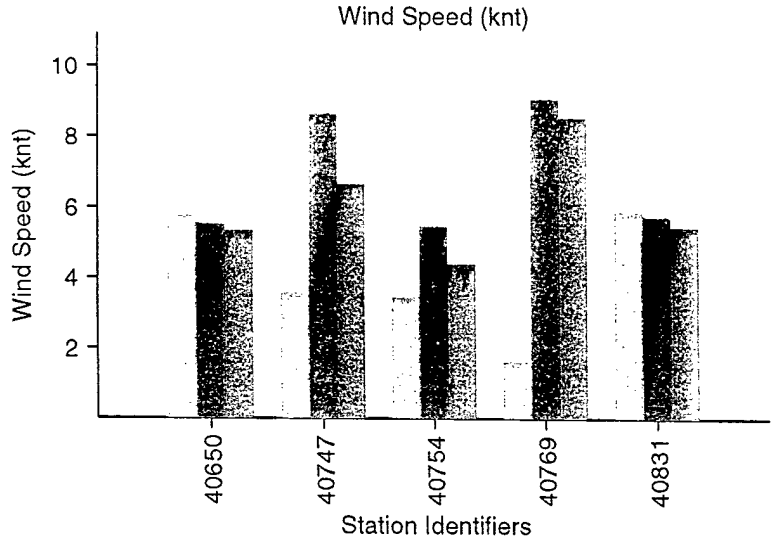

Attachment 10

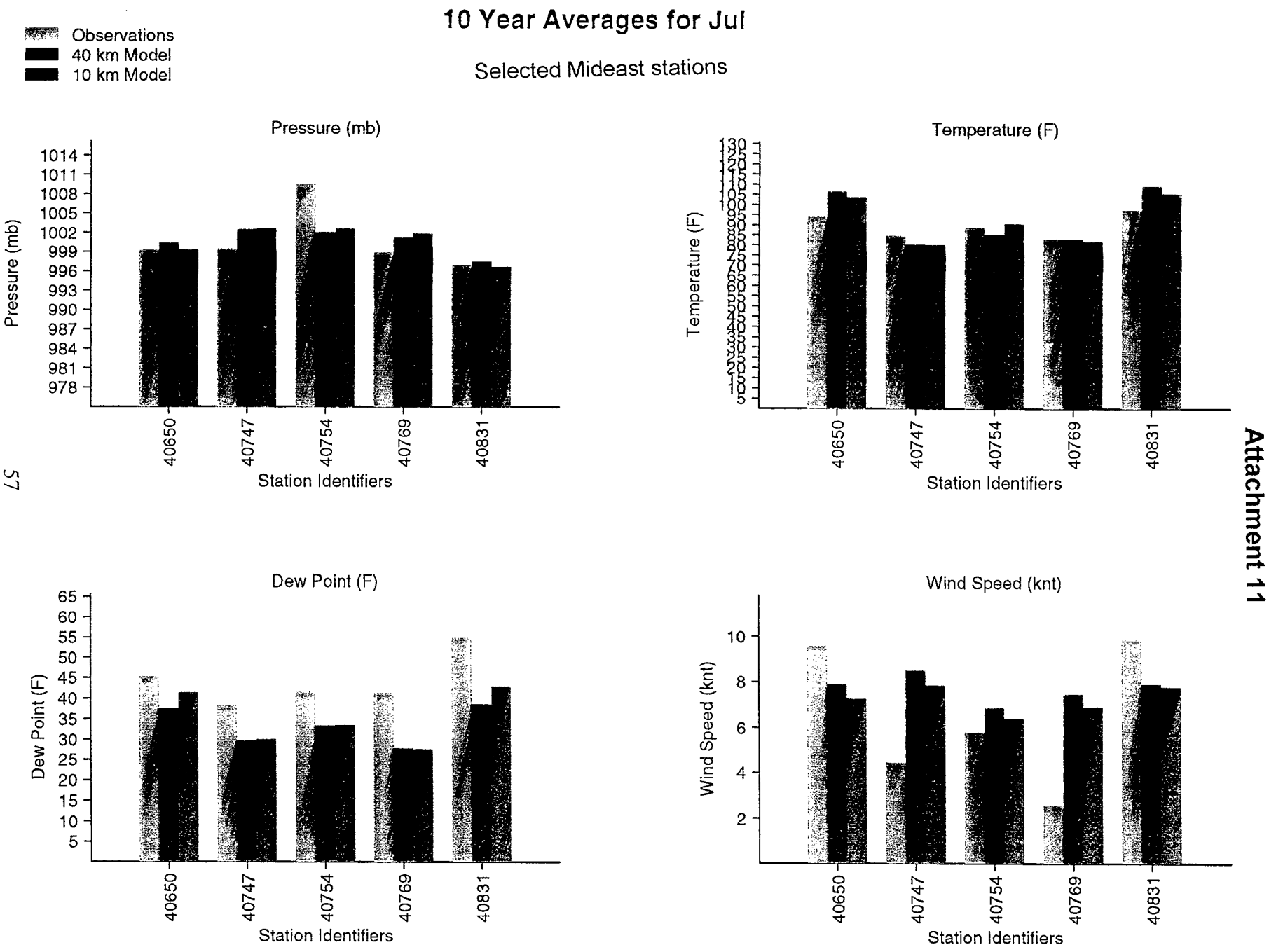

Attachment 11

Observations
Model

Analysis of 47122 for Jan, Coarse Model

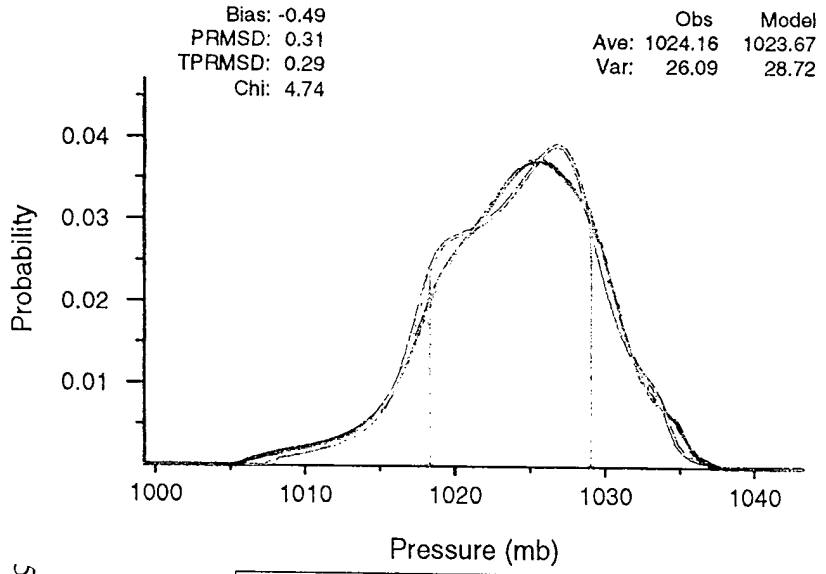

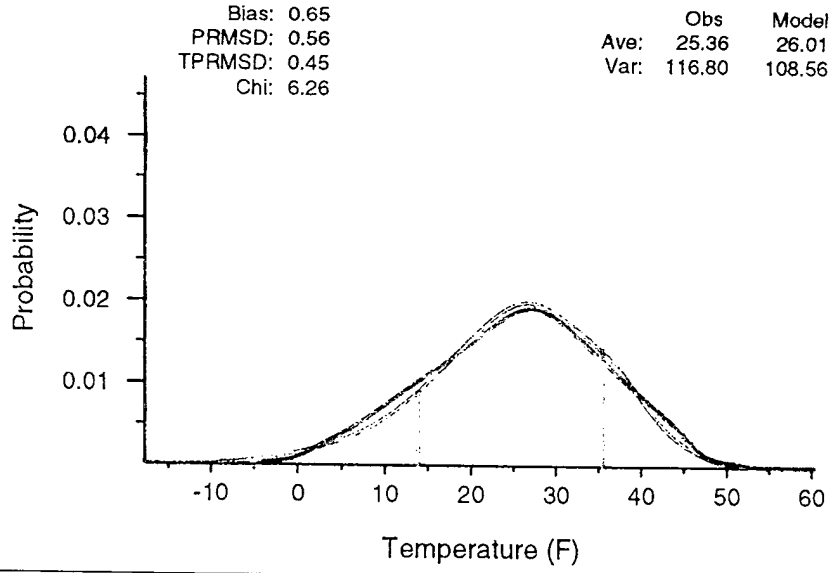

--- Red lines represent the 10% (left) and 90% (right) tails of the distribution for a charts of this type (Attachments 12-19). TPRMSD is the error calculated only looking at the tails of the distribution as a check of the extremes of the distribution.

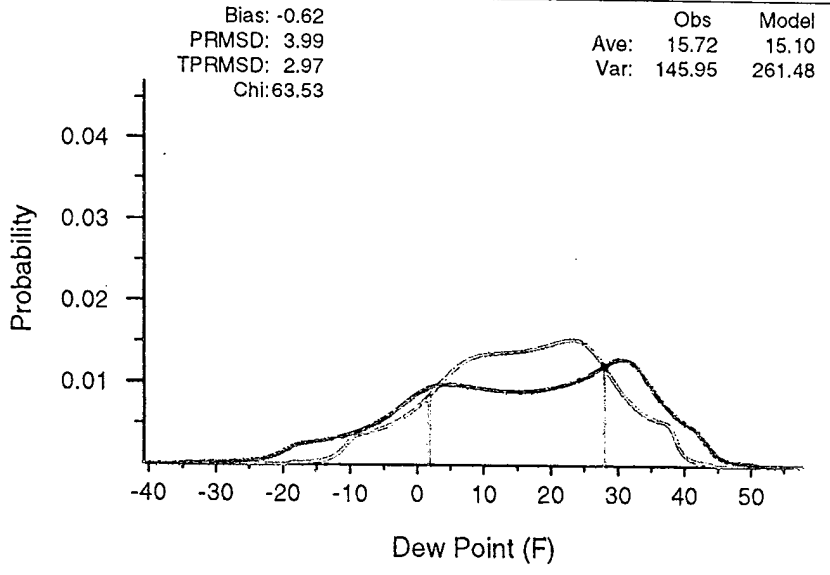

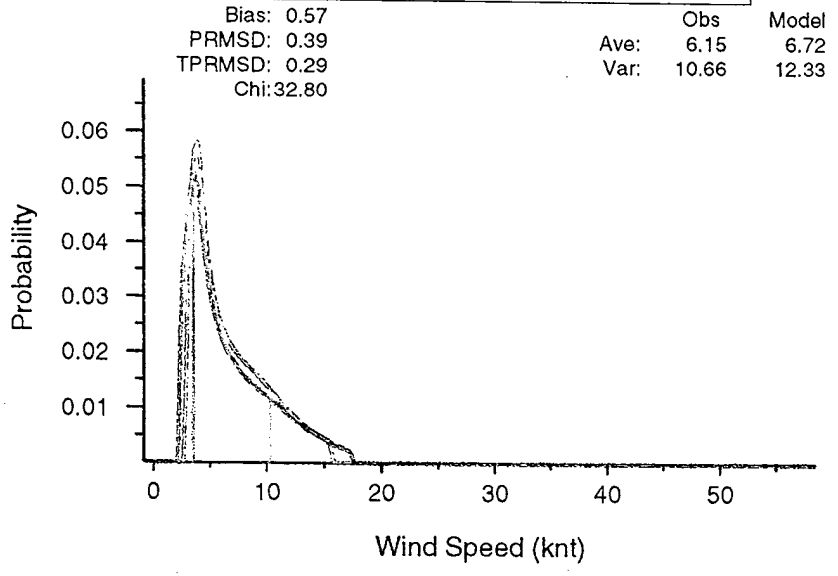

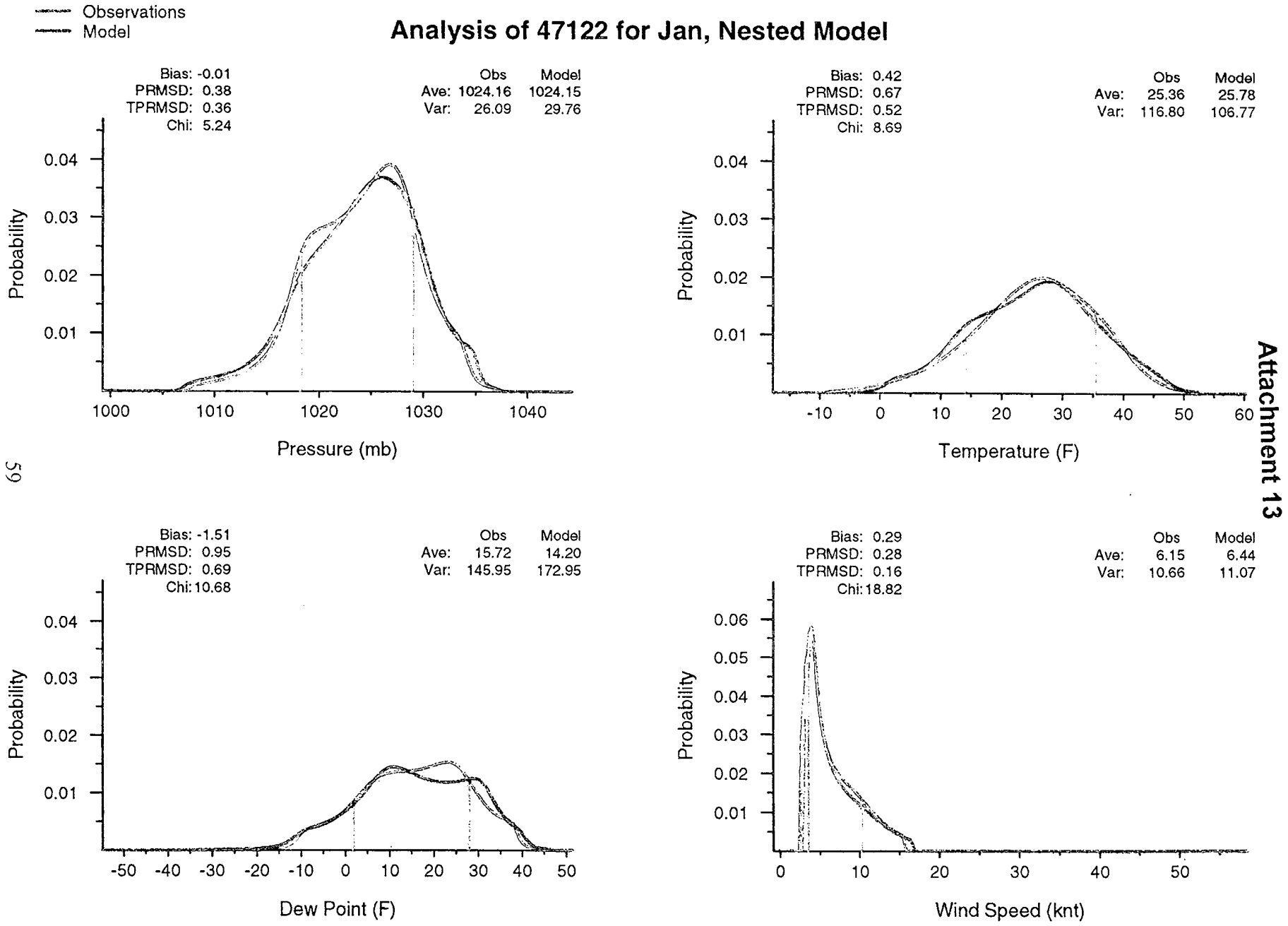

Attachment 13

Observations
Model

Analysis of 40754 for Jan, Coarse Model

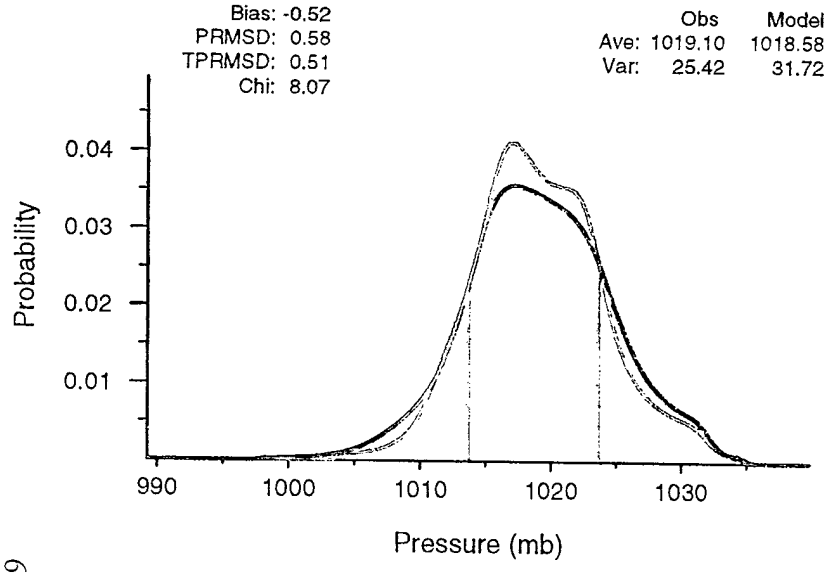

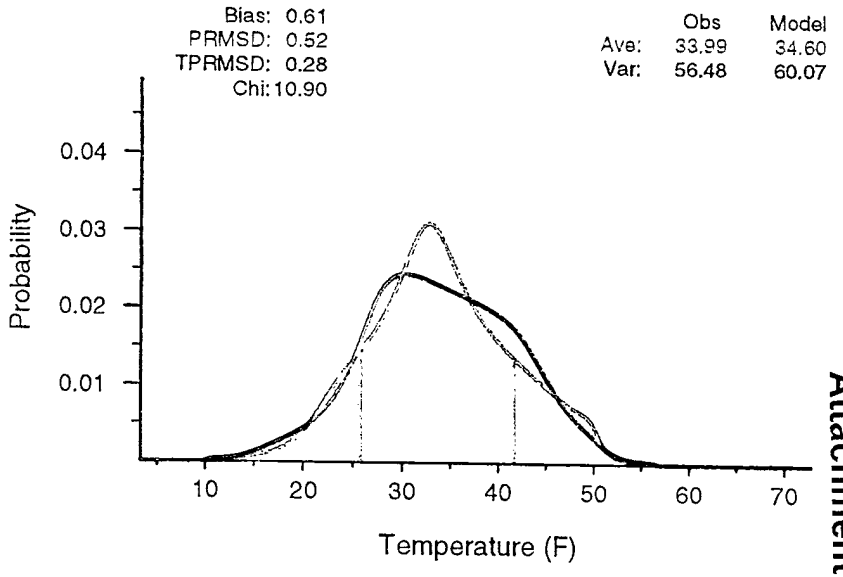

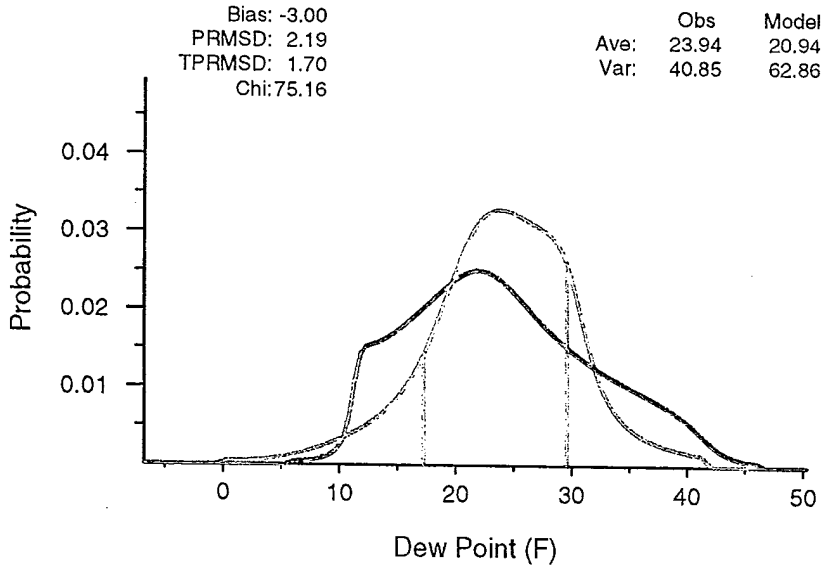

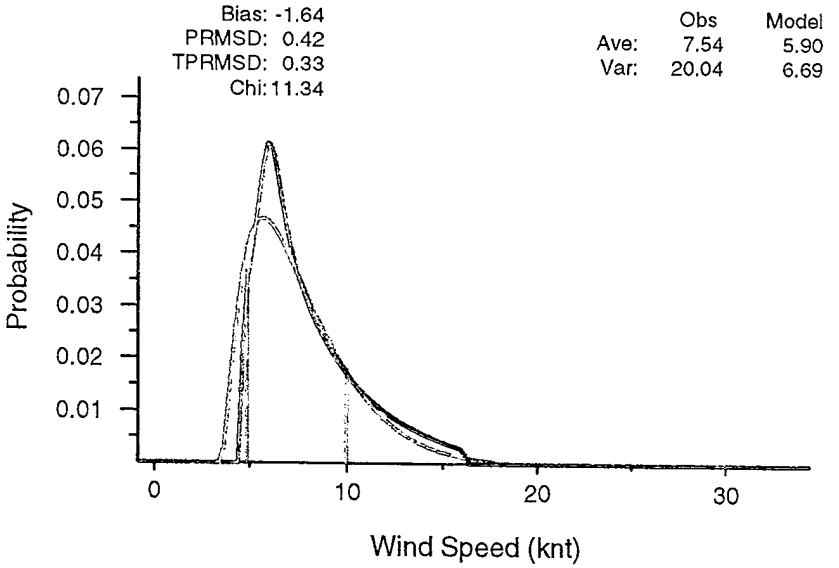

Attachment 14

09

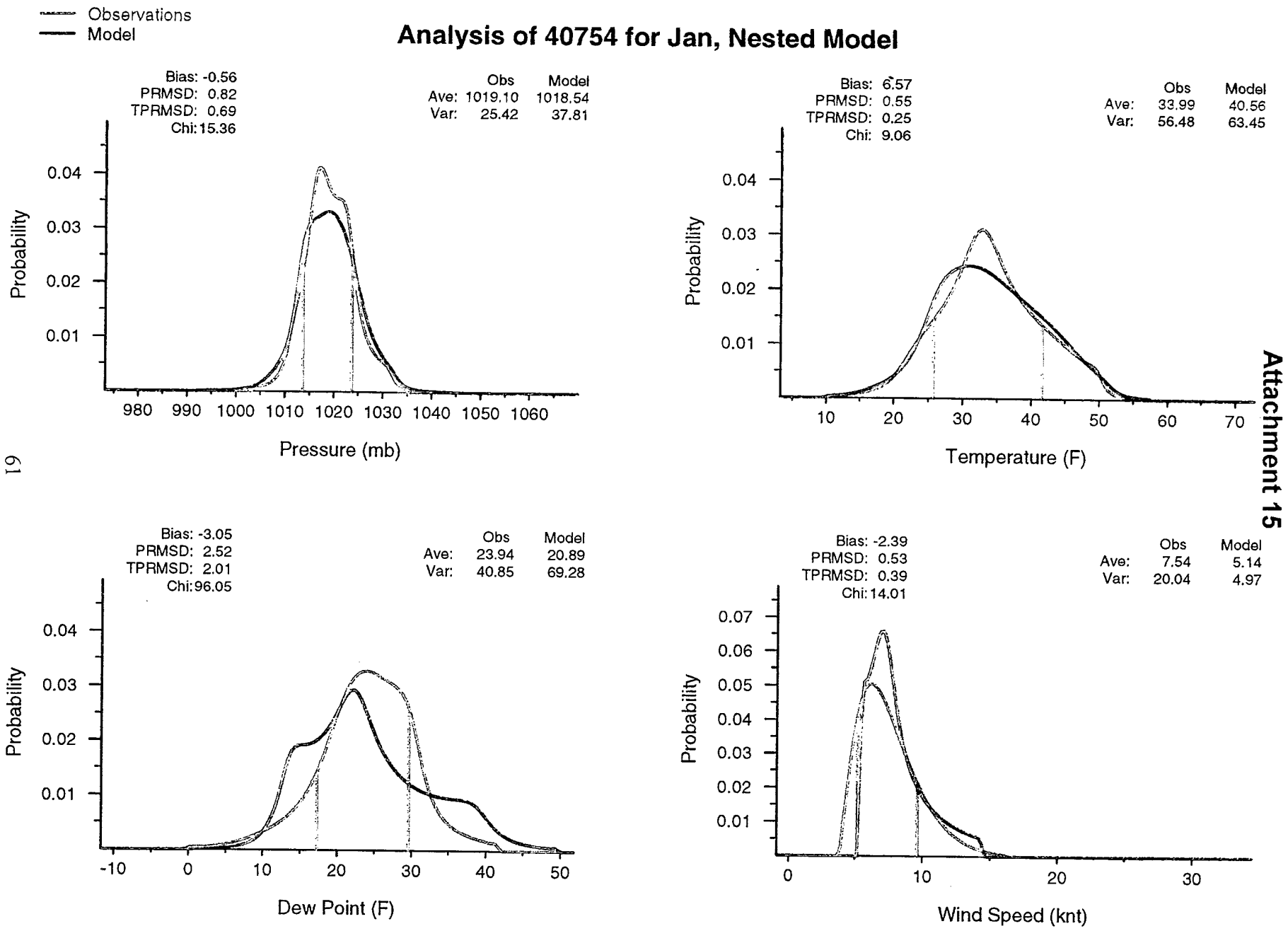
Observations
Model
Analysis of 40754 for Jan, Nested Model
Bias: -0.56
PRMSD: 0.82
TPRMSD: 0.69
Chi: 15.36
Obs Model
Ave: 1019.10 1018.54
Var: 25.42 37.81
Probability
0.04
0.03
0.02
0.01
980 990 1000 1010 1020 1030 1040 1050 1060
Pressure (mb)
Bias: 6.57
PRMSD: 0.55
TPRMSD: 0.25
Chi: 9.06
Obs Model
Ave: 33.99 40.56
Var: 56.48 63.45
Probability
0.04
0.03
0.02
0.01
10 20 30 40 50 60 70
Temperature (F)
Bias: -3.05
PRMSD: 2.52
TPRMSD: 2.01
Chi: 96.05
Obs Model
Ave: 23.94 20.89
Var: 40.85 69.28
Probability
0.04
0.03
0.02
0.01
-10 0 10 20 30 40 50
Dew Point (F)
Bias: -2.39
PRMSD: 0.53
TPRMSD: 0.39
Chi: 14.01
Obs Model
Ave: 7.54 5.14
Var: 20.04 4.97
Probability
0.07
0.06
0.05
0.04
0.03
0.02
0.01
0 10 20 30
Wind Speed (knt)

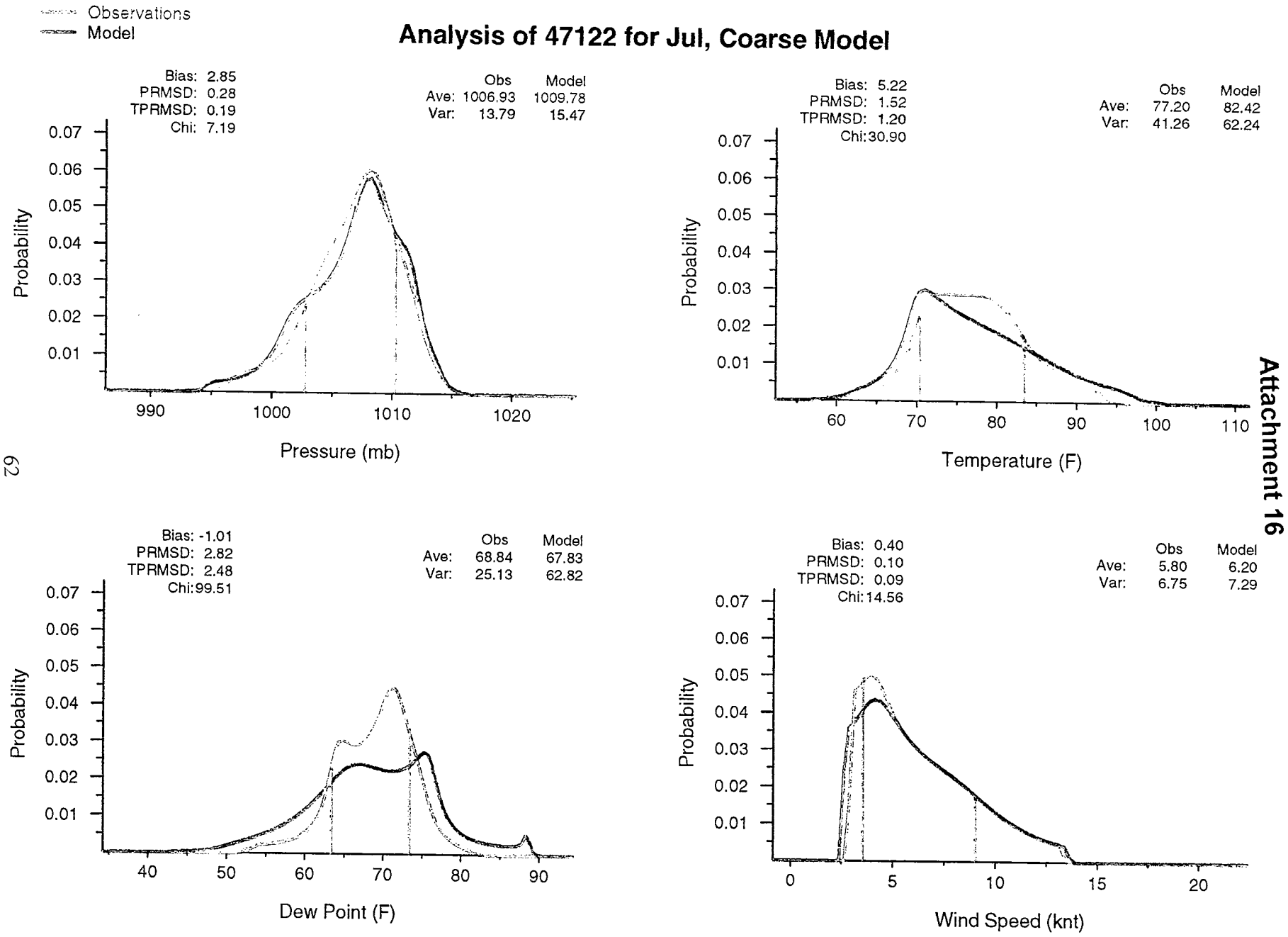
Observations
Model
Analysis of 47122 for Jul, Coarse Model
Bias: 2.85
PRMSD: 0.28
TPRMSD: 0.19
Chi: 7.19
Obs Model
Ave: 1006.93 1009.78
Var: 13.79 15.47
Probability
Pressure (mb)
Bias: 5.22
PRMSD: 1.52
TPRMSD: 1.20
Chi:30.90
Obs Model
Ave: 77.20 82.42
Var: 41.26 62.24
Temperature (F)
Bias: -1.01
PRMSD: 2.82
TPRMSD: 2.48
Chi:99.51
Obs Model
Ave: 68.84 67.83
Var: 25.13 62.82
Dew Point (F)
Bias: 0.40
PRMSD: 0.10
TPRMSD: 0.09
Chi:14.56
Obs Model
Ave: 5.80 6.20
Var: 6.75 7.29
Wind Speed (knt)

Observations
Model

Analysis of 47122 for Jul, Nested Model

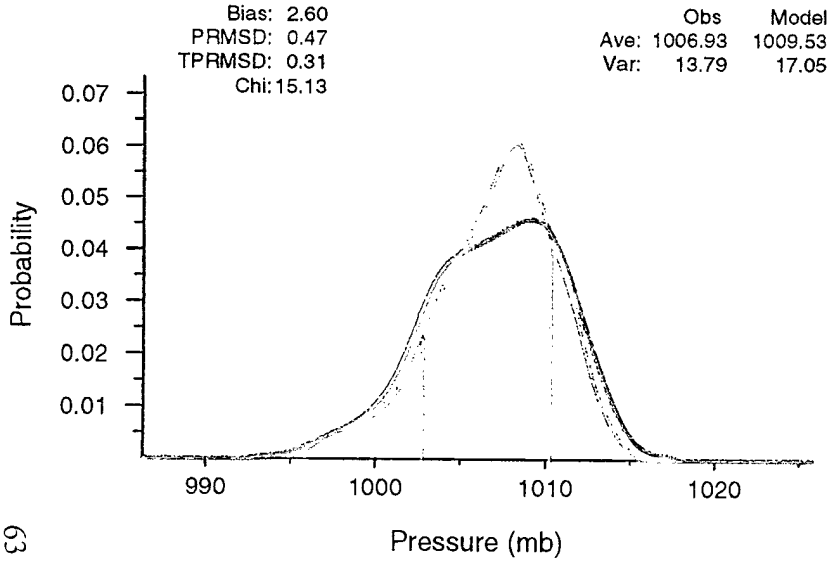

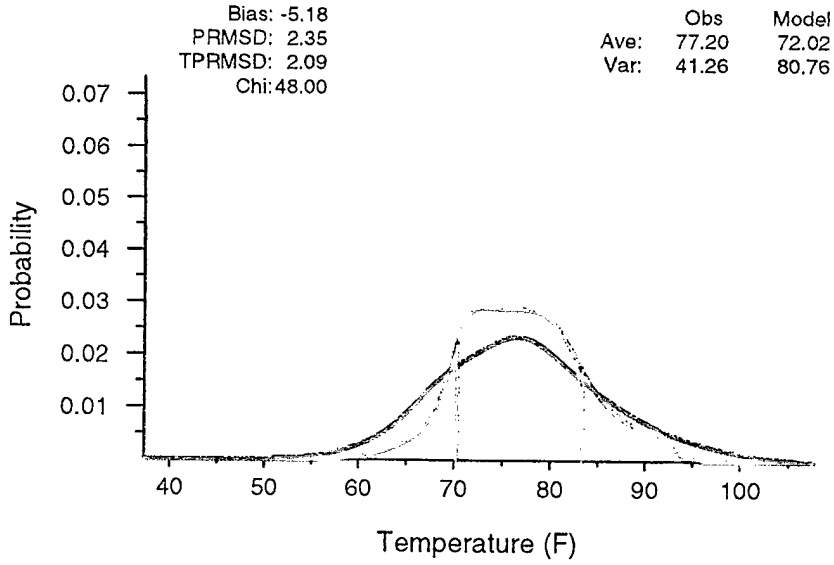

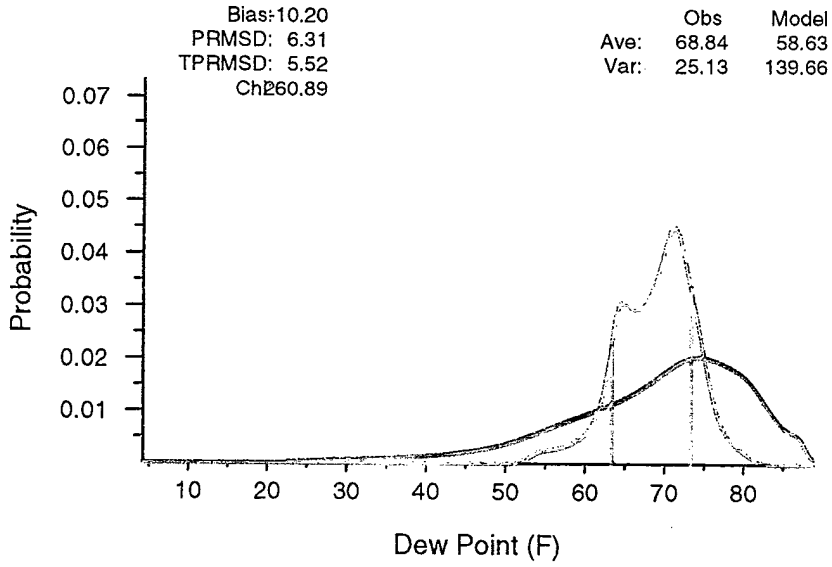

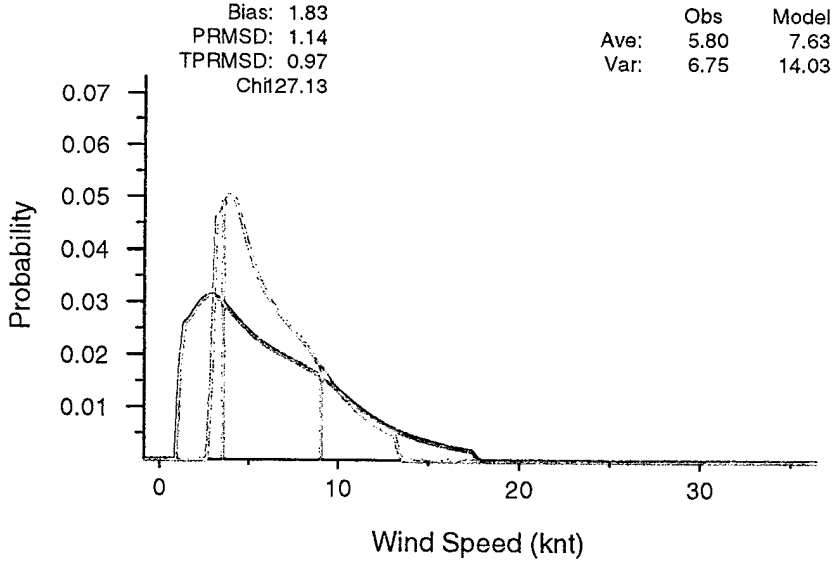

Attachment 17

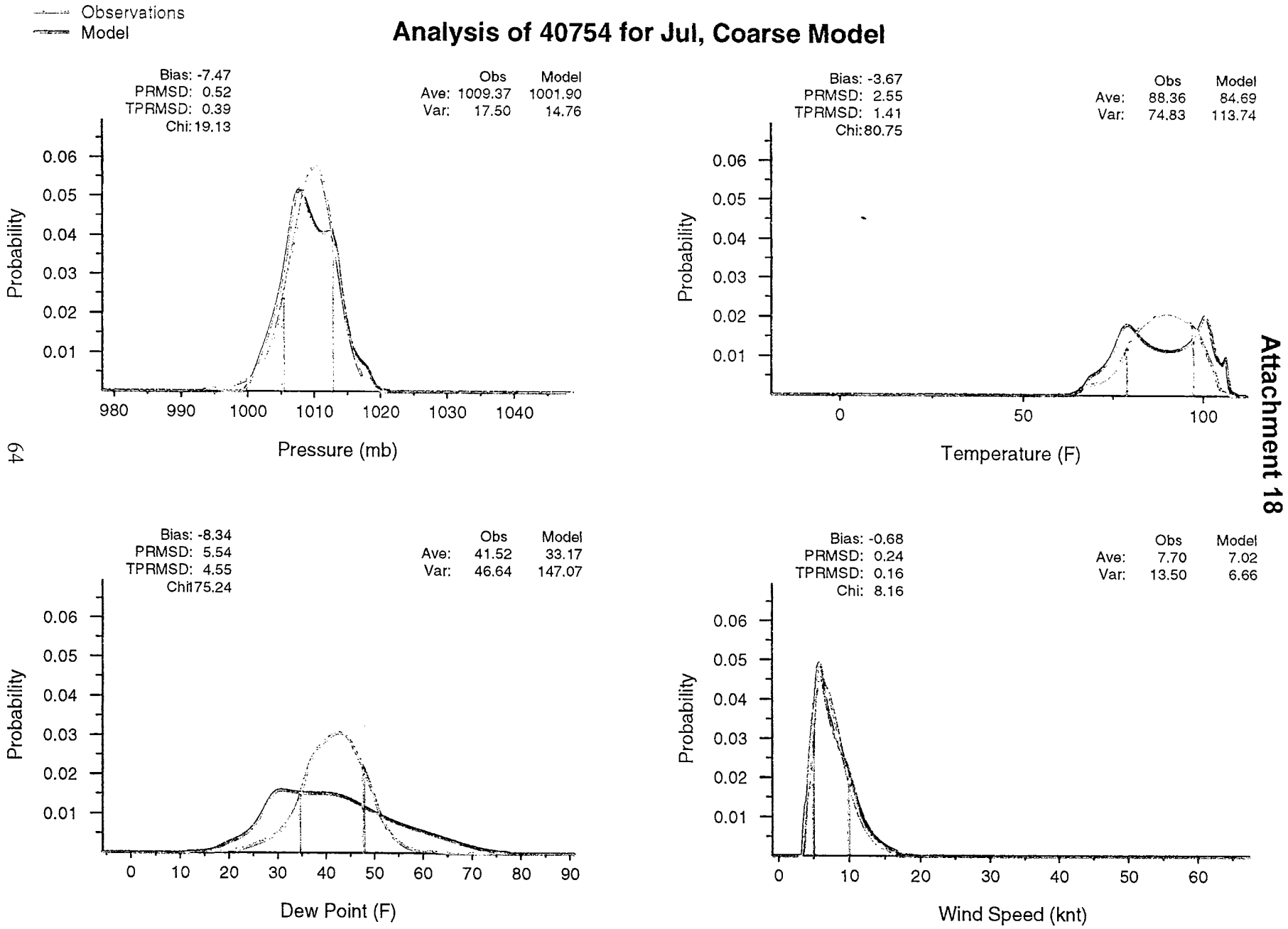

Attachment 18

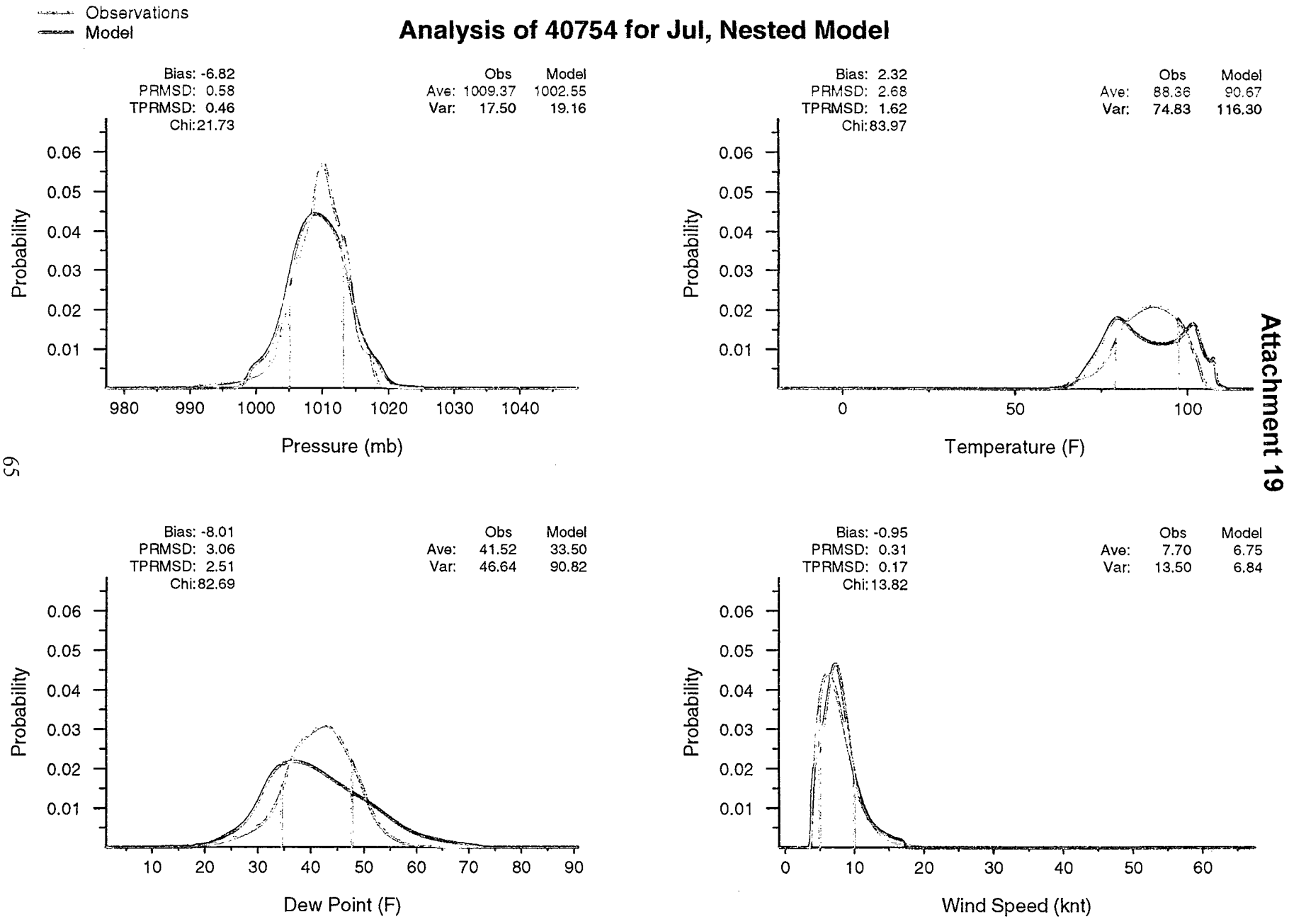

Attachment 19

Attachment 20

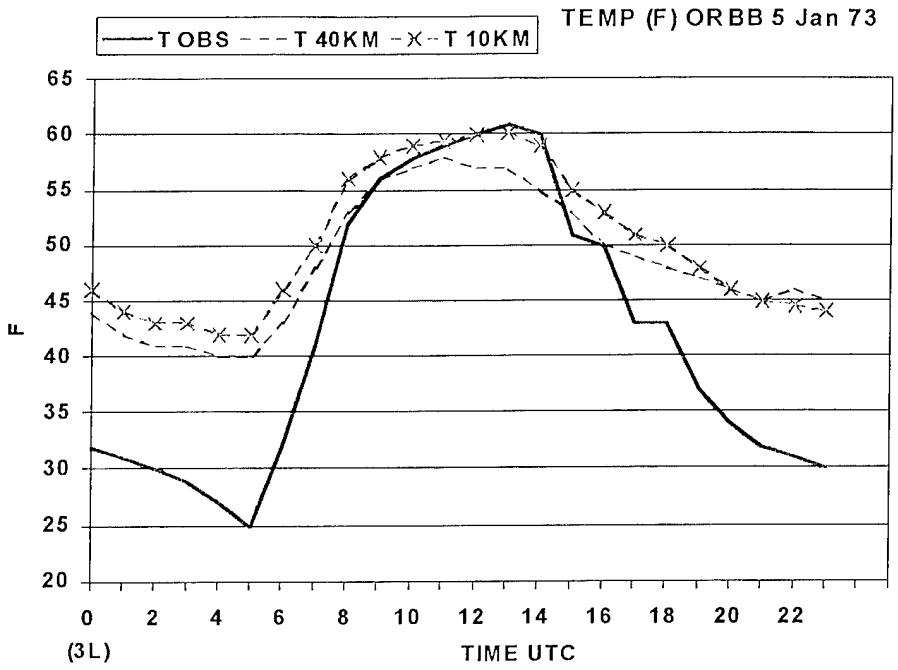

Attachment 20A. The surface temperature (T) comparison for the observed (OBS), 10 km and 40 km domains for 5 January 1973 at Baghdad, Iraq (ORBB) before soil moisture was adjusted.

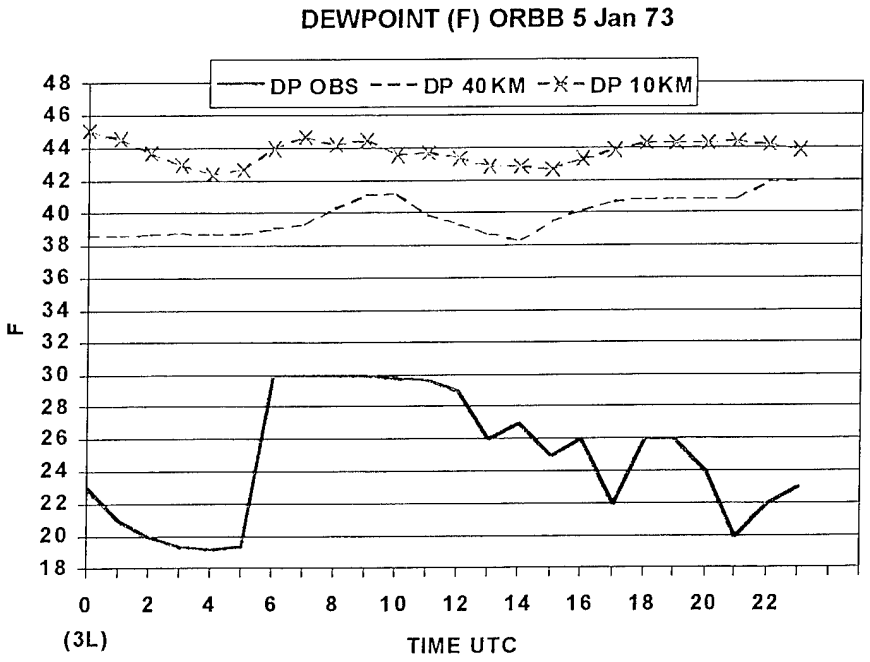

Attachment 20B. Surface dewpoint (DP) temperature comparison for the observed 10 km and 40 km for 5 January 1973 at Baghdad, Iraq (ORBB) before soil moisture was adjusted.

Attachment 21

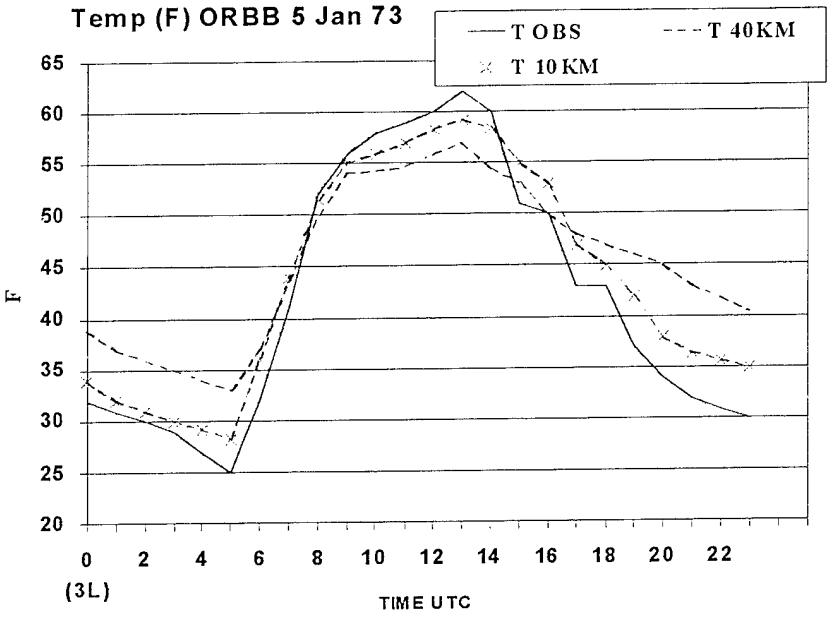

Attachment 21A. The surface temperature (T) comparison for the observed (OBS) 10 km and 40 km for 5 January 1973 at Baghdad, Iraq (ORBB) after soil moisture was adjusted.

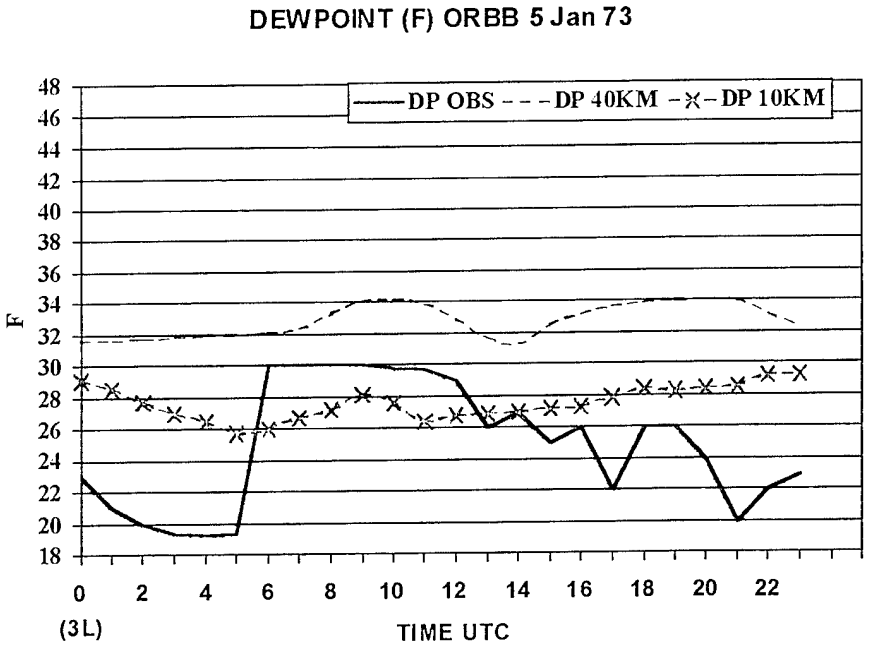

Attachment 21B. The corrected surface dewpoint (DP) comparison for the observed (OBS), 10 km and 40 km for the 5 January 1973 at Baghdad, Iraq (ORBB) after soil moisture was adjusted.

Attachment 22

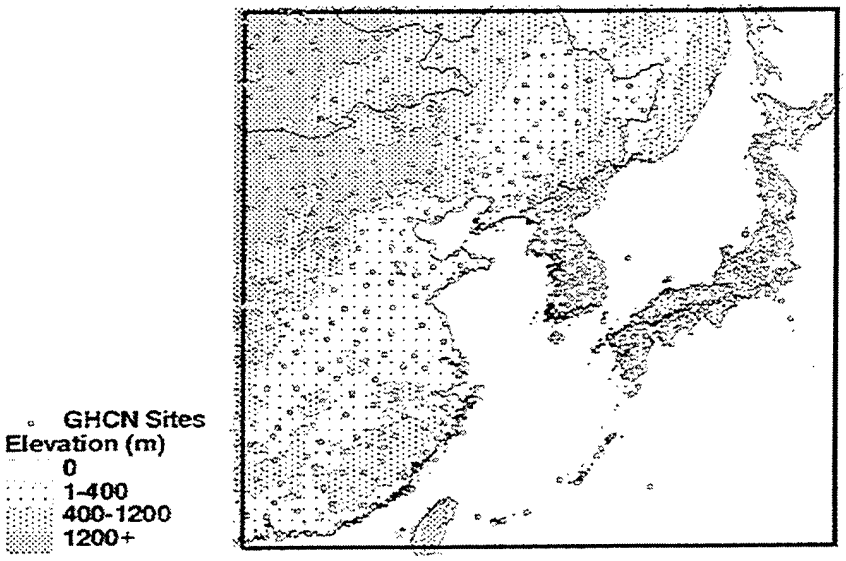

Attachment 22A. Location of the model domain at 40 km resolution. Locations of NCDC's Global Historical Climatology Network (GHCN) temperature observing sites are indicated with terrain elevation in meters.

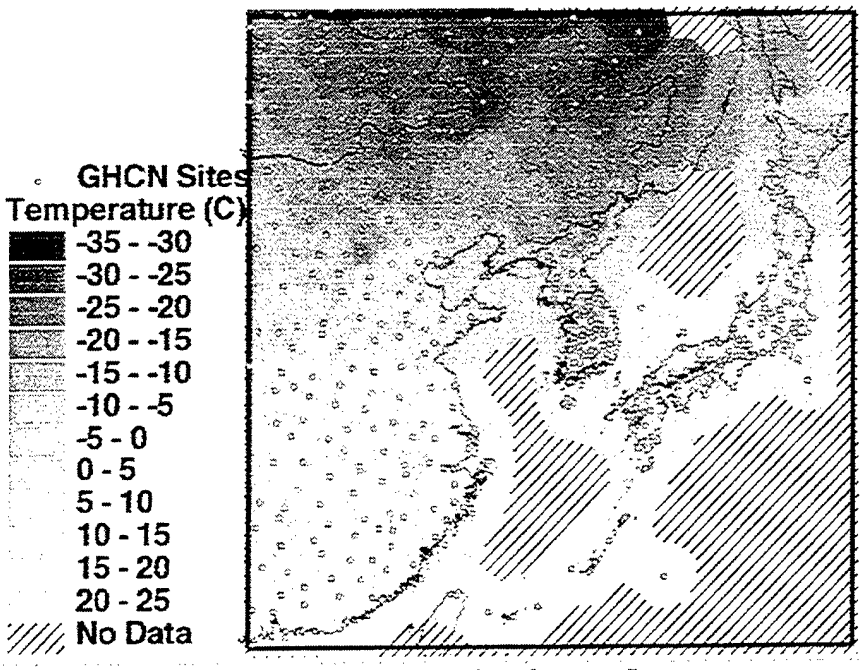

Attachment 22B. Contoured analysis of mean January temperature from the GHCN. Hatched regions indicate areas beyond 250-km range to the nearest observing site.

Attachment 23

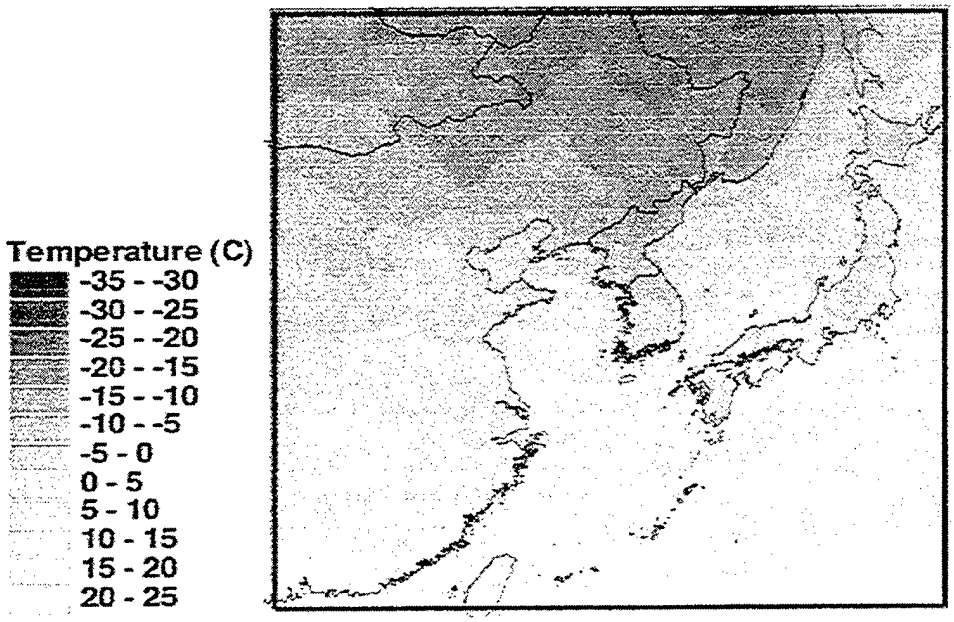

Attachment 23A. Mean January temperature from the 40 km model domain.

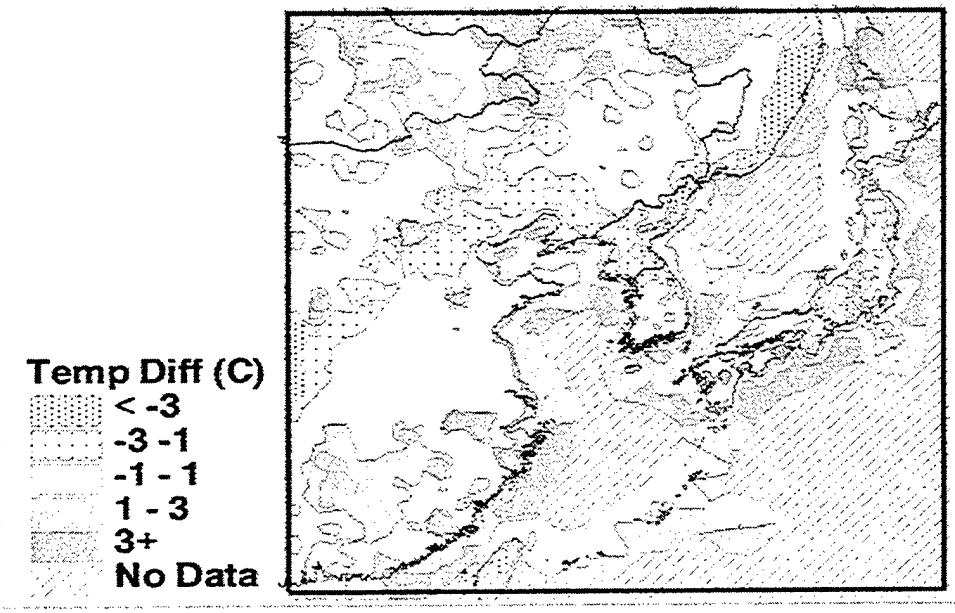

Attachment 23B. Difference between modeled and observed mean January temperature. Solids indicate regions where the model is warmer than observed.

Attachment 24

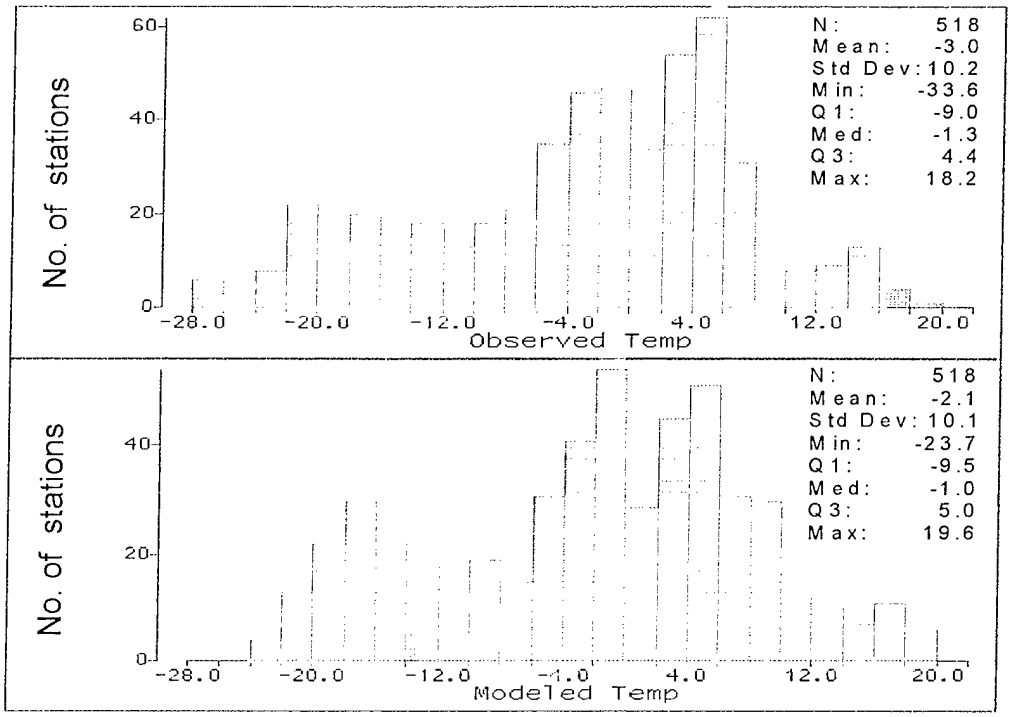

Attachment 24A. Distributions of observed mean temperature (C) (top) and modeled mean temperature (bottom) at the NCDC's Global Historical Climatology Network (GHCN) locations.

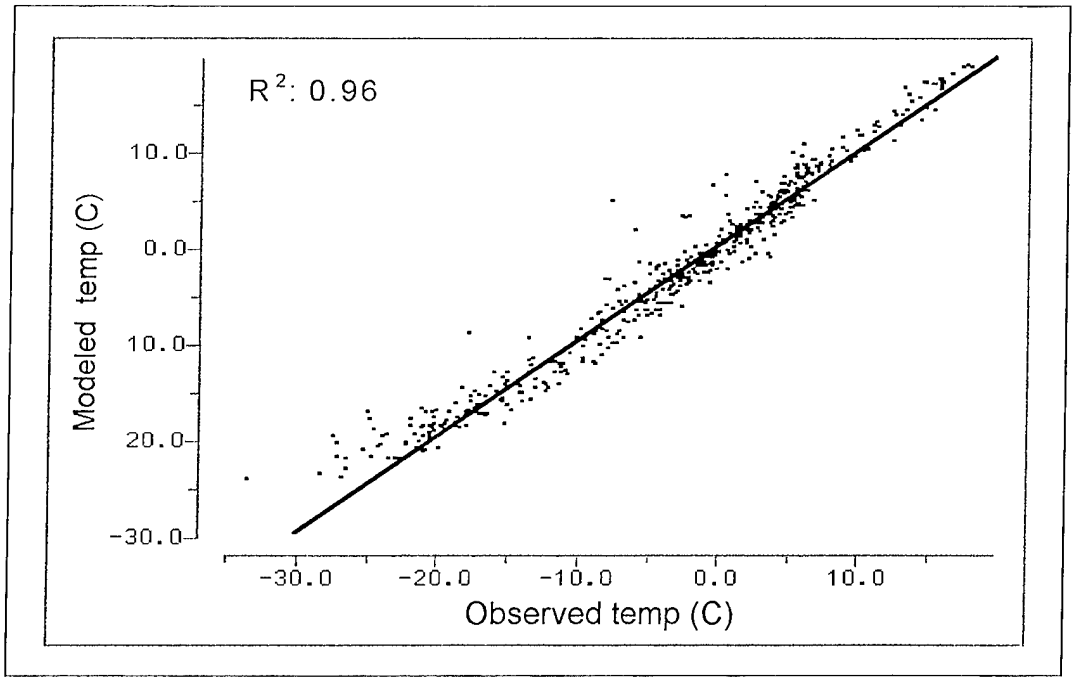

Attachment 24B. Comparison of modeled vs. observed mean January temperature at GHCN observing locations in Far East Asia.

Attachment 25

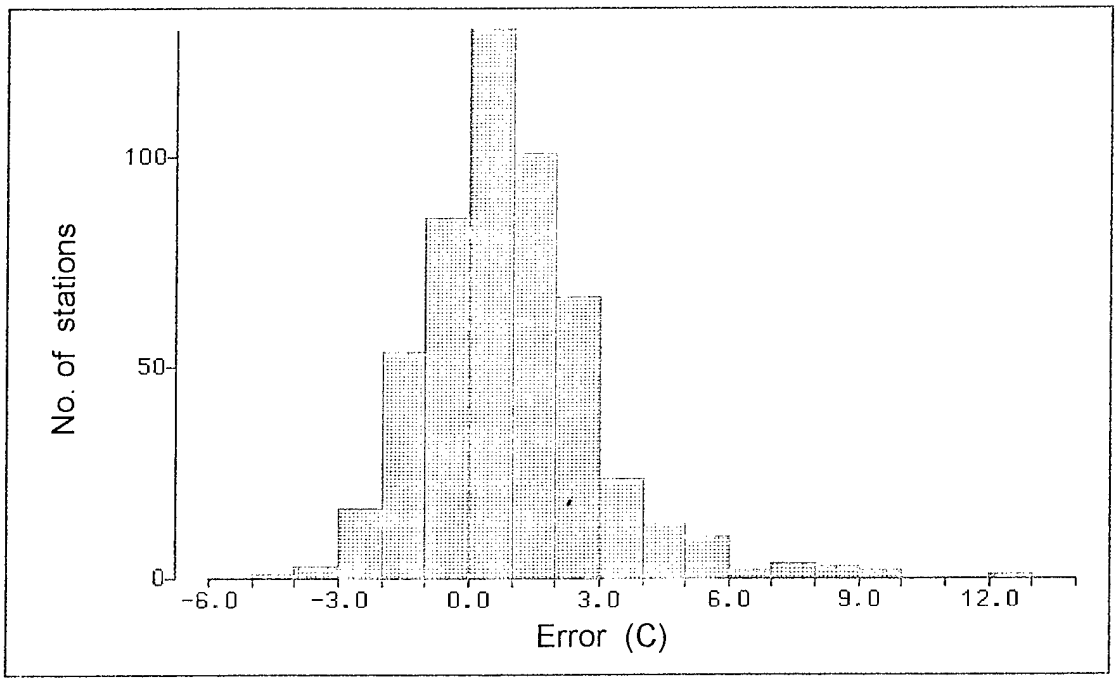

Attachment 25A. Distribution of the errors in modeled mean January temperature.

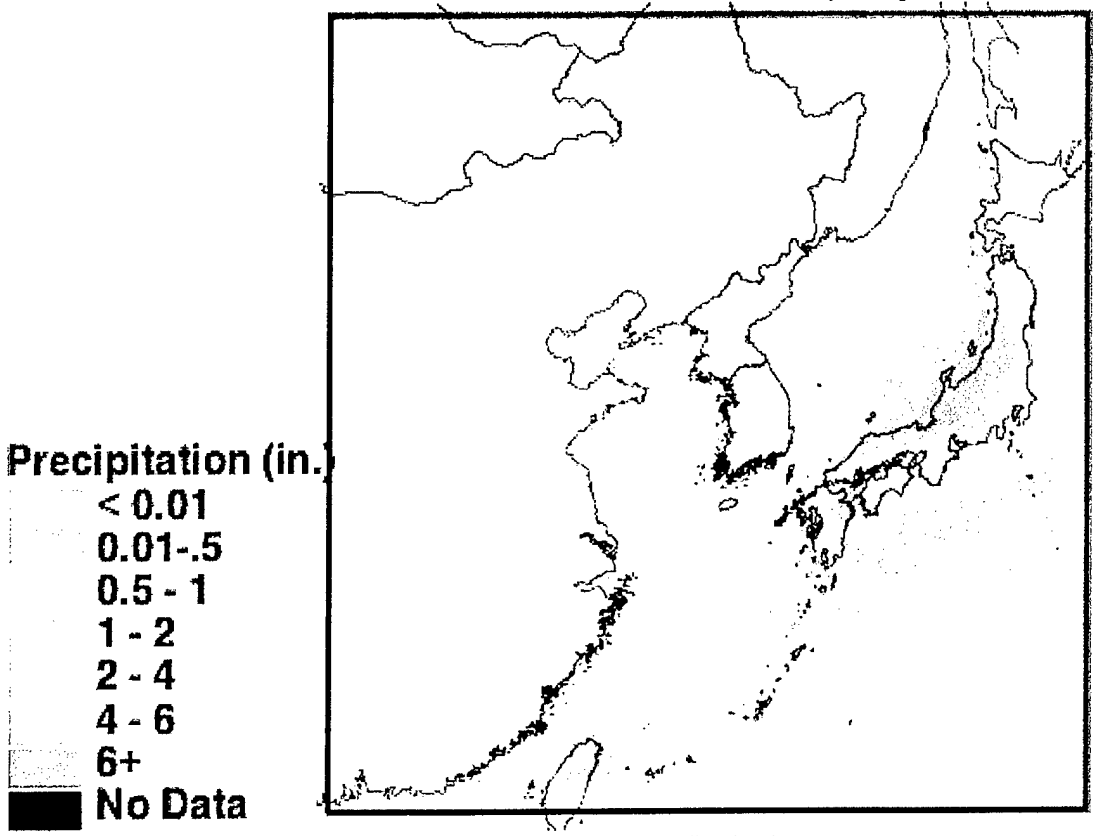

Attachment 25B. Modeled mean January precipitation (inches).

Attachment 26

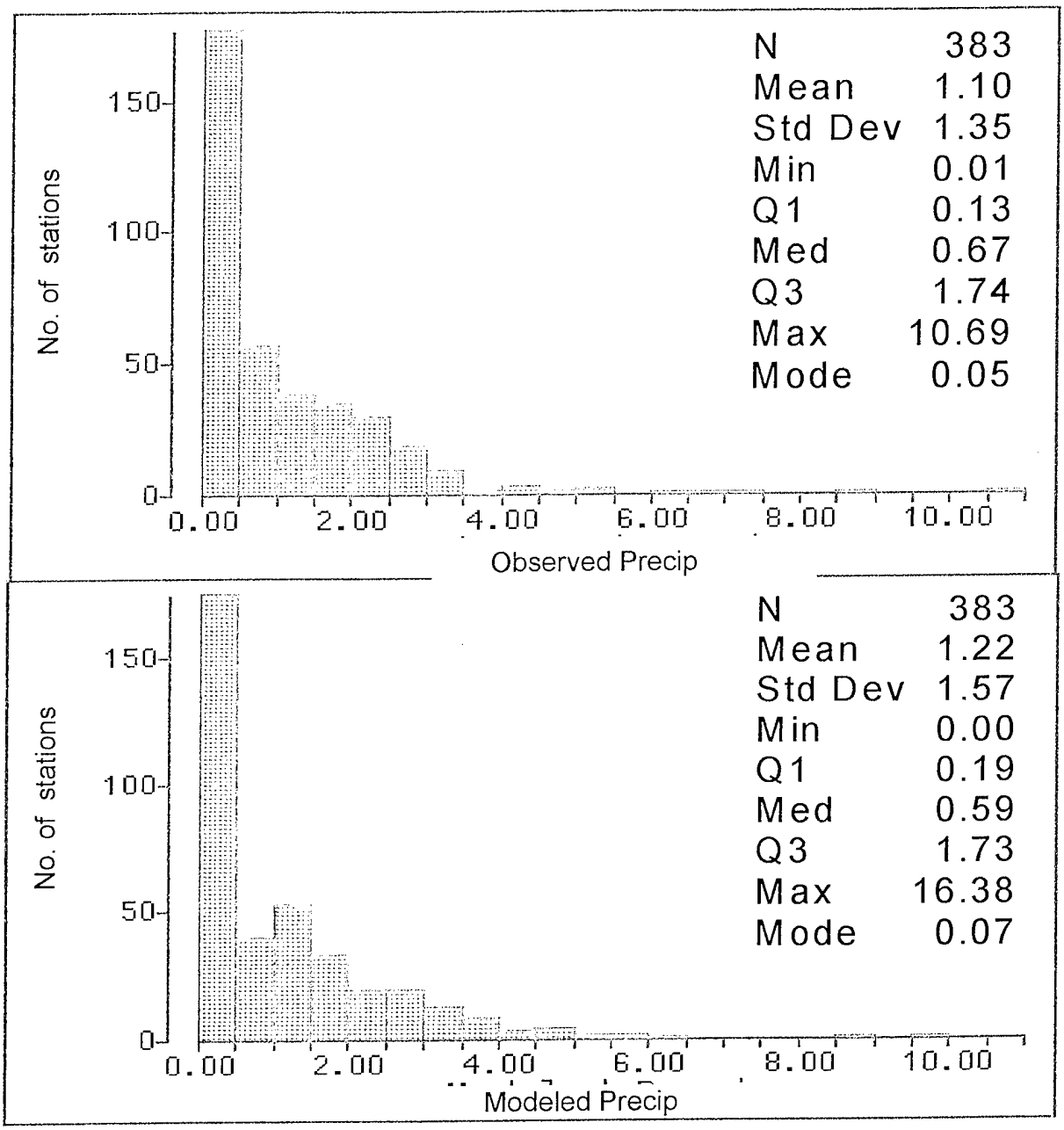

Attachment 26. Frequency distributions of observed (top) and modeled (bottom) mean January precipitation at 383 of NCDC's Global Historical Climatology Network (GHCN) sites around Far East Asia.

Attachment 27

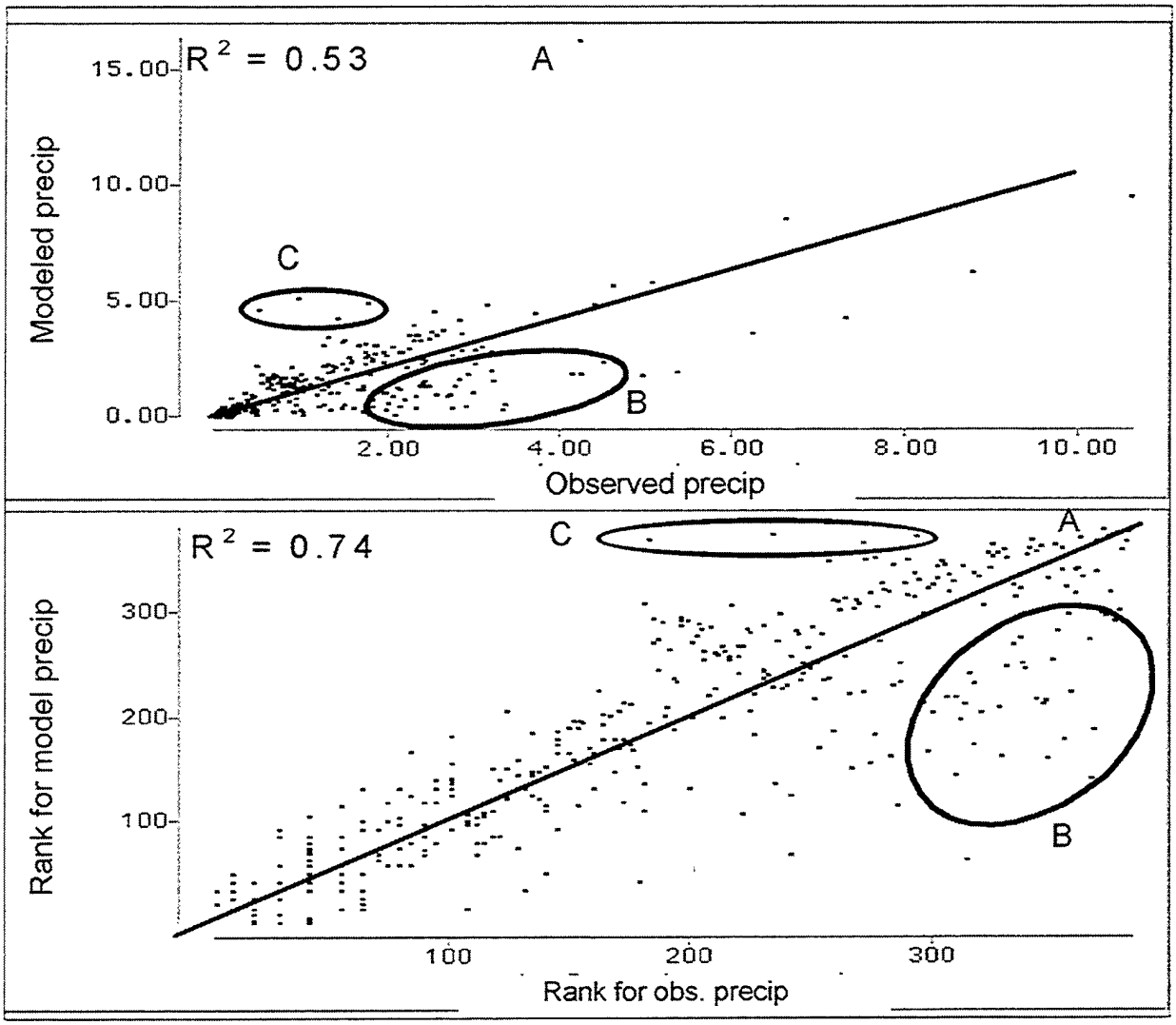

Attachment 27. Modeled vs. Observed mean January precipitation at 383 of NCDC's Global Historical Climatology Network (GHCN) stations. Bottom is ranked values where the lowest ranks are the driest stations. The solid lines show the expected 1-1 correlation.

A – Taipei, Taiwan

B – Continental Southeast China

C – Four sites in Japan.

Attachment 28

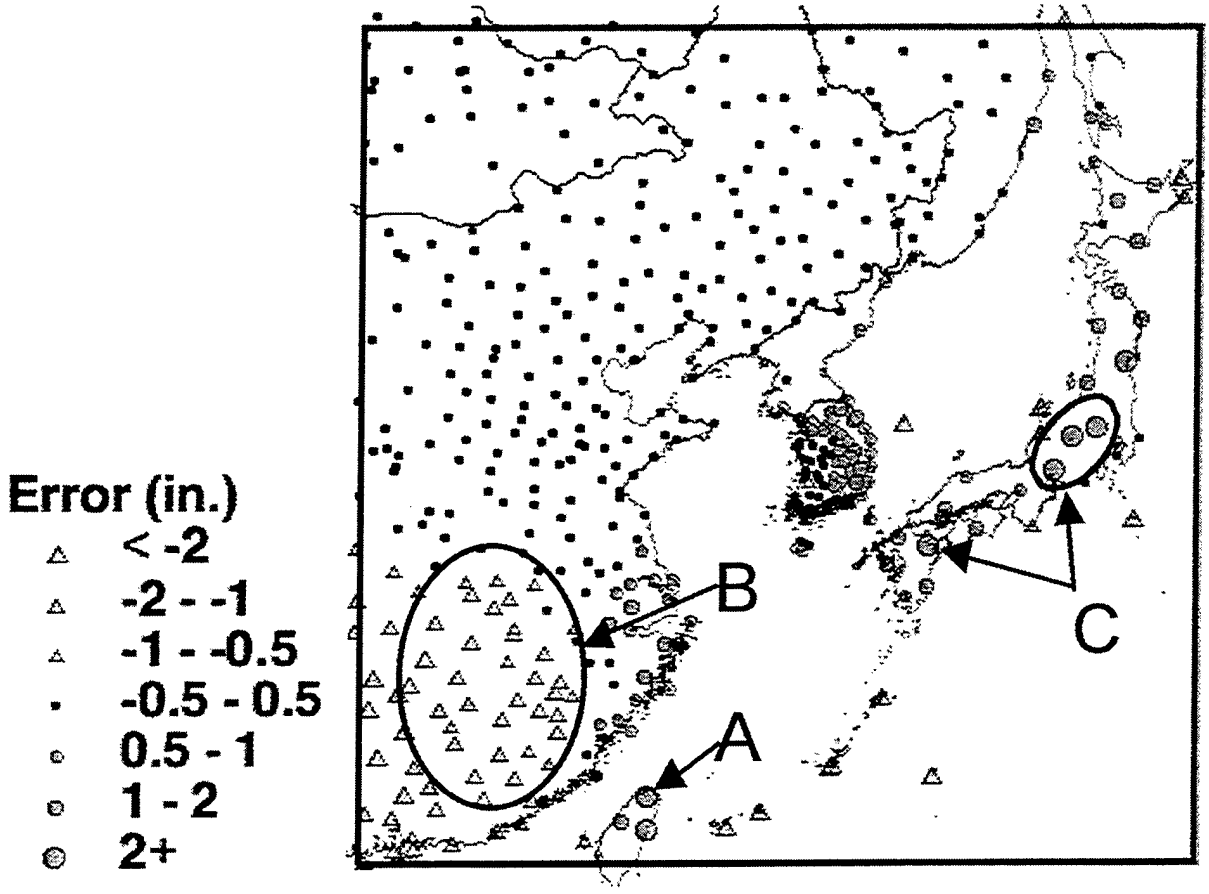

Attachment 28. Model error at GHCN locations. Positive values (circles) indicate regions where the model is wetter than observed.

A – Taipei, Taiwan;

B – Continental Southeast China;

C – Four sites in Japan.

Attachment 29

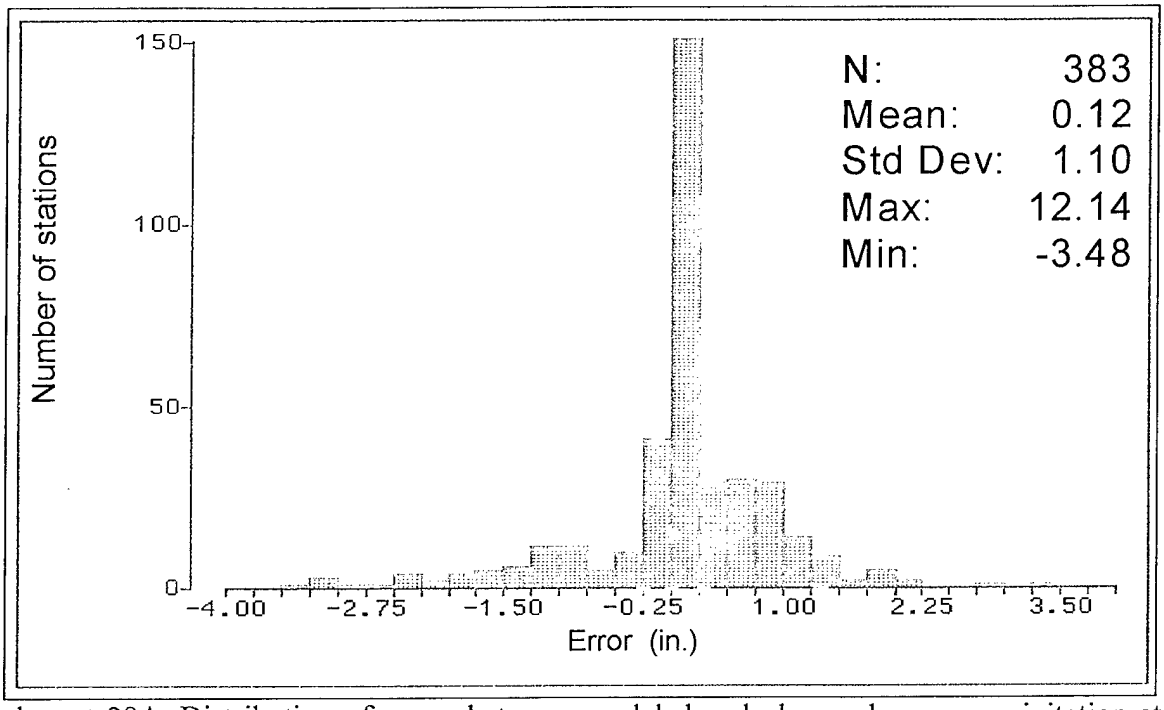

Attachment 29A. Distribution of errors between modeled and observed mean precipitation at NCDC's Global Historical Climatology Network (GHCN) locations in Far East Asia.

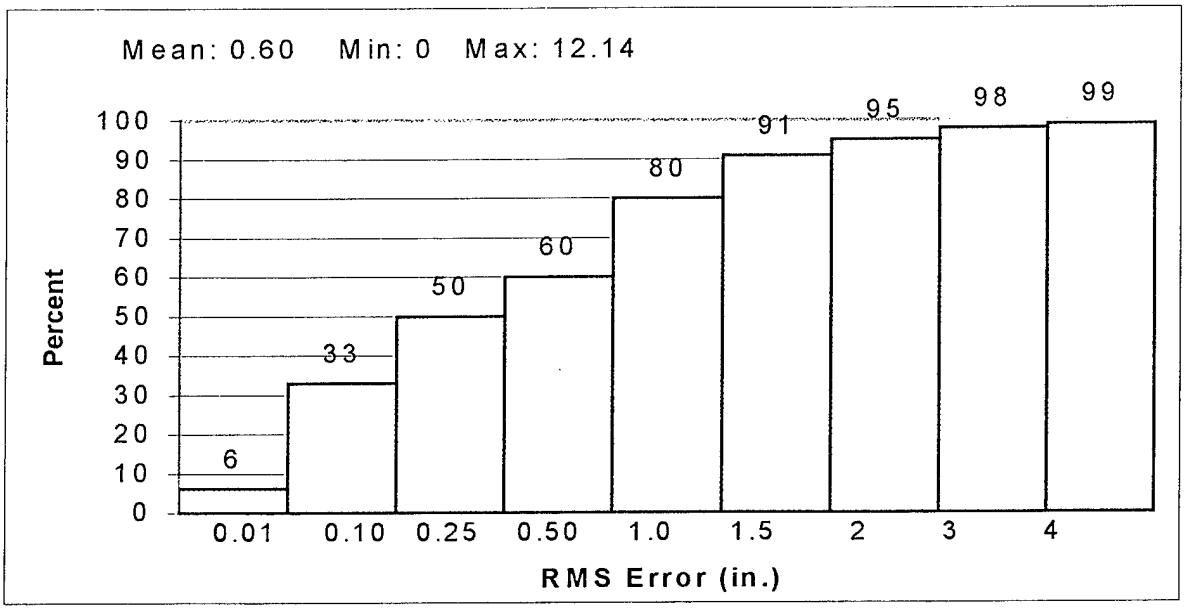

Attachment 29B. Cumulative frequency distribution of root mean square (RMS) errors between modeled and observed mean precipitation.

Attachment 30

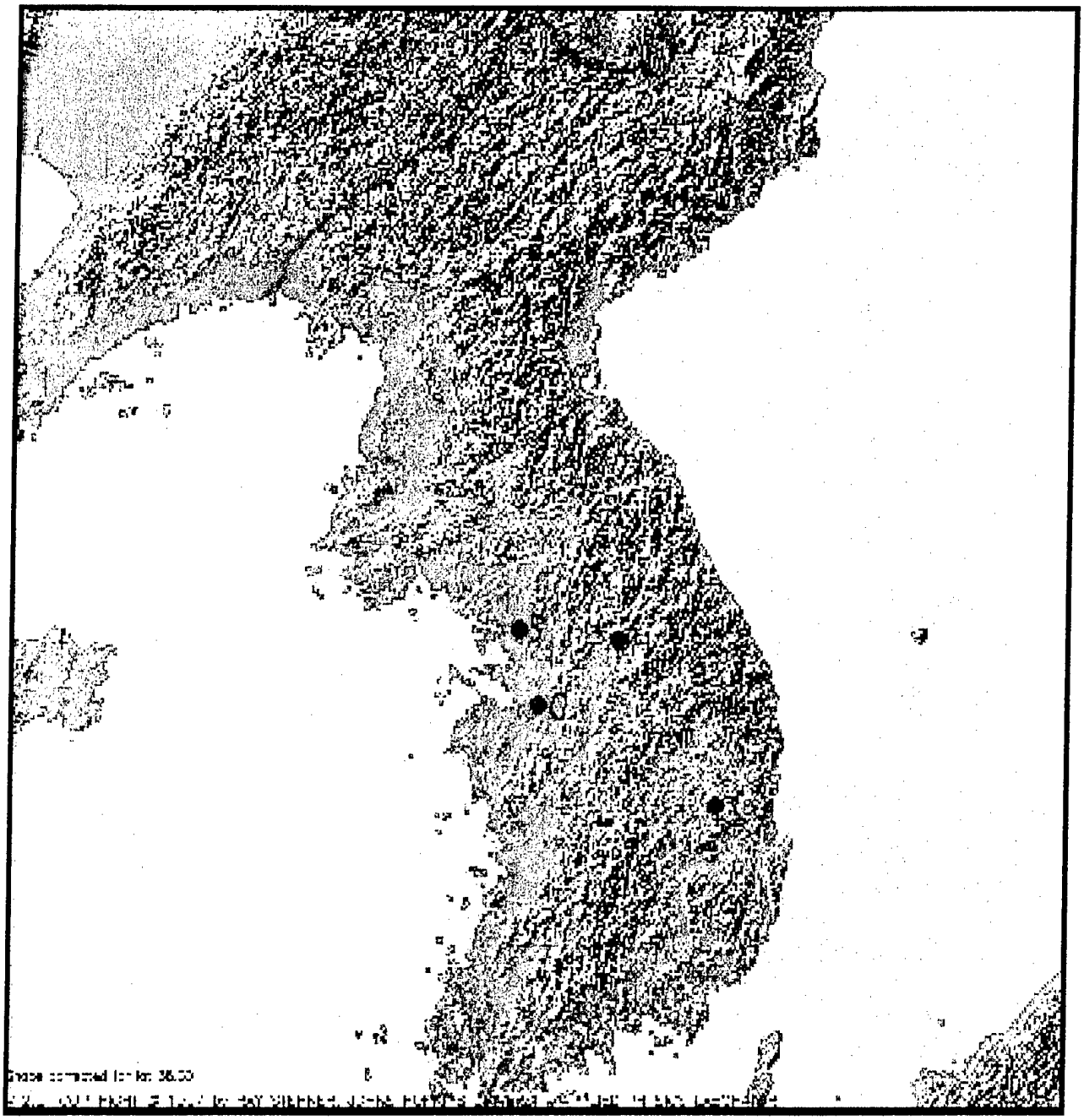

Attachment 30. The locations of the four stations used in the spatial variability experiments. Seoul (S), Osan (O), Hoengsong (H); Taegu (T).

Attachment 31

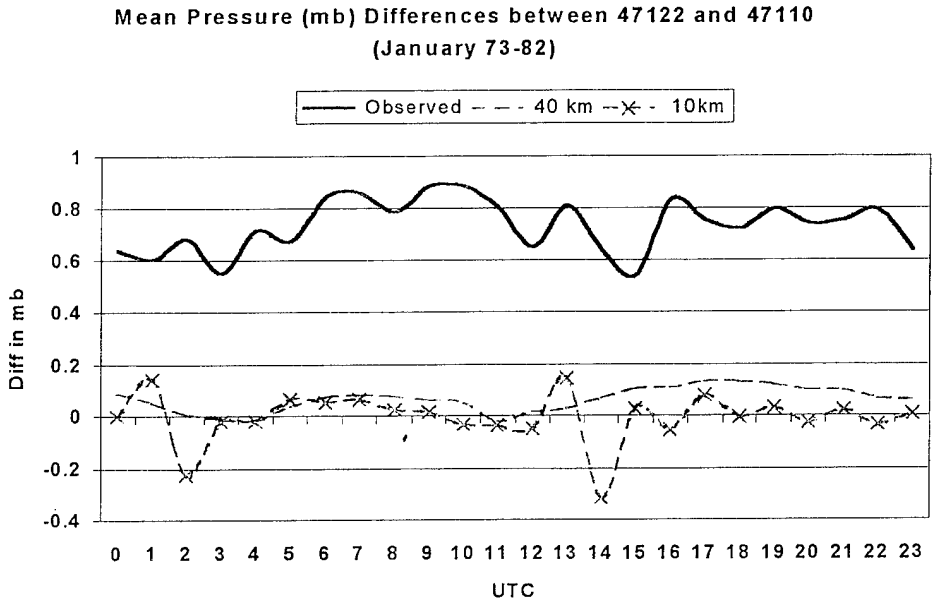

Attachment 31 A. January pressure comparison Osan (RKSO) and Seoul (RKSS).

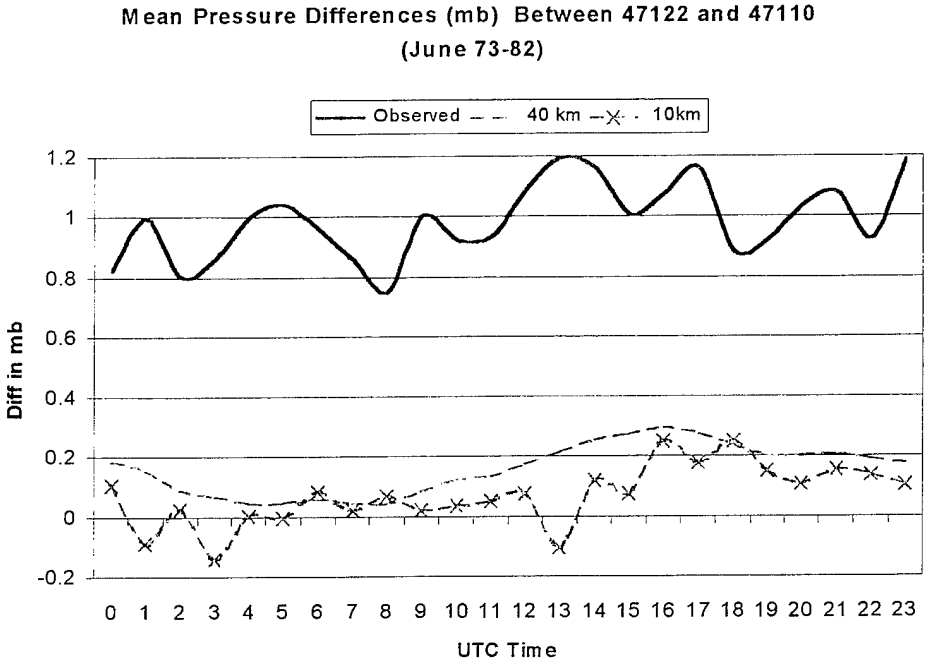

Attachment 31 B. June pressure comparison Osan (RKSO) and Seoul (RKSS).

Attachment 32

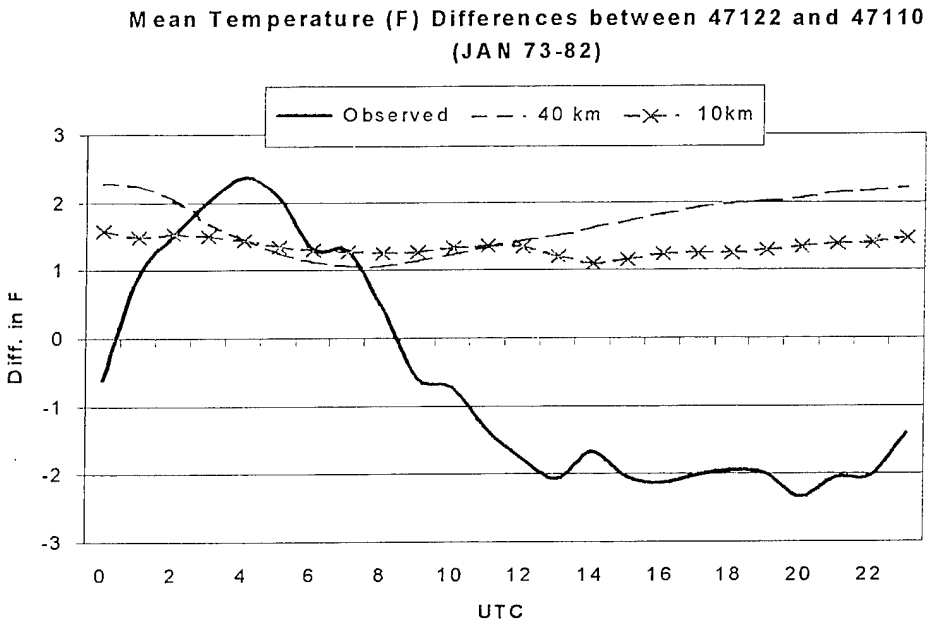

Attachment 32A. January mean temperature comparison Osan (RKSO) and Seoul (RKSS).

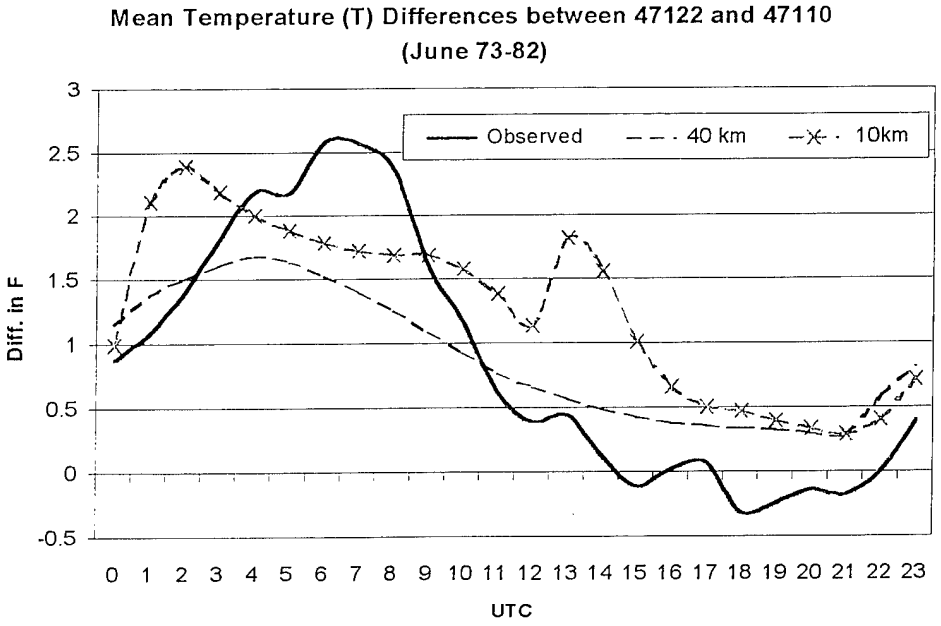

Attachment 32B. June mean temperature comparison Osan (RKSO) and Seoul (RKSS).

Attachment 33

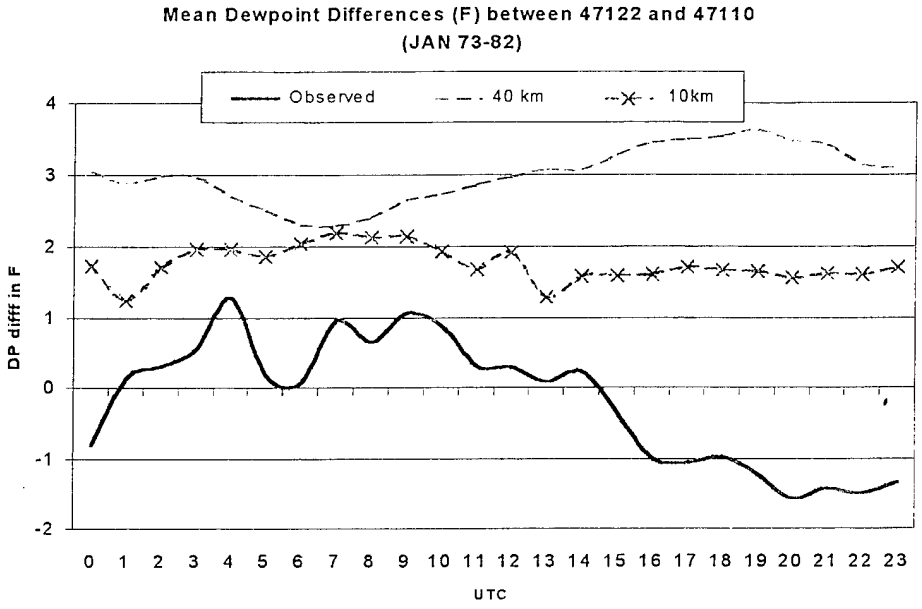

Attachment 33A. Comparison of mean January dewpoints, Osan (RKSO) and Seoul (RKSS).

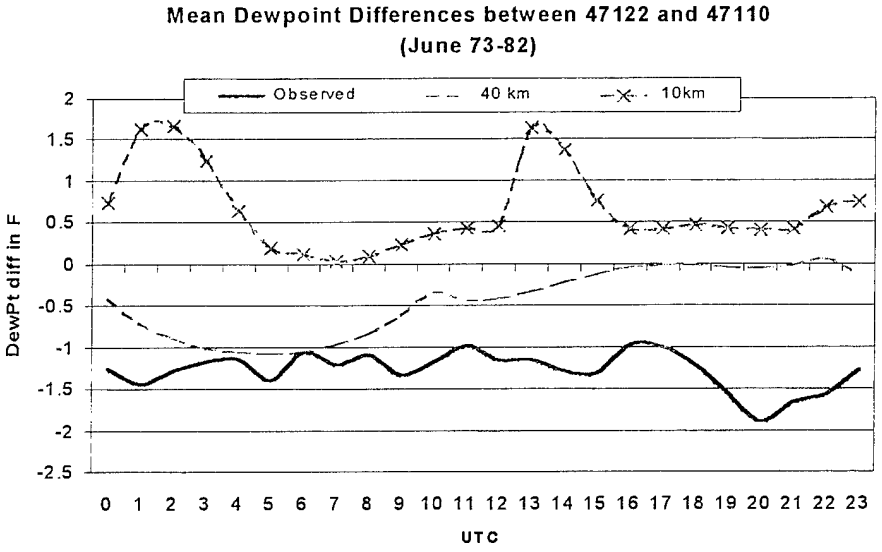

Attachment 33B. Comparison of mean June dewpoints, Osan (RKSO) and Seoul (RKSS).

Attachment 34

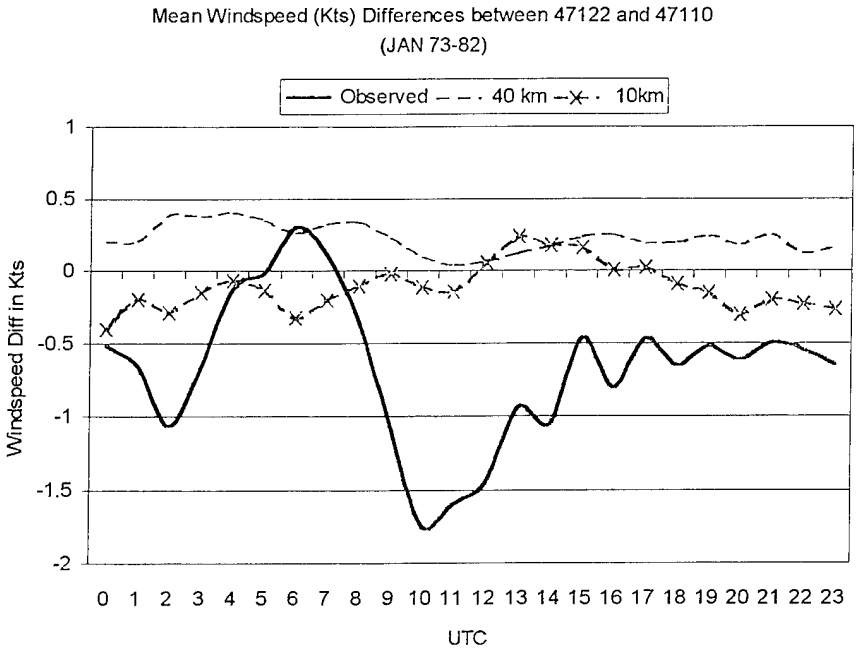

Attachment 34A. Comparison of mean January wind speeds, Osan RKSO - Seoul RKSS.

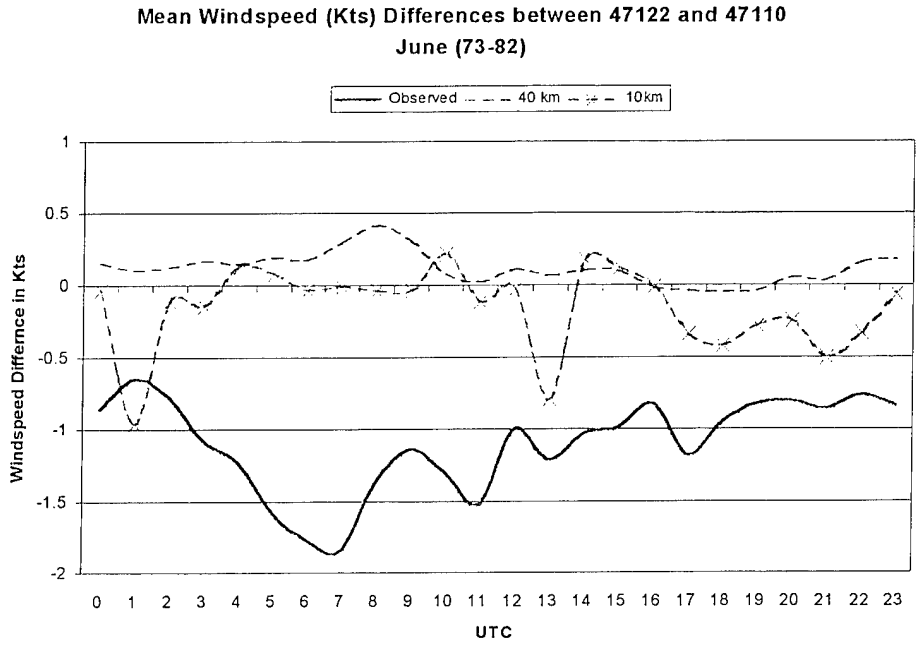

Attachment 34B. Comparison of mean June wind speeds, Osan RKSO - Seoul RKSS.

Attachment 35

Analysis of Extreme Values for the 10 Km Nest over Korea 1973-82

Vrbl Number	Variable Label	Unit	Minimum	Maximum	Range
1	Mean Surface Temperature	F	-1.8231	86.6807	88.5038
2	Std Dev of Sfc Temperature	F	1.0832	13.9147	12.8315
3	Max Surface Temperature	F	26.7033	86.7517	60.0484
4	Min Surface Temperature	F	-59.7046	74.3540	134.0586
5	Mean Surface Dew Point	F	-13.3622	75.6625	89.0247
6	Std Dev of Sfc Dew Point	F	3.0525	22.0626	19.0101
7	Max Surface Dew Point	F	20.6665	97.5308	76.8643
8	Min Surface Dew Point	F	-158.755	61.6766	220.4316
10	Mean Sea Level Pressure	mb	1004.420	1027.120	22.7000
11	Max Sea Level Pressure	mb	1016.300	1091.320	75.0200
12	Min Sea Level Pressure	mb	959.3340	1010.070	50.7360
13	Frequency of Precip	%	0.0000	52.2816	52.2816
14	Mean Hourly Precip.	in	0.0000	0.1354	0.1354
15	Std Dev of Hourly Precip.	in	0.0000	0.0006	0.0006
16	Max Hourly Precip.	in	0.0000	9.9564	9.9564
17	Mean Monthly Precipitation	in	0.0000	36.0351	36.0351
18	Mean Sfc Wind Speed	kts	3.6984	28.7256	25.0273
19	Max Sfc Wind Speed	kts	14.0567	115.3130	101.2563
20	Min Sfc Wind Speed	kts	0.0010	1.8731	1.8721
21	Prevailing Sfc Wind Dir.	deg	45.0000	360.0000	315.0000
22	Prevailing Sfc Wind Speed	kts	3.6180	32.0464	28.4285

Attachment 36

Analysis of simulated climatologies compared with observed climatologies provided by Capt Matt Doggett AFCCC/DOC.

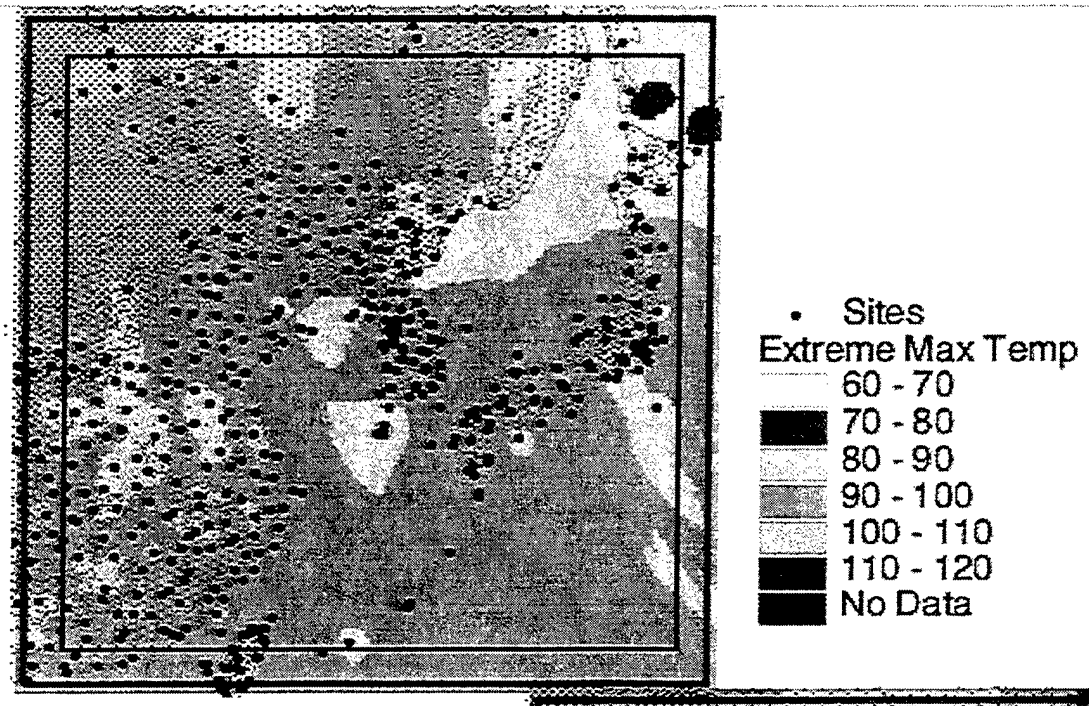

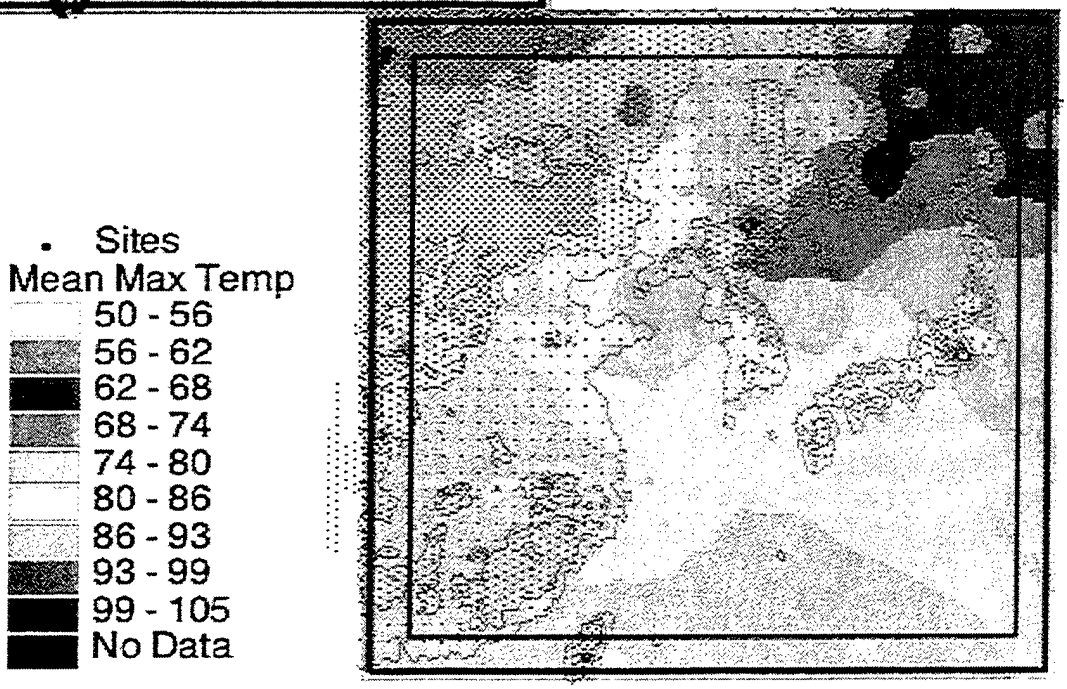

(Obtained from surface, land-based observations. Use caution over oceans and data-sparse mountain regions)

Mean Daily/Extreme Max:

Highest values over continental China and southern Pacific upper 80s to low 90s (86-93). Lowest in mountainous locations and northern Japan, northeast China; upper 50s to low 60s (56-62). Korean peninsula averages highs in 70s-80s except in the mountains with highs only in the 60s. Extreme Max Continental China gets extremes of 100-110. Large portion of the rest of the area has maximums of 90-100. Northern Japan islands coolest with extremes of 70-80. Extremes on Korean peninsula from 90-100.

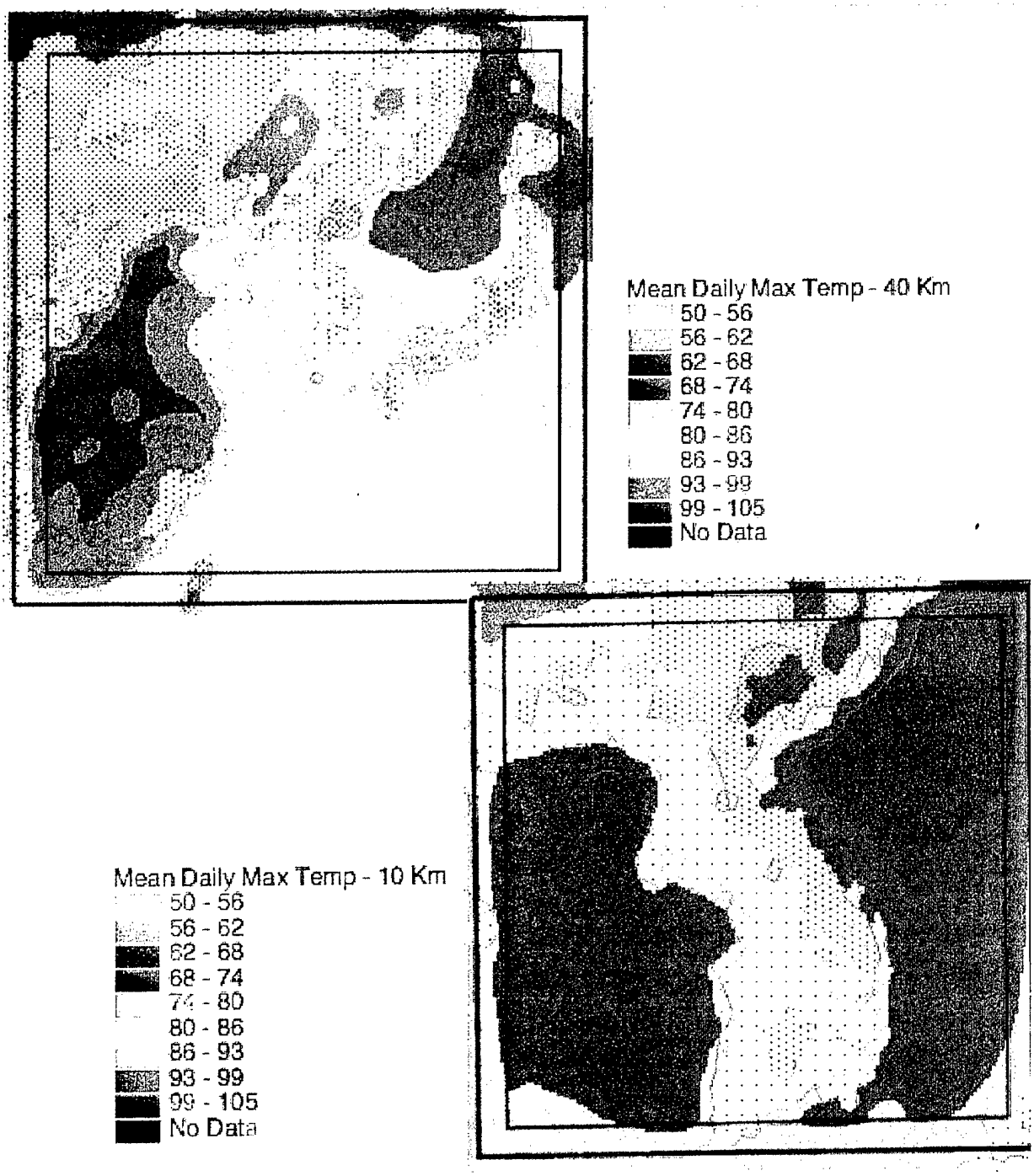

Mean Daily Maximum Temperature - July

- 40 km. Hottest temperatures across continental China in the 90s to over 100. Appears to be about 10 degrees too hot. Northern islands of Japan appear nearly 20 degrees too warm. Japan & Korea in general appear 5-10 degrees too warm. Observed mean daily highs are in 80s (80-86) while modeled are 86-93.
- 10 km: Temps generally ~6 degrees (one category) cooler than shown in 40 km. Daily highs much closer to observed than at 40 km. Most dramatic difference between 40 & 10 km is over the oceans which are as much as 12 degrees (two categories) cooler than in 40 km. The same ocean SST data is used in both cases and so it is surprising that there is such a difference between 40 & 10 km. Also, there aren't any features over the ocean that are resolved at 10 km that aren't resolved at 40 km.

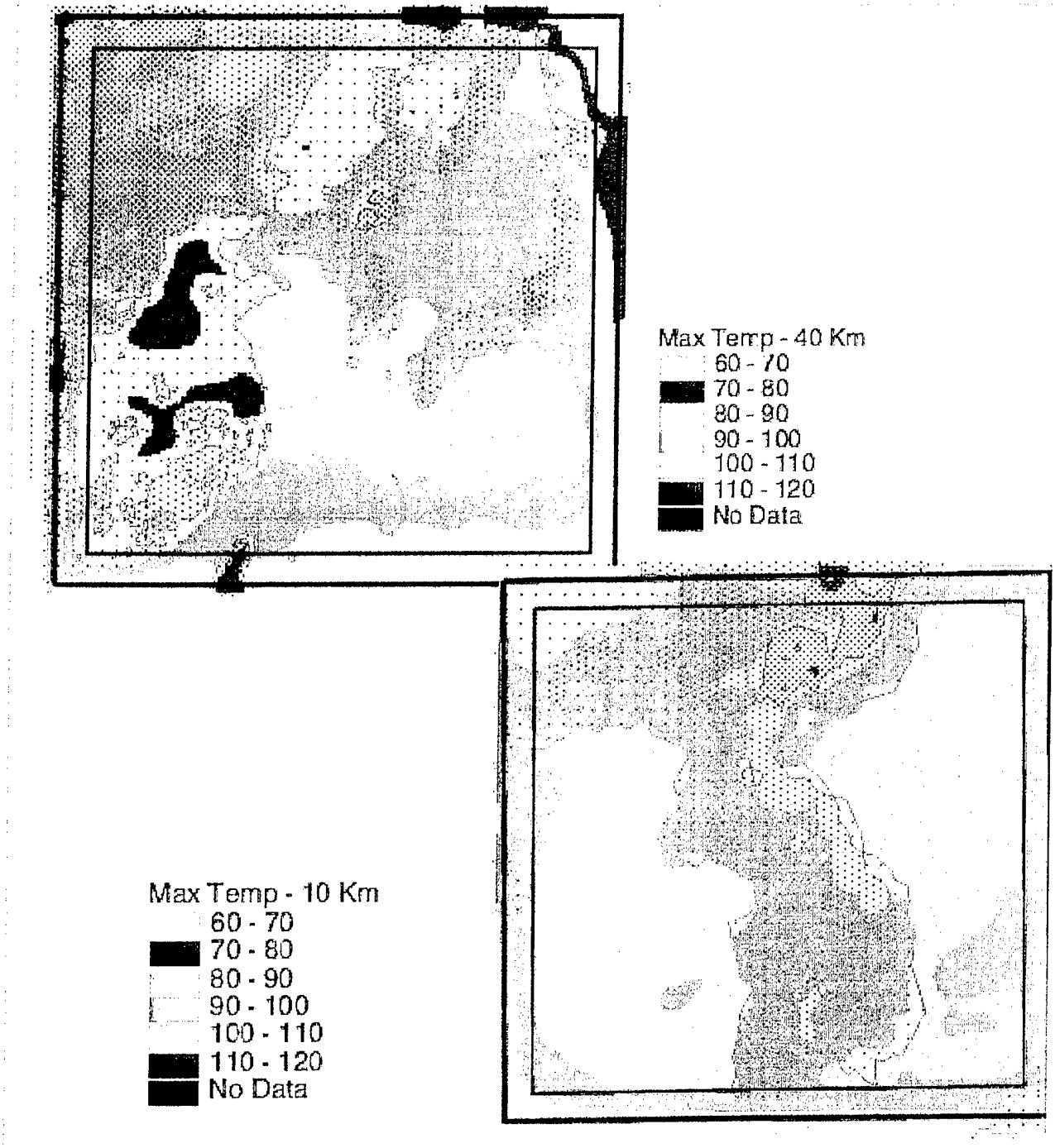

Extreme Maximum Temps – July

Overall the extreme max temps look reasonable although the extremes over mainland China appear too hot.

- 40 km. Hottest temperatures over continental China 110-120 are about 10 degrees too hot. Coolest over the Northern Pacific Ocean are fairly close to observed.. Identifies minimums in temperature extremes in the mountainous terrain of China and Japan. Maximums over the oceans seem to be much too high. Extremes of 90-100 over Korea and Japan are close to observed of 90-100. Minimums of 70-80 over Taiwan are about 10 degrees *colder* than observed of 80-90.
- Suspicious that the extreme temperatures around Korea are higher over the ocean than over the land; exactly opposite of what is expected. Same over southern Japan islands.
- 10 km. Corrects for the discrepancy over the oceans noted above in the 40 km data. Temps over the oceans are cooler than over the land and dramatically cooler than at 40 km.

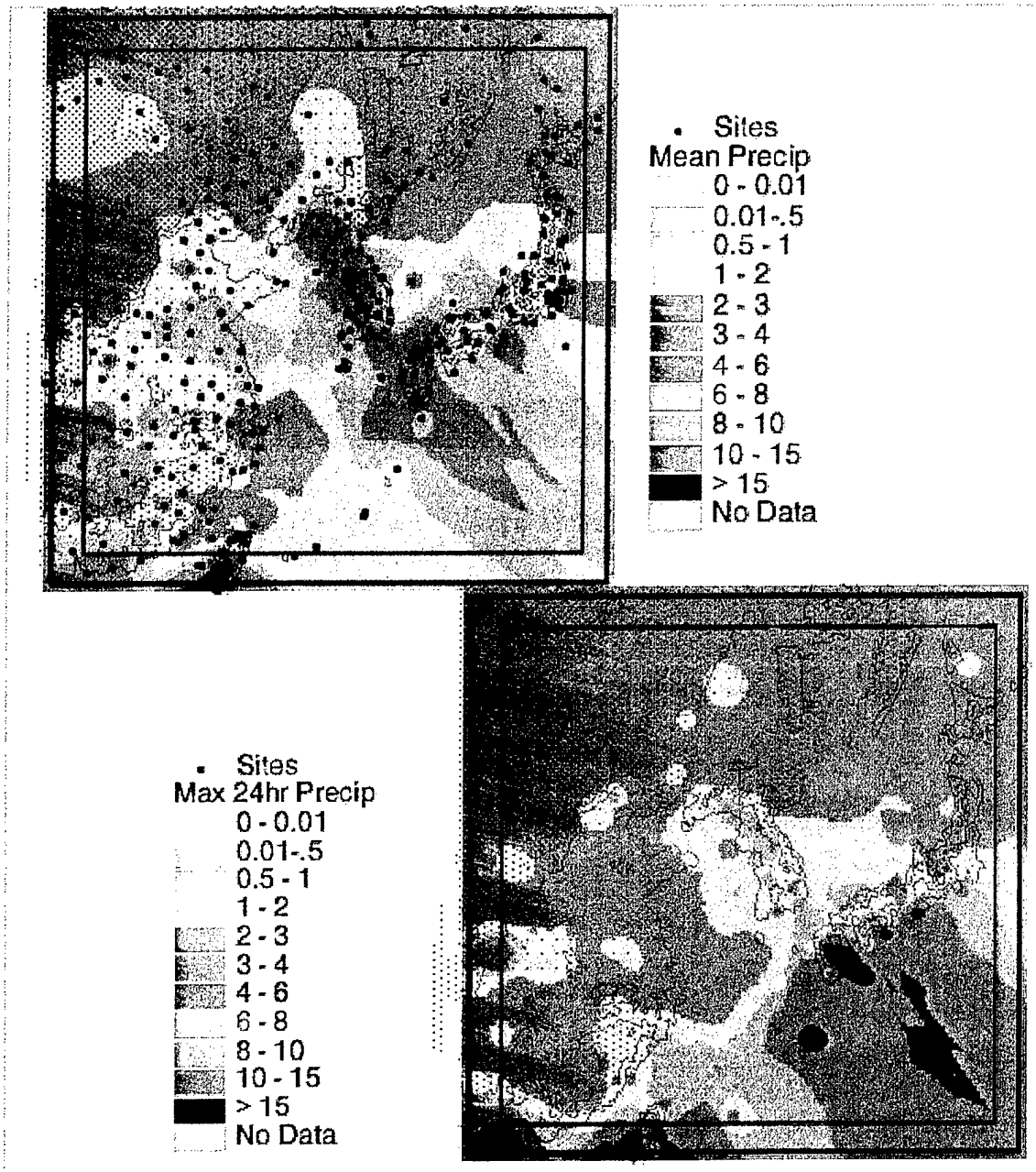

Observed Precipitation – July

(obtained from surface, land-based observations. Use caution over oceans and data-sparse mountain regions)

Mean Monthly Precip

Maximums along Korean peninsula (10-15 in), southern Japan islands (10-15 in) and southern island of Taiwan (>15 in). Minimums observed in continental China of 1-2 inches. Broad region of 4-6 in. from mountainous continental China extending into northeast China and across to northern islands of Japan.

Max 24-hr Precip

Maximums along tropical maritime China, Taiwan, and Japan (>15 in).

Minimums in continental China of < 1 in.

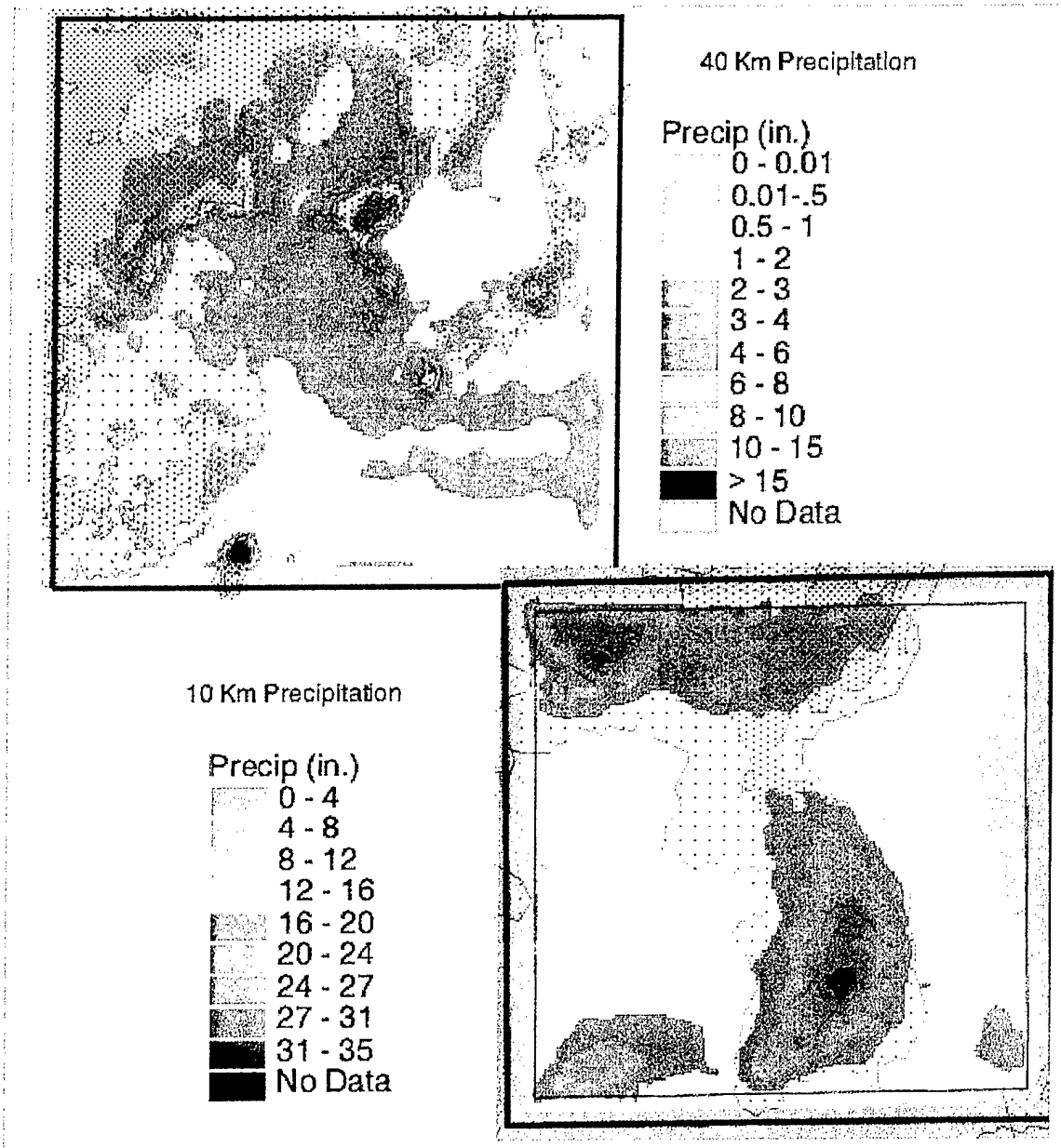

Modeled Mean Monthly Precipitation

40 km

In general, the model is much too dry compared to observed. Severely too dry over southern China and northern Japan's islands (modeled < 1 in vs. observed of 4-6 inches). Also the western half of Korean peninsula is too dry (2-4 inches model vs. 10-15+ inches observed). Central China 1-4 inches compared to observed in excess of 8 inches.

10 km

Huge differences between 10 km and 40 km. 31-35 in maximum over S. Korea and northern N. Korea far in excess of observed 10-15 in. The frequency of precip value in the model averages 24% for all gridpoints. Most are somewhere between 22-27%.

Attachment 36 cont.

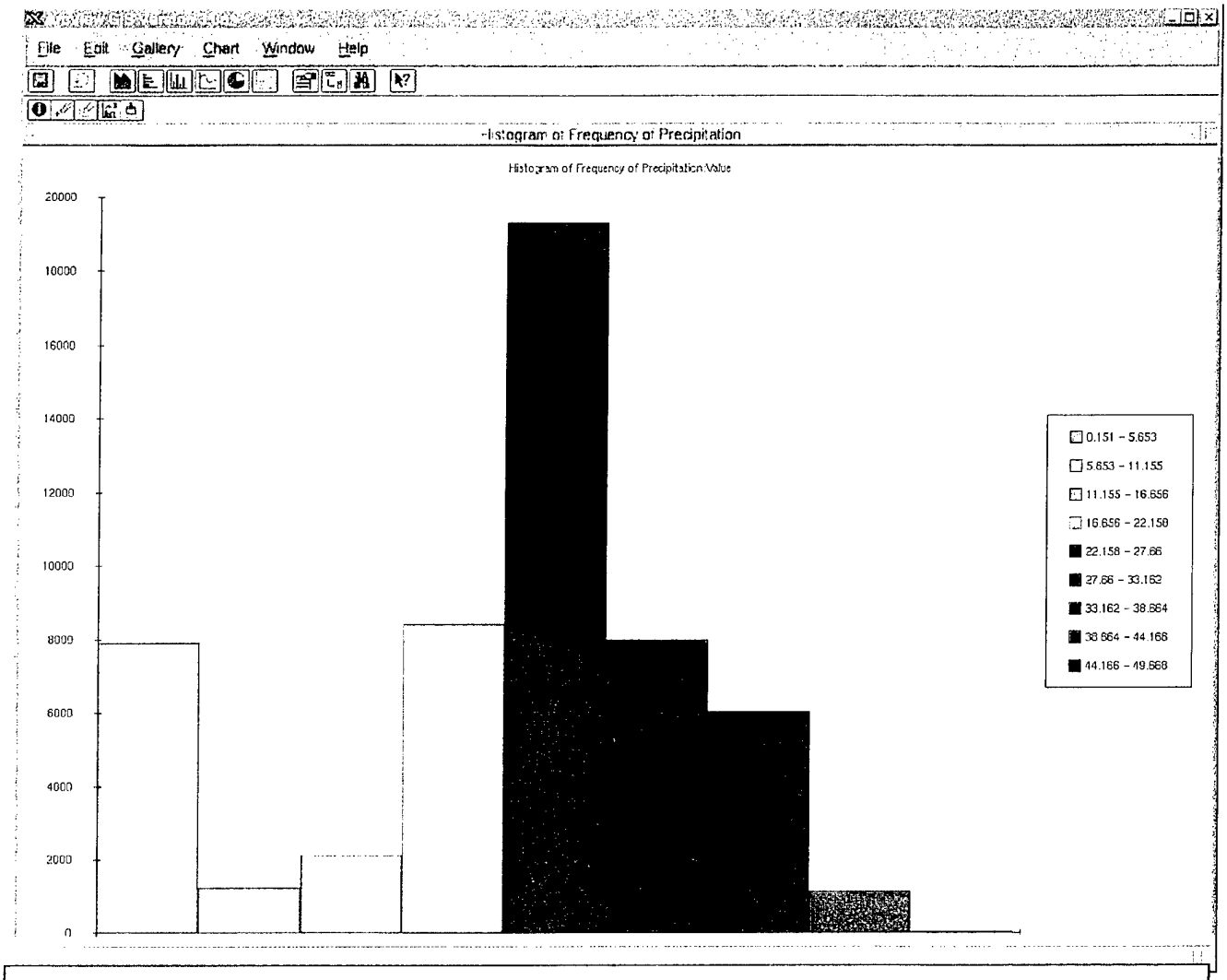

Frequency distribution of precipitation frequency - July - 10 km Korea.

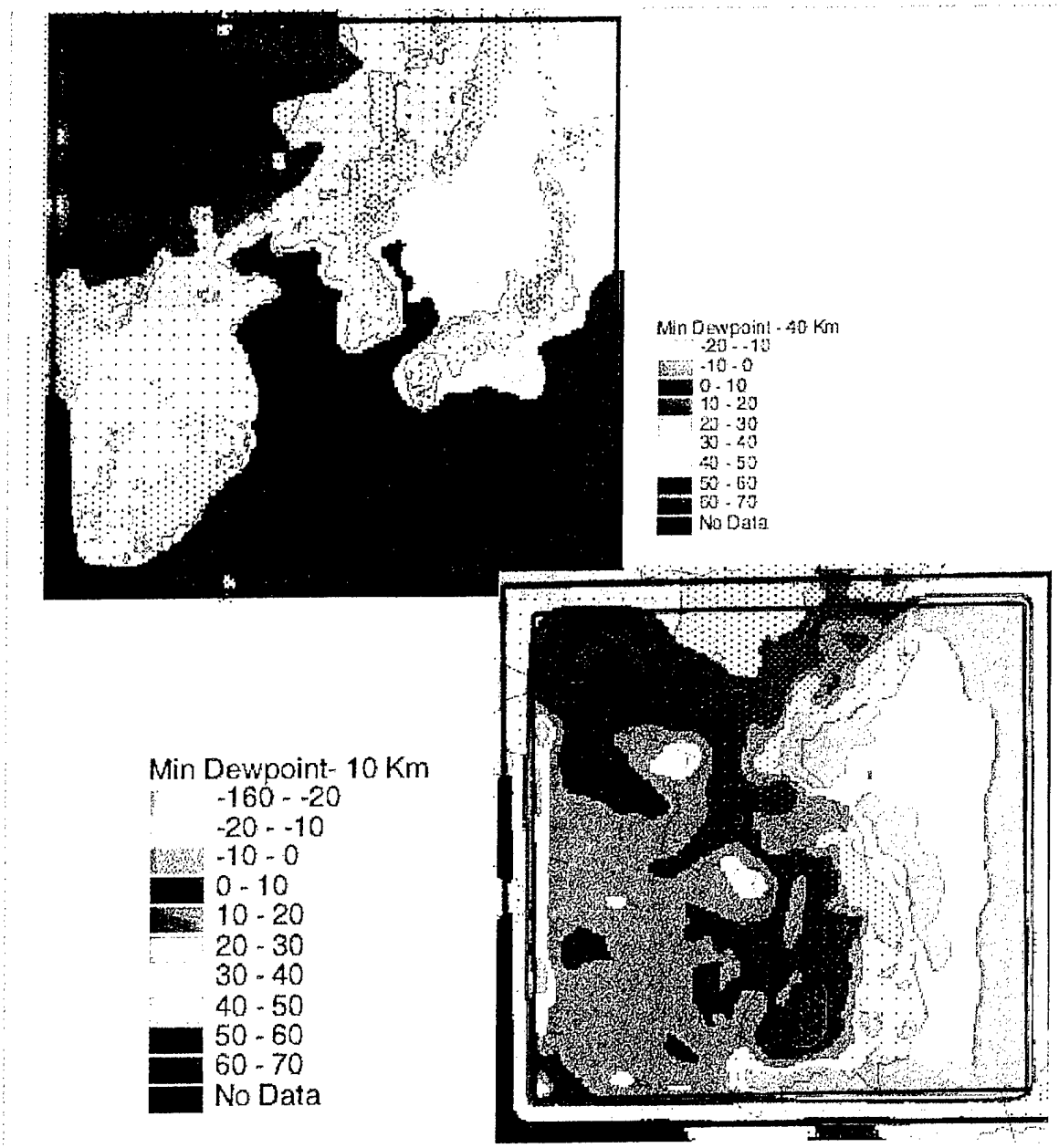

Minimum Dewpoint – July – All Hours

The 40 km dewpoint minimums appear to be reasonable. No observed min dewpoints are readily available to compare data
Very obvious and significant differences between 40 & 10 km data.
Obviously bogus values well below zero over the ocean waters at 10 km. Clearly the minimum dewpoint should not be lower over the oceans than over the land.

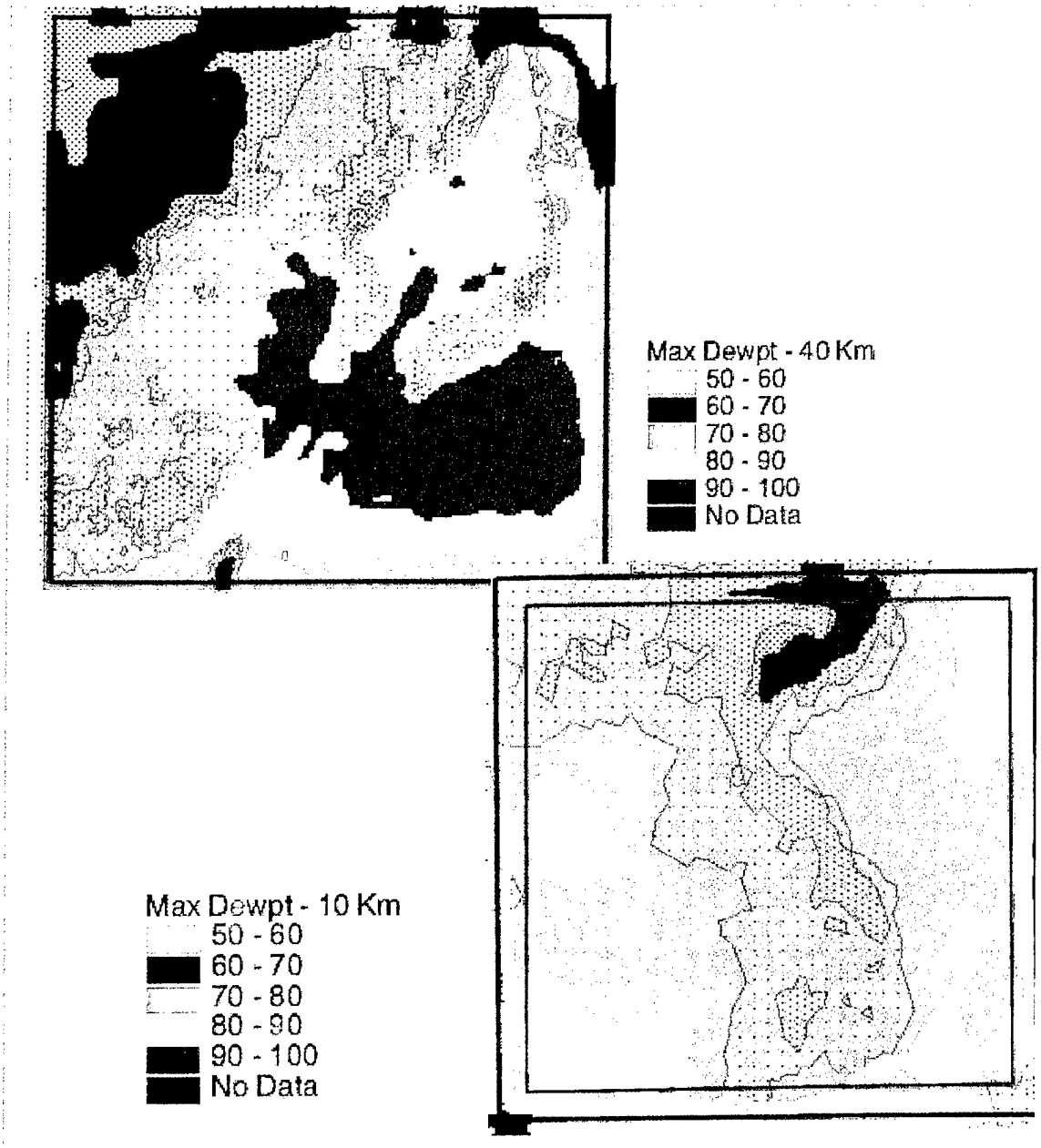

Maximum Dewpoint – July – All hours

Again, no maximum dewpoint observations from Operational Climate Data Center (OCDS) to readily compare with. However, a qualitative analysis appears to indicate reasonable values at both 40 & 10 km.

40 km

Maximums over the oceans and minimums over mountainous terrain and continental areas.

10 km

Values run about 10 degrees less than at 40 km over the same region. Values over water generally higher than over land. Properly identifies a minimum over the northern mountains.

Attachment 37

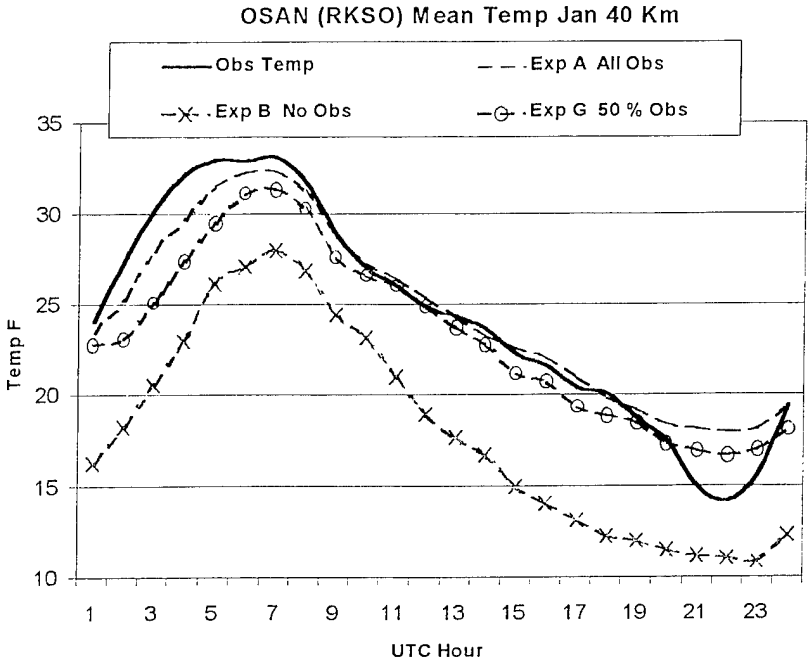

Attachment 37A. Data Denial Experiment results for RKSO temperature January (1973-75, 77 and 79) 40 km nest.

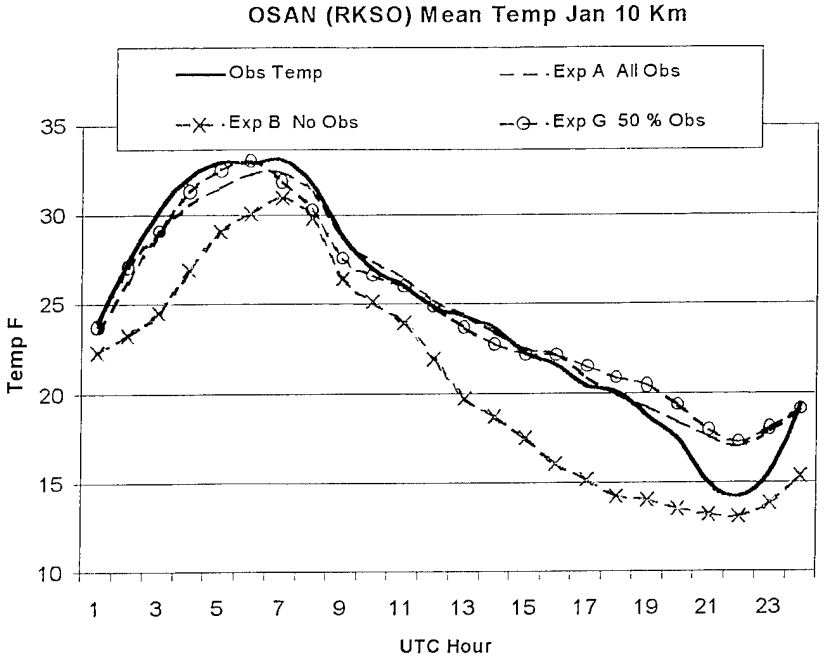

Attachment 37B. Data Denial Experiment results for RKSO temperature January (1973-75, 77 and 79) 10 km nest.

Attachment 38

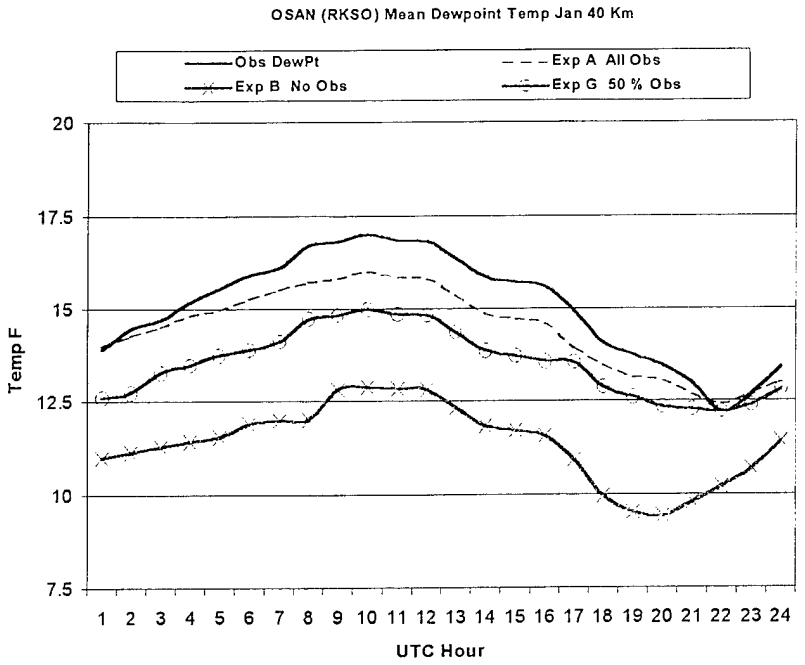

Attachment 38A. Data Denial Experiment results for RKSO dewpoint January (1973-75,77-79) 40 km nest.

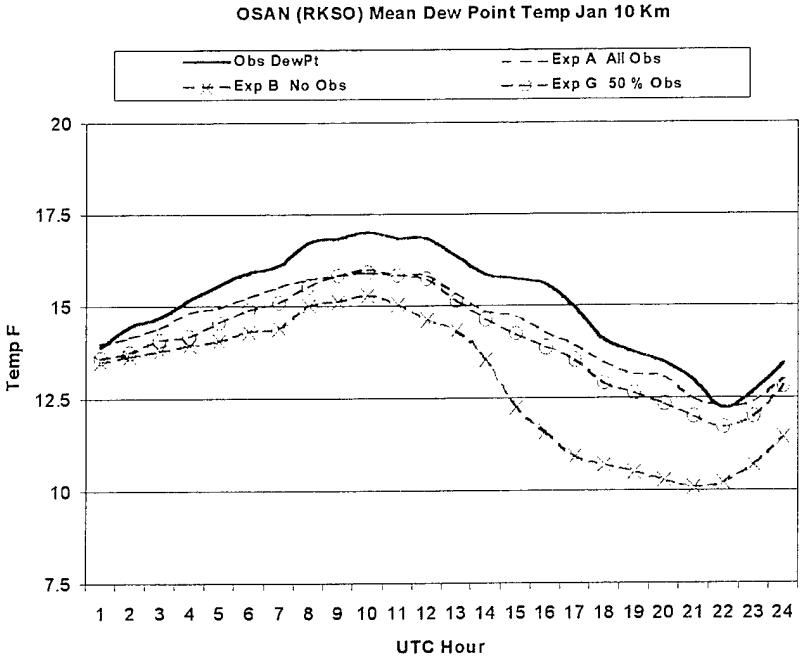

Attachment 38B. Data Denial Experiment results for RKSO dewpoint January (1973-75,77-79) 10 km nest.

Attachment 39

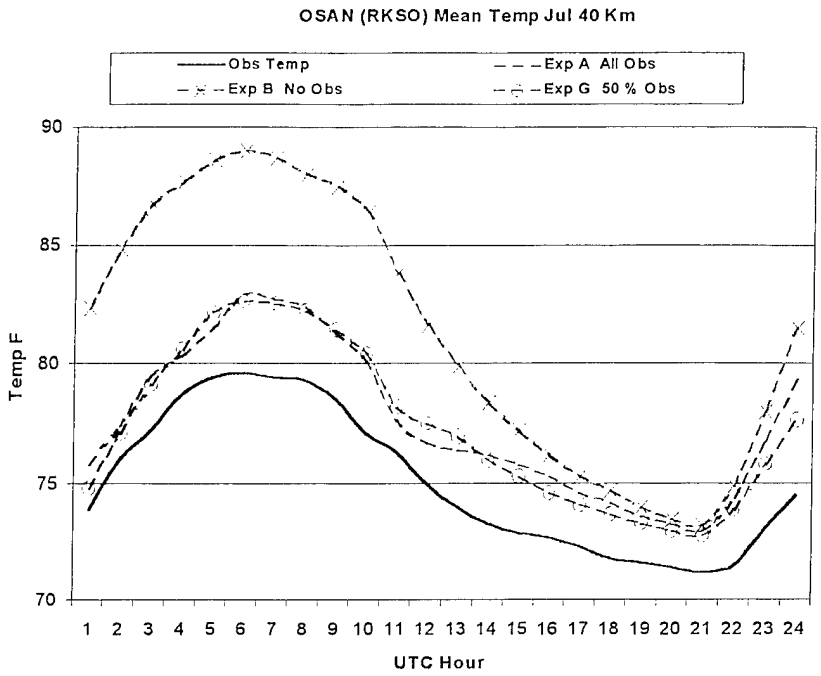

Attachment 39A. Data Denial Experiment results for RKSO temperature July (1973-75,77-79) 40 km nest.

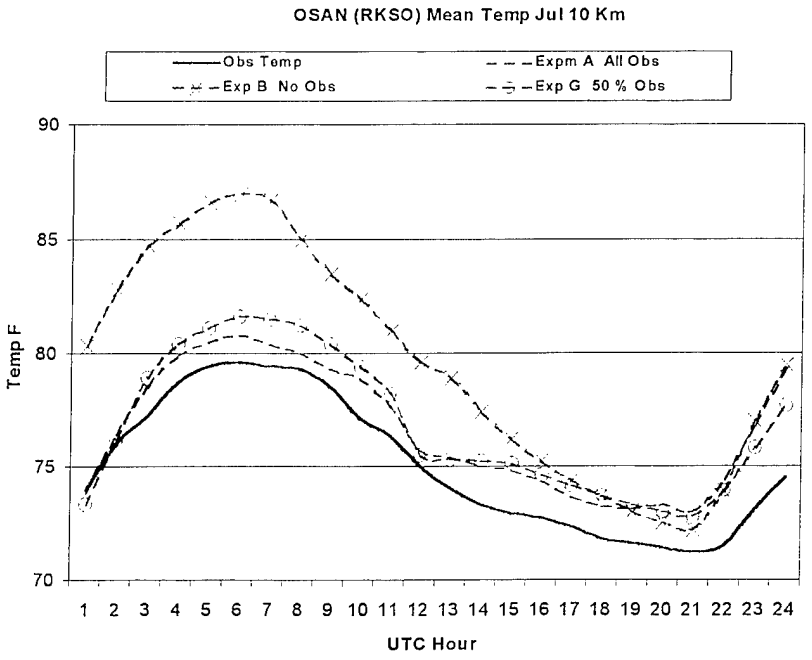

Attachment 39B. Data Denial Experiment results for RKSO temperature July (1973-75,77-79) 10 km nest.

Attachment 40

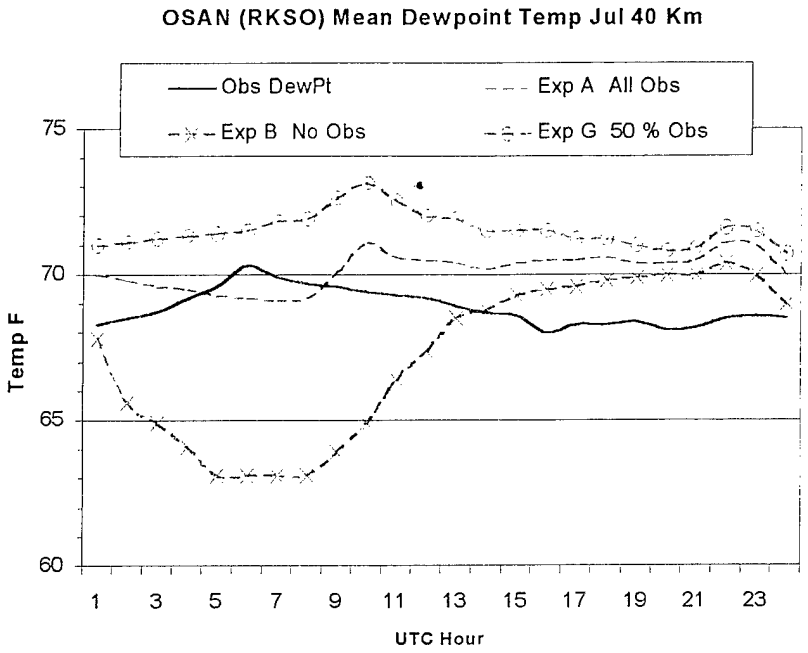

Attachment 40A. Data Denial Experiment results for RKSO dewpoint July (1973-75,77 and 79) 40 km nest.

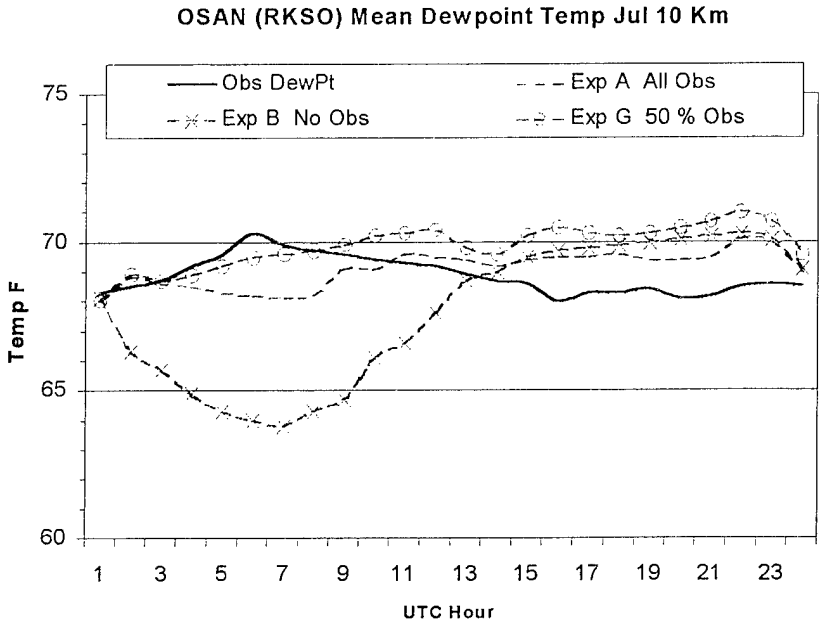

Attachment 40B. Data Denial Experiment results for RKSO dewpoint July (1973-75,77 and 79) 10 km nest.

Attachment 41

LOWTRAN 7 IR Transmissivity Compared with CLIMOD IR Transmissivity

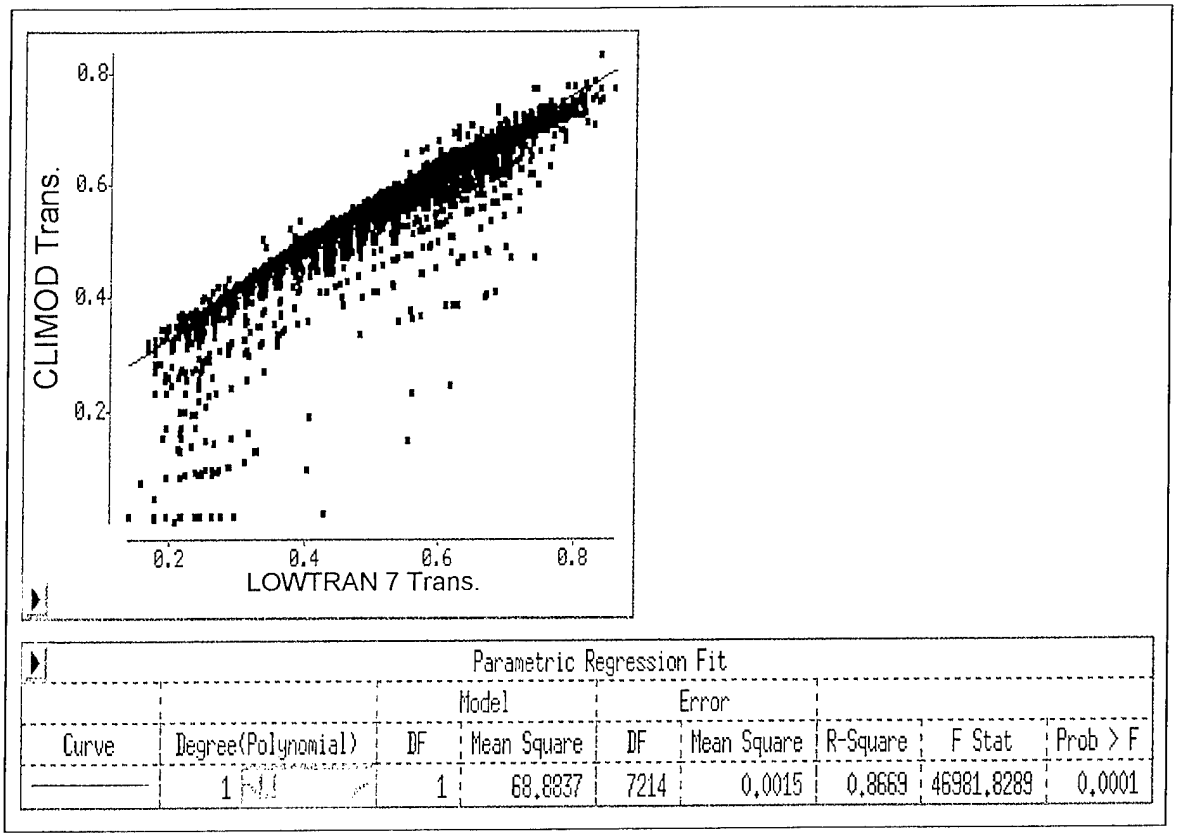

Parametric Regression Fit

		Model		Error				
Curve	Degree(Polynomial)	DF	Mean Square	DF	Mean Square	R-Square	F Stat	Prob > F
———	1	1	68.8837	7214	0.0015	0.8669	46981.8289	0.0001

Attachment 41. Example of assessment of algorithm for the 8-12 micrometer band done by AFCCC/DOC. LOWTRAN 7 transmissivity values (x axis) compared with CLIMOD algorithm transmissivity values (y axis).

REFERENCES

Brown, B. G., G. Thompson, R. T. Bruintjes, R. Bullock, and T. Kane, 1997: Intercomparison of in-flight icing algorithms. Part II: Statistical verification results. *Wea. Forecasting*, **12**, 890-914.

Cairns, M., R. J. Miller, J. Chen, J. L. Mahoney, S. G. Benjamin, J. E. Ramer, and T. L. Smith, 1994a: A Second Evaluation of Aviation-Impact Variables Generated by MAPS. *NOAA Tech. Memo.* ERL FSL-13, NOAA/FSL, Boulder, CO 80303. 96 pp.

Doggett, M. K., M. Squires, and R. Kiess, 1999: An evaluation of the quality of local climate statistics generated from the output of a 3-d mesoscale atmospheric. Preprints, *11th Conference on Applied Climatology*, Dallas, TX, Amer. Meteor. Soc., 344-349.

_____, 1999: ACMES extreme value analysis study. 15 Dec 1999 (unpublished paper available at AFCCC/DOC)

_____, 2000: Modeling snowfall climatologies using a mesoscale model. Preprints, *12th Conference on Applied Climatology*, Asheville, NC, Amer. Meteor. Soc., 9-11.

Ellrod, G. P., and D. I. Knapp, 1992: An objective clear-air turbulence forecasting technique: Verification and operational use. *Wea. Forecasting*, **7**, 150-65.

Gagan, J., and C. E. Graves, 1999a: *Korea Statistics: July - December, 10 Years.* [available from Dr. Charles E. Graves, Saint Louis University, 3597 Leclede Avenue, St. Louis, MO. 63103-2010] 280 pp.

_____, _____, 1999b: *SW Asia Statistics: July - December, 10 Years.* [available from Dr. Charles E. Graves, Saint Louis University, 3597 Leclede Avenue, St. Louis, MO. 63103-2010] 200 pp.

_____, _____, 1999c: *Korea Statistics: Denial Experiments, January and July.* [available from Dr. Charles E. Graves, Saint Louis University, 3597 Leclede Avenue, St. Louis, MO. 63103-2010] 200 pp.

Graves, C. E, and. J. Gagan, 1999: *SW Asia Statistics: January - June, 10 Years.* [available from Dr. Charles E. Graves, Saint Louis University, 3597 Leclede Avenue, St. Louis, MO. 63103-2010] 190 pp.

Graves, C. E., and K. A. Poage, 1998: *AFCCC/ACMES Results, Climate Statistics: Korea: January - June.* [available from Dr. Charles E. Graves, Saint Louis University, 3597 Leclede Avenue, St. Louis, MO. 63103-2010] 300 pp.

Kneizys, F. X., E. P. Shettle, L. W. Abreu, G. P. Anderson, J. H. Chetwynd, W. O. Gallery, J. E. A. Selby and S. A. Clough, 1988: *Atmospheric Transmittance/Radiance: the LOWTRAN 7 model, AFGL-TR-88-0177.*

Lee, J. E., and M. Girodo, 1998: Use of the Eta model to determine the role of static stability in forecasting surface winds. Preprints, *16th Conference on Wea. Anal. and Fore.*, Phoenix, Amer. Meteor. Soc. 56-58.

MESO, 1995: *MASS Version 5.6 Reference Manual.* MESO, Inc., 185 Jordan Rd. Troy, NY 12180, 118 pp.

Pielke, R. A., 1984: *Mesoscale Meteorological Modeling.* Academic Press, 612 pp.

Ramer, J. E., 1993: An empirical technique for diagnosing precipitation type from model output. Preprints, *5th Conference on Aviation Weather Systems*, 2-6 August, Vienna, VA, Amer. Meteor. Soc.

Thompson, G. R., R. T. Bruintjes, B.G. Brown, and F. Hage, 1997: Intercomparison of in-flight icing algorithms. Part I: WISP94 real-time icing prediction and evaluation program. *Wea. Forecasting*, **12**, 878-889.

Thompson, J. S., 1999: ACMES desert dewpoint bias study. 22 Sep 1999 (unpublished paper available at AFCCC/DOC)

_____, 2000: An examination of ceiling and wind event frequency modeling by the Advanced Climate Modeling and Environmental Simulations (ACMES). Preprints, *12th Conference on Applied Climatology*, Asheville, NC, Amer. Meteor. Soc., 9-11.

Van Knowe, G. E, J W. Zack, S. Young, M. D. Bousquet, P. E. Price C. E. Graves and K. Poage, 1999: An evaluation of the sensitivity of local climate statistics generated from the output of a 3-d mesoscale atmospheric model to model configuration, data assimilation, resolution and subgrid parameterization schemes. Preprints, *11th Conference on Applied Climatology*, Dallas, TX, Amer. Meteor. Soc., 513-516.

Vose, R. S., Richard L. Schmoyer, Peter M. Steurer, Thomas C. Peterson, Richard Heim, Thomas R. Karl, and J. Eischeid, 1992: *The Global Historical Climatology Network: long-term monthly temperature, precipitation, sea level pressure, and station pressure data.* ORNL/CDIAC-53, NDP-041. Carbon Dioxide Information Analysis Center, Oak Ridge National Laboratory, Oak Ridge, Tennessee.

Zack, John W, G. E. Van Knowe, P. E. Price, M. D. Bousquet, S. Young, and C. E. Graves, 1998: Scientific Report No. 1: Development of methods to generate high resolution climatological databases to support DOD modeling and simulation programs,. AFRL-VS-HA-TR-98-0047. Air Force Research Laboratory, Space Vehicles Directorate, Hanscom Air Force Base, MA. 46 pp.